AD-A062 417 NAVAL RESEARCH LAB WASHINGTON D C F/G 20/4
THE INFLUENCE OF YAW ANGLE UPON THE VORTEX WAKES OF STATIONARY --ETC(U)
AUG 78 S E RAMBERG
UNCLASSIFIED NRL-MR-3822 SBIE-AD-E000 238 NL

1 OF 2
AD
A062417

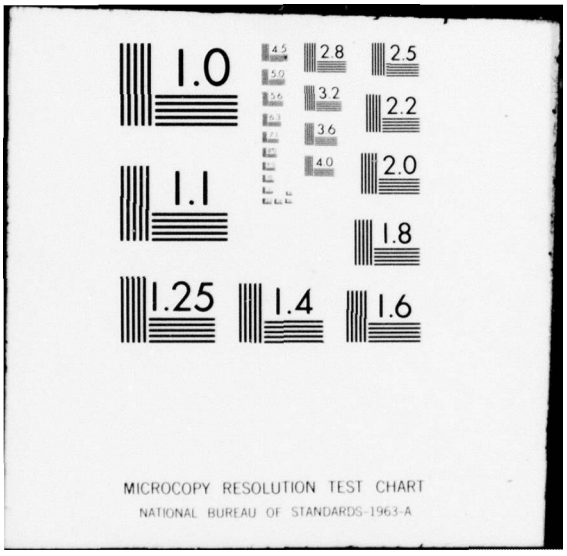
1.0
1.1
1.25
1.4
1.6
1.8
2.0
2.2
2.5
2.8
3.2
3.6
4.0
4.5
5.0
5.6
MICROCOPY RESOLUTION TEST CHART
NATIONAL BUREAU OF STANDARDS-1963-A

NRL Memorandum Report 3822

The Influence of Yaw Angle Upon the Vortex Wakes of Stationary and Vibrating Cylinders

Steven E. Ramberg

Applied Mechanics Branch
Ocean Technology Division

August 1978

NAVAL RESEARCH LABORATORY
Washington, D.C.

(18) SBIE

(14) NRL-MR-3822

SECURITY CLASSIFICATION OF THIS PAGE (When Date Entered)

REPORT DOCUMENTATION PAGE

READ INSTRUCTIONS BEFORE COMPLETING FORM

1. REPORT NUMBER: NRL Memorandum Report 3822
2. GOVT ACCESSION NO.
3. RECIPIENT'S CATALOG NUMBER

(9) Final rept.

4. TITLE (and Subtitle): (6) The Influence of Yaw Angle Upon the Vortex Wakes of Stationary and Vibrating Cylinders
5. TYPE OF REPORT & PERIOD COVERED: Final report on one phase of a continuing problem
6. PERFORMING ORG. REPORT NUMBER

7. AUTHOR(s): (10) Steven E. Ramberg
8. CONTRACT OR GRANT NUMBER(s): (16) RR023-01

9. PERFORMING ORGANIZATION NAME AND ADDRESS: Naval Research Laboratory, Washington, Dc 20375
10. PROGRAM ELEMENT, PROJECT, TASK AREA & WORK UNIT NUMBERS: 61153N-23-RR023-01, 84F02-24; PO-4-0009(PDM-03), 84F02-36

11. CONTROLLING OFFICE NAME AND ADDRESS: Office of Naval Research, Wash. DC; Civil Engineering Laboratory, (NCBC), Port Hueneme, CA
12. REPORT DATE: (11) August 1978
13. NUMBER OF PAGES: 114

14. MONITORING AGENCY NAME & ADDRESS (if different from Controlling Office): (12) 119p.
15. SECURITY CLASS. (of this report): UNCLASSIFIED
15a. DECLASSIFICATION/DOWNGRADING SCHEDULE

16. DISTRIBUTION STATEMENT (of this Report): (17) RR023041

Approved for public release; distribution unlimited

(19) AD-E000 238

17. DISTRIBUTION STATEMENT (of the abstract entered in Block 20, if different from Report)

18. SUPPLEMENTARY NOTES

19. KEY WORDS (Continue on reverse side if necessary and identify by block number)

Vortex wakes
Flow-induced vibrations
Yawed cylinders
Cosine Laws
Fluid forces
Drag

This report investigates

20. ABSTRACT (Continue on reverse side if necessary and identify by block number)

The present investigation considers the influences of yaw angle and end condition upon the vortex wakes of finite-length, yawed circular cylinders. The standard for comparison is the Independence Principle which produces the so-called Cosine Laws for yawed body flows. These expressions have found widespread use even though their validity cannot be proved theoretically for separated, unsteady or turbulent flows. Many previous empirical checks of the Principle under these conditions have produced conflicting reports. → (cont'd)

DD FORM 1 JAN 73 1473 EDITION OF 1 NOV 65 IS OBSOLETE i
S/N 0102-014-6601

SECURITY CLASSIFICATION OF THIS PAGE (When Date Entered)

251 950

Measurements of the vortex shedding frequency, the shedding angle, the base pressure, the vortex formation length and the wake width were obtained for both stationary and vibrating yawed cylinders in the range of Reynolds numbers Re = 160 to 1100. The influence of end conditions was assessed for free-ended cylinders of varying end geometries and for cylinders fitted with adjustable endplates. The cylinder lengths varied from about 20 to nearly 100 diameters. Based upon the experimental results and upon some fundamental considerations of the vorticity discharged at separation it is concluded that the use of the Independence Principle is not valid for separated, yawed cylinder flows except in two special cases. The first case concerns the transverse vibration of the yawed cylinders when the vortex shedding processes are captured in a manner equivalent to the use of the Cosine Laws. The second instance is a result of substantial end effects upon the wakes of finite-length, stationary yawed cylinders. In this case, a particular configuration--endplates aligned with the flow--can produce results comparable to the Cosine Laws, but this configuration is shown to be inconsistent with the Independence Principle by vorticity considerations and by a simple model of the interaction of the end flow with the base region flow.

For the first time the "universal" Strouhal number concept for scaling the vortex wakes of bluff bodies at normal incidence is found to be valid for inclined cylinders. A discussion of this finding indicates that simple experiments, as done in the past, could neither ascertain the validity of the Independence Principle nor identify the exact flow appropriate to an infinitely long yawed stationary cylinder.

CONTENTS

CONTENTS (Continued)

THE INFLUENCE OF YAW ANGLE UPON THE VORTEX WAKES OF STATIONARY AND VIBRATING CYLINDERS

1.0 INTRODUCTION

The influence of yaw angle on the vortex wakes of stationary and vibrating circular cylinders has been investigated in a range of Reynolds numbers between 150 and 1100. The issue under investigation is the proper use of the so-called Independence Principle or Cosine Laws for scaling the vortex wake phenomena and ultimately for describing the vortex-induced vibrations of yawed bluff bodies. According to the Independence Principle, which is derived from the steady laminar boundary layer equations for an infinitely long yawed cylinder [51], velocity and pressure gradients exist only in a plane normal to the cylinder axis. Further, the flow development within this plane is equivalent to the flow about a cylinder which is perpendicular to a lower free stream velocity. The velocity is then reduced by the cosine of the yaw angle. In this way the three-dimensional problem is simplified to a well-studied two-dimensional problem governed by the normal component of the incident velocity. This convenient result cannot be obtained theoretically for flows that possess boundary layer separation, unsteadiness, turbulence or finite length effects. Since most flows of practical interest contain one or more of these effects, empirical relations are usually sought.

The search for empirical relations has centered on efforts to support the use of the normal component of velocity to characterize yawed body flows regardless of separation, unsteadiness, etc. The motivation for this approach is of course its simplicity, but the importance of the spanwise velocity component and possible three-dimensional aspects of the flow can be seriously underestimated. As a result there is no physical basis for assessing the accuracy of individual experiments or for explaining the differences that have arisen between reported results. To overcome this difficulty the present study was undertaken to examine, in some detail, the three-dimensional vortex wake flows behind several

Manuscript submitted June 30, 1978.

yawed cylinders. The Independence Principle is then examined in light of the new experimental data to find when and how it can justifiably be used. Also, an explanation is offered to account for many of the discrepancies between previously reported results. Finally, the results of the present study are applied to the problem of the vortex-excited vibrations to determine the manner in which existing models can be modified to include the influences of yaw angle.

1..1 Review of the Problem.

The flow about a circular cylinder that is perpendicular (normal) to a uniform, incident flow is a classical problem in fluid mechanics. The interest in this problem stems from the manifold and complex flow phenomena that can occur for such a simple but common structural shape. In this section some of the literature for the normal incidence case is reviewed and compared to the relatively scant literature on the flow about yawed cylinders. In the absence of yawed body results the normal incidence case is discussed in relation to the Independence Principle and some simple physical arguments. With this in mind the effects of turbulence, separation, vibrations and finite length are discussed individually and the relevant literature is cited. The yaw angle and all other angles are measured from the axis of a cylinder perpendicular to the freestream flow direction and may take on positive or negative values. A sketch with the appropriate nomenclature is shown in Fig. 1.

1.1.1 The Effects of Turbulence. Practical flow problems are most often turbulent and rarely amenable to theoretical analysis. The first parameter encountered is, of course, the Reynolds number which is a product of a characteristic dimension and a velocity divided by a kinematic viscosity. The selection of a characteristic velocity and dimension depend upon the flow process and convention. In its usual or free stream form for cylinders, the Reynolds number is based upon the free stream velocity U_o and a cylinder diameter

D. For yawed cylinders the normal component of velocity $U_n = U_o \cos \theta$ is often taken as the reference value. In either case the body cross-sectional shape must be specified separately as another parameter of the problem. Roshko [47] has proposed that all bluff bodies can be considered as one class by properly selecting a characteristic velocity and a dimension for the flow. He based his "universal" Reynolds and Strouhal numbers on certain wake parameters since all bluff body wakes exhibit similarity for many freestream Reynolds numbers. With this approach Roshko unified the results of measurements on diverse shapes (cylinder, wedge, flat plate) with or without wake interference (splitter plates). Bearman [1] expanded on the approach and included other shapes and other wake interference (mass injection) while Richter & Naudascher [44] demonstrated that blockage or freestream flow convergence can be taken into account. Most recently, Griffin [23] found that vibrating bluff bodies are also compatible with the concept. In the present study the term "Reynolds number" by itself will always refer to the freestream Reynolds number $Re = \frac{U_o D}{\nu}$ for a circular cylinder of diameter D. Unless otherwise clearly noted the term "cylinder" will mean circular cylinder.

Turbulent flow occurs in the wake of a cylinder at normal incidence for Reynolds numbers between 200 and 5×10^5. Thereafter, the transition to turbulence moves forward into the attached or unseparated boundary layers on the cylinder. The process can be described [5] as a transition to turbulence wherein the transition steadily moves from the far wake to the attached boundary layers with increasing Reynolds number. An infinitely long, yawed cylinder can be expected to exhibit somewhat similar behavior, but the occurrence of a spanwise velocity component prevents a simple analogy with the unyawed cylinder. This can be shown as follows. If the development of the normal and spanwise boundary layers are uncoupled, as the Independence Principle assumes[1], then a spanwise

[1] See Chiu & Lienhard [9], but beware of getting the cart before the horse [48].

turbulent boundary layer will be encountered long before turbulence becomes important in the crossflow. As a consequence the normal and spanwise flows are necessarily coupled and the direct analogy breaks down. At lower, subcritical Reynolds numbers ($Re < 10^4$), for finite cylinders and small yaw angles this coupling will be weakest and may partly account for the reports of the apparent dominance of the normal component of velocity [10, 29,32, 42]. The importance of this coupling at higher Reynolds numbers can be seen in the works of Glenny [20], Smith, Kao & Moon [53] and particularly in the works of Bursnall & Lofting [7]. In each of these studies the results are consistent with the idea of an early transition to turbulence in the boundary layers due to the yawing of the cylinder away from normal incidence. The critical Reynolds number occurs earlier than is predicted by the use of the Independence Principle and drag measurements are greater than those predicted for subcritical Reynolds numbers. These factors are discussed further in the section on flow separation.

Another important parameter in the turbulent flow around bluff bodies is the level of turbulence in the freestream. The simplest characterization of freestream turbulence is the ratio of the RMS level u'_{rms} to the freestream velocity U_o. An improvement on this characterization is to also determine the frequency spectrum of the turbulent fluctuations. It is usually assumed that broadband, low level freestream turbulence ($u_{rms}/U_o < 0.01$) has at most a second-order influence for non-transitional phenomena. This view is taken in the present study.

1.1.2 Two-Dimensional and Three-Dimensional Separation. Bluff bodies owe their designation to the occurrence of boundary layer separation and to the formation of a large recirculating flow region aft of the body. The fluid forces, (e.g. the drag) on a bluff body are greatly increased by separation because the fore and aft pressure distributions become unequal and a net pressure or form

drag is created. In fact, for many Reynolds numbers the form drag far exceeds the drag due directly to viscous shear at the surface. The pressure distribution on a bluff body is largely imposed through the boundary layers from the accelerating outer potential flow. With these insights and the assumption of a uniform base pressure distribution Kirchoff attempted to determine more realistic computations of form drag by using a potential flow model that incorporated a free-streamline. The free-streamline emanated from the body surface and divided the flow behind the body onto an outer potential flow and an unspecified inner wake flow as shown in Fig. 2. In this approach the base pressure was determined from Bernoulli's equation evaluated along the free-streamline. Kirchoff took the free streamline velocity U_F as a constant everywhere so that it was equal to the velocity U_o at infinity. As a result the base pressure P_b must equal the free stream pressure P_o and does not account for the base suction, $P_b < P_o$, that is known to occur. Riabouchinsky [43] later addressed this difficulty by "closing" the wake of a flat plate by introducing an image plate some distance downstream. The analytical advantages stem from symmetry but more importantly U_F and therefore P_b are free to assume realistic values. Moreover the base pressure becomes inversely related to a characteristic longitudinal cavity or wake dimension. Fig. 3 is a plot of Riabouchinsky's results in a range of values of the base pressure coefficient near the observed values for a flat plate.

More recently, Roshko [46] reconsidered the bluff body problem and proposed that

$$U_F = k\, U_o \,, \quad k \geq 1 \tag{1}$$

which can be substituted into Bernoulli's equation to obtain the base pressure

$$P_b = P_o + \rho/2\, (U_o^2 - U_F^2). \tag{2}$$

Written as a base pressure coefficient this becomes

$$C_{P_b} = \frac{P_b - P_o}{1/2\rho U^2_o} = 1 - \frac{U_F^2}{U_o} = 1 - k^2 \quad . \qquad (3)$$

It is assumed that $U_F = k\, U_o$ is a constant near the body and this must eventually be reconciled with the velocity at infinity. If this is done by introducing a step change in velocity at the location where the free streamline becomes parallel to the free stream flow, then the result is a notch in the otherwise circular mapping of the flow onto the hodograph plane. Hence the term "notched hodograph" theory. It is interesting to note that Roshko also computed an elliptical hodograph that permitted a gradual change in U_F, but the computed streamline positions and pressure distributions in the early wake failed to match observations as well as the notched hodograph method. In any case the solution depends on the parameter k which must be determined by some other consideration; Roshko ultimately related it to a characteristic wake width as will be discussed shortly. The theories of Riabouchinsky and Roshko not only provide a means to obtain better agreement with experiments but also introduce some characteristic(s) of the wake into the formulation. This places the intuitive notion of a coupling between the forces on the body and it's wake on a more rigorous basis. Although this discussion is based on two dimensional bluff body flows, the influence of yaw angle upon either free-streamline analysis can be assessed quite simply. The potential flow analysis will decompose according to the Independence Principle with no further assumption other than the absence of axial gradients. However, three-dimensional effects can still influence the outcome through changes in the wake parameters or differences in the separation process.

The traditional criterion for boundary layer separation is that the surface shear stress must vanish. For two-dimensional steady, laminar separation this condition is sufficient, but in the presence of unsteadiness, turbulence or a third velocity component other conditions may be necessary. For

example, it has been suggested that unsteady separation occurs when the shear stress and velocity vanish together [60]. In the case of three-dimensional steady flows two types of separation have been postulated [60]. The first, termed singular separation, is a result of both surface shear stress components simultaneously going to zero. The second type of three-dimensional separation, termed ordinary, occurs when one stress component is much larger than the other. In the latter situation the projections of the streamlines nearest the surface onto the surface will converge. From continuity this convergence in one plane will be balanced by divergence in perpendicular planes and the flow will begin to depart from the surface. The separating flow will, in general, possess vorticity vectors whose direction is not parallel to the separation line. Also, the shear stress on the inside of the shear layer need not be zero. This is quite different from the two-dimensional case and has not been taken into account during studies of the flow about yawed cylinders.

The separation process for a yawed cylinder is at once unsteady, three-dimensional and possibly turbulent, so that a quantitative description of the flow is not possible at the present time. Nevertheless, an important qualitative difference between the separation mechanisms for yawed and unyawed cylinders can be identified. Whereas the flow separation from an unyawed cylinder is of the two-dimensional singular variety, the separation from a yawed cylinder is of the three-dimensional ordinary type. Surry [55] has presented several photographs of surface flow patterns on yawed cylinders that clearly show flow convergence leading to ordinary separation. This important difference between yawed and unyawed separation is a direct result of the spanwise flow that occurs on the yawed cylinder. All else being equal, the presence of a spanwise shear stress would tend to promote separation somewhat before the crosswise shear stress vanished. In other words, one could expect slightly earlier separation on yawed cylinders as compared to unyawed cylinders and this would in

turn tend to increase the steady drag above the value predicted using the Independence Principle. In terms of the free-streamline theories this ought to correspond to a slightly larger base pressure parameter k. Examination of Roshkos curves [Ref. 46, Fig. 5] near k=1.4, a typical value for circular cylinders, reveals that a 1 degree change in the separation azimuth corresponds to $\Delta k \simeq 0.02$ or a change in drag of about 6 percent.

Among the first measurements of steady drag on yawed cylinders were those made by Relf & Powell [42] for $Re \simeq 10^4$. Based on wind tunnel force measurements on inclined ($\theta \leq 80°$) smooth and stranded wires, it was concluded that the normal or crosswise component of drag approximately varied as $\cos^2\theta$. This suggested the use of the normal component of velocity to characterize the drag as

$$C_{D_n} = \frac{\text{normal component of drag/unit length}}{1/2\ \rho\ (U_o \cos\theta)^2} \qquad (4)$$

$$= f\ (Re_n), \qquad Re_n = \frac{U_o \cos\theta\ D}{\nu},$$

which is, of course, also a result of the Independence Principle. The approximate nature of this conclusion is evident from Relf & Powell's experimental findings and is remarked upon in the text. A single series of tests by Relf & Powell on a smooth cylinder clearly shows a monotonic increase of C_{D_n} with yaw angle such that the drag was 10 to 20 percent higher at $\theta = 60°$ to $80°$. Similar trends have been reported by Bursnall & Lofting [7] and Smith, Kao & Moon [53] with regards to the pressure distribution on yawed cylinders. Bursnall & Lofting were particularly concerned with boundary layer transition for yawed cylinders where $\theta \leq 60°$ and they measured the base pressure for Reynolds numbers in the transition and subcritical ranges. They found that the critical Reynolds number

Re_c could not be determined solely by the normal component of velocity and that subcritical base pressure coefficients did not vary as $\cos^2\theta$. Smith, Kao & Moon employed circumferential pressure measurements to compute the pressure or form drag as a function of yaw angle in a range of subcritical Reynolds numbers. They found that the normal component of form drag was greater than that predicted using the Independence Principle; C_{D_n} increased by as much as 25 percent as θ increased from 0° to 60°. Each investigator has identified the spanwise velocity as the underlying cause of the observations. The concensus is that the spanwise flow promotes earlier turbulent transition in the wake for subcritical Reynolds numbers by "tripping" the boundary layer and thereby reducing the critical Reynolds number. In this writer's opinion the difference between the separation mechanisms for yawed and unyawed cylinders is equally important because this difference occurs for all Reynolds numbers and can vary with yaw angle. Further, these differences point to the influence of the spanwise velocity both in occurrence and in magnitude. In the following discussion we shall see a similarly important influence of the spanwise flow upon the wake development.

The separated shear layers behind a bluff body roll-up to form vortices that, for most Reynolds numbers, alternately detach from the base region of the cylinder and move away downstream. The alternate shedding process causes an oscillatory movement of the separation lines and ultimately produces a staggered discrete vortex pattern in the wake. As a result of the separation line movement, fluctuating lift and drag forces are generated at the shedding frequency f_s and twice the shedding frequency, respectively. Clearly the shedding frequency is an important parameter of the problem and was first systematically documented by Roshko [45] for a variety of unyawed cylinders. In the nondimensional form $St^1 = \frac{f_s D}{U_o}$ the shedding frequency depends primarily upon

---

[1] St is the Strouhal number.

the Reynolds number. The Independence Principle preserves this relationship between the Strouhal and Reynolds numbers for yawed cylinders if both quantities incorporate the normal components of velocity: $St_n = f_s D/U_n$ and $Re_n = U_n D/\nu$. As a practical matter St is essentially constant for Re between 10^3 and 5×10^5, so that one would expect the shedding frequency to vary as cos θ in this range. A number of investigators have tested this proposition and have reported it to be the case. An interesting exception to this trend is the rather precise experiments of Van Atta [58] who concluded that the shedding frequency versus Re_n did not follow the Independence Principle within his range of Reynolds numbers Re $\leq$ 300. Furthermore, his results are within the error bounds of many other workers who report bounds and claim to have verified the Cosine Law at large Reynolds numbers. The precision of Van Atta's experiment was in part possible because the wake velocity spectra are sharply peaked at low Reynolds numbers.

The alternating vortex pattern in the wake of a cylinder is usually termed a von Karman vortex street in recognition of von Karman's classical analysis for staggered arrays of potential vortices. Von Karman showed the only linearly stable arrangement for an inviscid vortex street was the familiar staggered pattern with a ratio of transverse to longitudinal vortex spacings equal to $h/\ell = 0.281$ [Ref. 34, pg. 155]. Although this finding and others which have followed are based on an infinitely long, two dimensional inviscid vortex street, it is possible to apply these or slightly modified results to real vortex wakes under certain conditions. After the shed vortices move away from the base region of the cylinder, vorticity is diffused away from the core of each vortex as the pattern is convected downstream. Eventually the vortex cores expand, begin to interact, and precipitate the breakdown of the regular vortex pattern. However, before this happens a stable arrangement exists for several cycles in the wake shortly after formation [22]. In the stable region turbulent or laminar diffusion effects are small except in the immediate neighborhood of the

vortex cores, and it is possible to apply an inviscid formulation. One such result is a relation between the vortex street convection velocity U_c, the individual vortex circulation K, and the transverse and longitudinal spacings h and ℓ:

$$U_c = f_s \cdot \ell = U \frac{K}{2\ell} \tanh \frac{\pi h}{\ell} . \qquad (5)$$

To the extent that the inviscid vortex street model is applicable in the two-dimensional case one can expect that it will be equally valid for the yawed cylinder because the linearity of the potential flow analysis will always permit a spanwise flow to be superimposed up on a cross flow solution. Once again this is equivalent to the use of the Independence Principle and axial gradients are not considered.

A real vortex street originates from a complex interaction between the separated shear layers in the base region of the cylinder. The complexity of this interaction can be indicated by a comparison between the vorticity discharged from the cylinder and the vorticity contained in the vortex street. The circulation per unit length of the separating shear layers is U_F and the average velocity is $1/2\ U_F$ so that the total rate of discharge of circulation is $1/2\ U_F^2$. The individual vortices in the street meanwhile possess a circulation K and are created at a rate f_s on one side of the street.

By defining

$$\epsilon \equiv \frac{\text{vorticity in street}}{\text{vorticity discharged}} = \frac{f_s K}{1/2\ U_F^2} \qquad (6)$$

one has a measure of the fraction of discharged vorticity that actually appears in the form of concentrated vortices. Various investigators [16, 23, 47] have reported values of this fraction in the range $\epsilon = 0.15$ to 0.85 which indicates

that much of the discharged vorticity is lost due to mixing in the formation region. Clearly, the vortex wake is very dependent on the complex formation processes. Meanwhile, Roshko and Riabouchinsky have shown that the base pressure or fluid forces are also sensitive to these processes. Roshko's "universal" Reynolds number concept was the first successful attempt to bridge the formation region and thereby join the free-streamline theory to the vortex wake.

Roshko's concept is based on the observation that two parallel shear layers require only two quantities to completely characterize them; the streamline velocity U_F and the distance between the layers d_F. Since the layers will eventually roll-up to form a periodic wake, the characteristic frequency of this wake must be proportional to the ratio U_F/d_F. This defines a "universal" Strouhal number S^* which is independent of the body that generated the shear layers;

$$S^* = \frac{f_s d_F}{U_F} . \tag{7}$$

Similarly, a universal Reynolds number can be defined as,

$$R^* = \frac{U_F d_F}{\nu} . \tag{8}$$

The above concept is not readily extended to include yawed cylinders because of the additional component of vorticity that is introduced by the spanwise flow. The simplest approach is to ignore changes in flow direction outside the shear layers and view the shear layers in a plane perpendicular to the resultant vorticity vector at separation. Based on the Independence Principle and Roshko's approach the components of vorticity at separation are

$$\Omega_{z'} = U_{F_N} = k\, U_n = kU_o \cos\theta \tag{9}$$

and

$$\Omega_{x'} = U_T = U_o \sin\theta \tag{10}$$

using the notation in Fig. 1. The angle γ between the resultant vorticity vector and the cylinder axis is then given by

$$\tan \gamma = \frac{\Omega_{x'}}{\Omega_{z'}} = \frac{\tan \theta}{k} . \tag{11}$$

If the mixing process in the formation region cancels equal percentages of $\Omega_{x'}$ and $\Omega_{z'}$ then the orientation of vortex filaments in the vortex street is also defined by γ. On the other hand Chiu's [8] computed velocity profiles, based on the Independence Principle, for a yawed cylinder show that the distributions of $\Omega_{x'}$ and $\Omega_{z'}$ are not equal and, in fact, the median of $\Omega_{z'}$ corresponds to about the 80th percentile of $\Omega_{x'}$. Thus a mixing process that cancels the inner portions of the shear layers will cancel more of $\Omega_{x'}$ than $\Omega_{z'}$. An extreme that is consistent with observation in the two-dimensional case might be that 50% of $\Omega_{z'}$ is cancelled along with 80% of $\Omega_{x'}$, so that

$$\tan \gamma = \frac{0.2\ \Omega_{x'}}{0.5\ \Omega_{z'}} = \frac{2 \tan \theta}{5k} . \tag{12}$$

This relation and the proceeding one are plotted in Fig. 4 in terms of shedding angle $\alpha = \theta - \gamma$ and $k \approx 1.4$. These estimates are generated from very simple arguments based in large part upon the Independence Principle. The result is a range of inclination angles for the vortex street filaments that is always less than the yaw angle. A number of flow visualization studies of yawed cylinder wakes [10, 30, 55] confirm this observation. However, inclined vortex lines are not unique to yawed cylinders and have been reported for unyawed cylinders by numerous investigators [18]. In the case of an unyawed cylinder, slantwise shedding is usually attributed to extraneous influences such as disturbances in the freestream, non-uniformity of the cylinder, or the influences of end conditions. Since these effects are also present in yawed cylinder experiments it is

difficult to identify and analyze the basic yawed cylinder flow patterns. For example, the self-induced vortex street velocity (Eq. 5) must be perpendicular to the vortex filaments, yet if the vortex filaments are inclined to the freestream direction then the vortex street will be convected at some angle to the freestream. From the results of Smith, Kao & Moon [53], the flow direction profiles at downstream distances of $\frac{x}{D} = 5$ and $\frac{x}{D} = 10$ differ very little and possess a residual angle of up to 10° from the freestream direction. This residual angle is indicative of slantwise shedding but bears no apparent relation to the yaw angle. Thus it is not possible to decide whether this is a result of yaw angle, extraneous influences or both.

1.1.3 The Effects of Finite Length Upon the Wake Flow. In addition to the cross-sectional shape and the yaw angle one other geometric variable remains -- the cylinder length L or, non-dimensionally, the cylinder's aspect ratio L/D. In the limit $L/D = \infty$, the flow over both yawed and unyawed cylinders is nominally two-dimensional. A classic experimental difficulty is to produce the desired (nominally) two-dimensional flow at finite values of L/D when the presence of end effects necessarily introduces a three-dimensional flow. For the case of an unyawed cylinder two general remedies have been employed. In the first, a large aspect ratio is selected and the end effects are assumed to be confined to the extremities of the cylinder. Measurements on the center section are usually checked for spanwise uniformity and an effective cylinder length is determined. This approach can be misleading, as Stansby [54] and Etzold & Fiedler [15] have shown. Stansby measured the base pressure of finite aspect ratio cylinders (L/D = 10 and 20) and showed that although the base pressure C_{pb} was essentially uniform over the center span, its value depended on the end conditions. Etzold & Fiedler examined the flow about an unyawed, cantilevered cylinder for $Re = 3 \times 10^4$ and $L/D \leq 10$. A spanwise velocity component existed over the entire span for all the aspect ratios tested. At

the largest ratios of L/D a uniform distribution of drag was approached near the bottom of the cantilever, but the flow was nowhere two-dimensional. The second remedy for undesirable end effects involves the use of thin end plates aligned with the freestream to control the end flow. Presumably, the end plates produce only three-dimensional disturbances of a size comparable to the boundary layer on the plate while spanwise pressure gradients and velocity components are largely prevented. This remedy is widely used and criteria have even been suggested for selection of the endplate size and geometry [19, 21, 54].

In the case of a yawed cylinder, the experimenter must recognize that a very specific spanwise velocity component should exist but no pressure gradients are permissible. As discussed earlier, both the separation process and the wake development are likely to be sensitive to whatever spanwise velocity and pressure gradients are present. This rules out flat endplates aligned with the freestream for small aspect-ratio yawed cylinders as a means to simulate infinite or very large aspect ratios. Thus the prime experimental technique in the zero yaw case cannot be applied in a straightforward manner to the yawed case. It remains to be seen whether curved endplates or plates set at an angle to the freestream can produce the desired effect; the difficulty is then to determine which effect is the desired one. During low Reynolds number experiments on a stationary unyawed cylinder, Gerrard [19] mounted the cylinder between airfoils that were slightly inclined to reduce the gap between them. Evidently the purpose of this arrangement was to insure a uniform flow over the center span of the cylinder, but this may have promoted or at least influenced the slantwise shedding that he observed. Gerrard did comment that the vortex shedding frequency at nearly seven diameters from the airfoil was modified in a manner consistent with the altered direction of the freestream velocity due to the inclined airfoil. Stated another way, an inclined endplate on an unyawed cylinder caused a local flow comparable to inclining the

cylinder. The observations of Stansby, Etzold & Fiedler and Gerrard taken together with the present discussion point to the importance of end effects and imply that these effects can act over the entire span of a finite cylinder even for aspect ratios large by usual standards (L/D>10).

Several investigators have studied the wakes of stationary finite-length cylinders at very large yaw angles near 90°. The problem addressed in these studies can be described as slender body aerodynamics for small inclination angles between the body axis and the freestream direction. The application is to missile flight so that compressibility effects are included and the Reynolds numbers are quite large. In addition, the influence of nose cone or forebody geometry on the flow is of special interest. In papers by Thompson & Morrison [56] and Lamont & Hunt [37], subsonic flows are observed where the compressibility effects appear to be of secondary importance to the vortex dynamics. The major feature of the wakes of these bodies is a fixed pattern of downstream trailing vortices. A schematic of the flow pattern, adapted from Thomson & Morrison, is shown in Fig. 5. On the basis of this wake configuration two methods of analysis have been utilized. The first is an impulse flow analogy [50] where the spatial changes in the wake are likened to the temporal wake changes behind an impulsively started cylinder, while the second is a von Karman vortex street analogy where the convection velocity is exactly balanced by a component of the freestream velocity. The aim of both analyses is to describe the steady in-plane and out-of-plane forces on the cylinder, where the in-plane forces are usually resolved into components normal and parallel to the cylinder axis. The spanwise distributions of these components depend upon the nose geometry as expected. Of importance to the present study is the observation that the in-plane normal force coefficient along the span rapidly approaches a uniform value that depends little on the nose geometry and is comparable to the usual drag coefficient for unyawed cylinders. The trailing

vortex pattern and therefore this result have been recorded for yaw angles as little as 15°. The point to be made here is that two distincly different flow patterns behind finite cylinders have been observed for overlapping ranges of yaw angles. Furthermore, in-plane force measurements (drag) cannot, by themselves, differentiate between the two flow regimes; only detailed wake measurements and/or flow visualization can identify the occurrence and form of the finite length effects.

1.1.4 Vortex-excited and Forced Vibrations of Cylinders. When a rigid cylinder vibrates in a uniform flow, a number of interesting fluid dynamic phenomena occur that depend on the frequency and amplitude of the vibration. If the cylinder is a lightly damped oscillator and possesses a natural frequency near the vortex shedding frequency (or some multiple or submultiple of it), then these vibrations can be self-excited and the responses of the fluid and the cylinder are coupled [4]. Vortex-excited vibrations have been a serious problem for designers of stacks, masts, towed and moored undersea cables, heat exchangers and offshore structures. The coupled structural and fluid motions are difficult to study, so one fruitful approach has been to isolate the fluid response by externally vibrating the cylinder. In this way the frequency and amplitude become independently controlled variables over a wide range that includes, but is not restricted to, self-excited conditions. It is worth noting that this approach has provided data which may be of use during future studies of vortex-excited vibrations in a shear flow where, in general, the vibrating body will not experience self-excitation forces over the entire span. The forced vibration approach is utilized in the present study.

The literature relating to vortex-excited vibrations has been largely concerned with unyawed cylinders that vibrate transversely to the incident flow direction. In-line vibrations have also been observed [49,61] and studied

[26,29,33] but they will not be considered here. Therefore the additional non-dimensional variables of interest to this investigation are the amplitude of transverse vibration scaled in body diameters, a/D, and the ratio of vibration frequency to the natural vortex shedding frequency, f/f_s. Another non-dimensional quantity, termed the reduced velocity, is often used in place of the frequency ratio when discussing self-excited vibrations at a natural structural frequency. The reduced velocity, $V_r = U_o/f_n D$ can be related to the frequency ratio as follows because $f = f_n$ by definition

$$V_r = {U_o}/{f_n D} = \frac{f_s}{f_n} \frac{U_o}{f_s D} = \frac{f_s}{f_n} St^{-1} \qquad (13)$$

It is well-known that a vibrating, unyawed cylinder will "capture" the vortex shedding over a region in the frequency-amplitude plane as shown in Fig. 6, taken from Koopmann [35]. This means that the natural vortex shedding process is suppressed in favor of a shedding frequency that is equal to the body vibration frequency. As a result of this locking-on or synchronization the wake structure becomes more regular and is essentially two-dimensional. The spanwise cross-correlations of the velocity and the pressure fluctuations all improve greatly [17,35,39,40] as the vortex filaments align with the cylinder axis. The vortex wake characteristics vary in relation to the amplitude and frequency [24,28]. Increasing the amplitude of vibration causes the transverse vortex spacing, h, in the fully-developed wake to decrease while the longitudinal vortex spacing, ℓ, varies inversely with the frequency ratio. The vortex circulation [12,24] also changes markedly and is a function of a "wake response parameter" [25] defined as $St_w = {f}/{f_s}\ (1 + {a}/{D})\ St$. The larger the value of this parameter the greater the vortex strength.

Griffin [22] has shown that a single characteristic length can scale much of the downstream wake development over a wide range of amplitudes, frequencies

Reynolds numbers. This characteristic dimension is the vortex formation region length ℓ_F, which is defined as the distance to the initial position of a fully formed vortex. The vortex formation length is also a function of the wake response parameter.

Comparable forced body experiments do not exist for yawed cylinders, though several investigations of the self-excited case have been made. Dale & Holler [10] have published flow visualization photographs of stationary and self-excited yawed cables towed in water for Reynolds numbers between 30 and 500, and with aspect ratios greater than 125. Since the cables were flexible and curved, the amplitude of vibration and the yaw angle varied along the span. Two important features have emerged from these experiments. First, large transverse vibrations did occur and, second, the vortex filaments that were shed at an angle to the curved stationary cable became aligned with the curved cable when it was vibrating. The three-dimensional vortex street so generated appears to be convected in the freestream direction and the individual vortex filaments persist for ten or more wavelengths in the wake. However, the wake behavior observed in these experiments cannot be generalized to other yawed cylinders because of the particular symmetry of the curved cylinders. Another study of a vibrating, yawed cylinder was undertaken by Koopmann [36] who measured the response of spring-mounted, rigid cylinders in a wind tunnel and reported that regular vibrations did not occur for yaw angles greater than 15°. In view of the aspect ratio (L/D = 4) and the use of end plates aligned with the freestream it is not possible to generalize these results to other situations.

The most recent study of the coupled problem provides more promising results. King [32] recorded the response of flexible, cantilevered cylinders in a water flume for Reynolds numbers in the range $Re = 3 \times 10^3$ to 2×10^4 and yaw angles between ± 45 degrees. The aspect ratios are not stated, but they seem to be no less than 20 and no greater than 40. King observed for these conditions

that the vortex-excited response could be scaled by cos θ and that the stationary cylinder drag scaled by $\cos^2 \theta$. He concluded that the Independence Principle is valid for both stationary and vibrating yawed cylinders. However, complete agreement was not achieved until a subsidiary set of cylinders was tested under conditions that changed the bottom end conditions from those of his main test apparatus. The presence of a bottom crossbeam during the main tests reduced the response amplitude by as much as 50 percent from that expected using the Independence Principle and later measured during the subsidiary tests. As King observed, the differences were not a simple matter of a reduction in the effective length of the cylinder. The indication seems to be that the cross beam modified all or most of the vortex shedding along the span regardless of whether the beam was on the upstream or downstream end. In view of these findings and in the absence of detailed flow measurements, it is difficult to assess the contribution of end effects in either the main or subsidiary tests. Hence, there is some uncertainty regarding the extent to which King's results can be generalized to other situations.

2.0. EXPERIMENTAL SYSTEMS

2.1 Wind Tunnel, Test Section, and Test Cylinders. The experiments were performed in an open jet wind tunnel with a 6-5/16 inch (160 mm) square exit. Immediately preceding the exit was a 6 inch (150 mm) long clear acrylic test section that was employed to minimize changes in the freestream flow over the length of a yawed cylinder. The sides of the test section could be removed as needed. Upstream from the test section the air flow was conditioned by a honeycomb flow straightener, several fine mesh screens, and a 20:1 area-ratio contraction section. A larger plywood box with access windows surrounded the test section and the free jet on four sides to eliminate interference from room drafts. A photograph of the wind tunnel and supporting equipment is shown in Fig. 7. As a result of these arrangements the flow inside and just after the test section was uniform to within 2 percent of the mean value for all but the thin boundary layers of the flow. A residual or freestream turbulence level of less than 1.5 percent was measured in the test section; within the frequency band 20-1000 Hz a level of less than 0.5 percent was obtained.

The cylinders were mounted at the end of the test section such that a zero yaw angle corresponded to a cylinder normal to the free jet. Various yaw angles were obtained by tipping one end of each cylinder into the acrylic test section, $+\theta$, or occasionally away from the test section, $-\theta$. This sign convention is made clearer by noting that the fixed end of each cylinder was imbedded in an extension of the test section floor that could be rotated to obtain the desired yaw angle up to a maximum of 60°. The cylinders themselves were either solid steel drill rods or precision brass tubes. The brass tubes were used in conjunction with endplates that could be soldered onto the tubes at various positions and orientations. A special clamping arrangement was manufactured in order to assemble the cylinder and endplate with some precision ($\pm$ 0.5°). The brass endplates were individually machined from 1/16 inch (1.6 mm) thick, 1-1/4

inch (32 mm) diameter brass disks. Each disk was tapered on the upstream and downstream edges. The streamwise dimension of the endplates was always greater than 5 cylinder diameters and was usually greater than 8 cylinder diameters. No attempt was made to polish the cylinder or endplate surfaces beyond their manufactured smoothness since it has been shown that slight to moderate surface roughness is not a significant variable under the present conditions [59]. A photograph of two cylinder-endplate combinations is shown in Fig. 8.

2.2 Forced Vibration Equipment. The forced vibration experiments were performed by oscillating a cylinder that was cantilevered from a trasversing beam located at the top end of the acrylic test section. The beam was flush with the roof of the test section and had holes drilled to produce six yaw angles of θ = 0, 10°, 20°, 30°, 40°, and 50°. The beam was driven side-to-side by an electromagnetic shaker connected to one end of the beam and the motion frequency and amplitude were derived from a signal generator and a power amplifier. The shaker-beam system had a limited oscillation amplitude in the frequency range of interest (20 - 40 Hz), so the cylinders were occasionally tuned to respond in a natural fundamental mode in order to obtain larger amplitudes. As a result, the amplitude of vibration sometimes varied along the cylinder span. The variation in amplitude along the span was not a handicap since it has been shown that locked-in vortex shedding largely depends on local amplitude [40].

The amplitude of motion at any point along the cylinder was measured by an optical tracking device located about 3 feet (1 meter) downstream from the test section. This instrument was capable of following the motion of one side of the cylinder if the background of the viewing area was brightly lit. The proper lighting was obtained by aiming 650-watt incandescent lamps through the wind tunnel contraction section. The electromagnetic shaker was mounted on vibration isolated supports to eliminate any transmissions to the wind tunnel and sensor systems.

2.3 Flow Visualization Equipment. The essential feature of the flow visualization system is a thin sheet of aerosol that spans the central vertical plane of the test section. The forced vibration apparatus described above was used to place the cylinder in the plane of the aerosol so that the spanwise flow development could be observed and photographed.

The aerosol was generated by bubbling compressed air through a liquid -- di(2-ethylhexyl)-phthalate, or DOP -- to obtain a suspension of small liquid droplets. Liquid DOP was used to duplicate earlier systems [24], but in principle other inert, nontoxic, noncorrosive, nonvolatile and nonhygroscopic liquids would have been suitable. After generation the aerosol was passed through a small jet that impacted on a flat plate. In this way the largest liquid droplets were stripped from the aerosol and the mean particle size was reduced to less than 1 μm [13]. A photograph of the aerosol generating arrangement is shown in Fig. 9.

The aerosol was injected into the freestream flow by means of a slender airfoil located in the contraction section of the wind tunnel. The airfoil vertically spanned the center of the converging tunnel and the aerosol emanated from the trailing edge along both sides of a wake splitter plate. Within the airfoil the aerosol entered through both ends into a cavity that was separated from the trailing edge slots by wads of fine mesh wind tunnel screen. The combination of a cavity, screens and a splitter plate was found to produce a very smooth and uniform aerosol sheet. The cavity and wadding provide uniformity of flow over the span while the splitter plate inhibits unsteadiness in the airfoil wake. It is worth noting that the airfoil was assembled in a few hours from material available at most any hobby shop and as seen in Figure 9 the generator system is equally simple. A schematic of the entire system is presented in Figure 10 and a photograph of the airfoil injector positioned in the wind tunnel contraction section is shown in Fig. 11.

The aerosol was illuminated by two strobe lights located on the opposite side of the sheet from the viewing position. This arrangement took advantage of the good forward scattering characteristics of the aerosol [27]. The strobes were driven by the same signal generator that excited the electromagnetic shakers so that locked-in vortex shedding was easily identified visually as a "frozen" wake pattern. Flow visualization photographs were obtained by using a 35mm camera with an f2.8, 35mm lens mounted to one side of the test section. In a fully darkened room the strobe lights were flashed once while the shutter was held open. The lighting levels thus produced were sufficient to permit normal processing of commonly available black and white film (ASA 400).

2.4 Anemometry and Signal Processing Systems. Two channels of constant-temperature, hot-wire anemometers (DISA types 55D05 and 55K) were employed in the experiments. The hot-wire probes were single element sensors (DISA type 55P01) with 5 μm diameter platinum plated tungsten wires. The probes were mounted on two traversing mechanisms that both permitted movement in each of three orthogonal directions. Both mechanisms were equipped with scales and verniers so that all displacements were measurable to $\pm$ 0.05 mm. One mechanism was motorized and capable of moving along two orthogonal axes; this was accomplished by means of a fixed-speed motor drive and a variable-rate stepping motor drive (DISA type 55H01 traversing mechanism with DISA type 52B01 sweep-drive unit). The motorized drives were used to plot or to record velocity profiles.

The anemometer signals were linearized by means of analog devices expressly made for this purpose (DISA type 55D10 linearizers). The calibration and linearization of these measuring systems were undertaken in several ranges that spanned the experimental tunnel speed requirements of 0.2 to 3.0 m/sec. The calibrations were accomplished by placing one of several unyawed reference cylinders into the wind tunnel and computing the flow speed from Roshko's empirical relations [39]

and the observed vortex shedding frequency. The calibration cylinder for a particular set of experiments was always of a different diameter than the test cylinders for that set.

The shedding frequencies were determined from spectra of the anemometer signal when the probes were positioned in or near the wake. The spectra were obtained from a 200-line Honeywell-Saicor Realtime Spectrum Analyzer and Digital Averager. The resulting spectrum in each instance was an average of eight or more sample spectra. On occasion the linearized and calibrated anemometer signals were recorded on a four-channel FM instrumentation tape recorder (Hewlett-Packard type 3946A) for later analysis. Mean flow velocities were obtained directly with an integrating digital voltmeter (DISA type 55D31) and fluctuating velocities were measured directly using a true RMS voltmeter (DISA type 55D35).

2.5 Pressure Measurements. Pressure measurements were taken with a null balance micromanometer whose vernier adjustments had a resolution of 0.01 mm of water column or about 1.4×10^{-4} psi. Base pressures were obtained from a single tap at the rear of the cylinder about midway along the span. The free-stream static pressure P_o and the stagnation pressure P_s were obtained with the aid of a pitot tube. Base pressure coefficients were obtained from the ratio

$$C_{P_b} = \frac{P_b - P_o}{P_s - P_o} = \frac{P_b - P_o}{1/2\rho U_o^2} \quad . \tag{14}$$

3.0 RESULTS FOR STATIONARY YAWED CYLINDERS

3.1 Shedding Frequency and Shedding Angle. The most important characteristic of vortex shedding is the shedding frequency f_s or, in nondimensional form, the Strouhal number $St = {}^{f_s D}/_{U_o}$. By incorporating the Independence Principle into Roshko's empirical relations [45] for the Strouhal number - Reynolds number dependence, the following results are obtained:

$$St_n = 0.212 \left(1 - {}^{A}/_{Re_n}\right) \tag{15}$$

where

$$Re_n = {}^{U_n D}/_{\nu} = Re \cos \theta$$

and

$$A = \begin{cases} 21.2, Re_n \leq 150, \\ 12.7, 300 < Re_n < 1500 \end{cases} \tag{16}$$

If the measured Strouhal number St is divided by the computed value of St_n, then the ratio ${}^{St}/_{St_n}$ should vary as cos θ regardless of the Reynolds number. Of course, the ratio ${}^{St}/_{St_n}$ will vary as cos θ only so long as the Independence Principle is valid. This approach was first used by Van Atta [58] because it suppresses Reynolds number variations and because it gives superior resolution for the variation of shedding frequency with yaw angle, particularly at large values of the angle. For these reasons the results for stationary yawed cylinders are normalized by the ratio ${}^{St}/_{St_n}$ in the present study.

The shedding angle α is poorly defined unless the shed vortex filaments are straight, or nearly so, and unless their orientation is steady. With two exceptions both conditions prevailed in the present study. The first exception was observed for cylinders with little or no yaw angle. The vortex filaments in the wakes of these cylinders were often wavy and exhibited some unsteadiness. The second exception was the result of a transition in the vortex wake pattern and will be discussed later in this section.

The shedding angle was determined from flow visualization photographs taken during each shedding frequency measurement. The cylinder and its wake were contained in the plane of the aerosol so that the vortex filaments appeared as lines of concentrated DOP. When the vortex filaments were straight it was a simple matter to measure their inclination angle with respect to the vertical ($\theta = 0$). If the filaments were not straight a median value was estimated, and error bounds included with the data point to encompass the entire range of angles observed. The shedding angle is introduced at this point because it was found to be closely related to the shedding frequency and because it is a simple but effective characterization of the various wake structures that were observed.

3.1.1 Free-Ended Cylinders. Preliminary tests using endplates produced conflicting results so it was decided to begin with free-ended cylinders and address the endplate situation separately. Thus, the initial experiments were designed to examine the wake structure as it was influenced by yaw angle aspect ratio, and free-end geometry for various Reynolds numbers. Fig. 12 contains all of the shedding frequency measurements obtained with free-ended cylinders. The aspect ratio L/D extends from about 20 to nearly 100 and the Reynolds number Re from about 160 to 1100. For yaw angles greater than 10°the spread in results is large despite a frequency resolution of $\pm$4% or better depending on the shape of the spectrum and on the analyzer range setting. It is interesting to note that a simple curvefit would probably pass close to the cos θ curve. Such an approach is inappropriate as shown by Fig. 13 which is composed of the fluctuating velocity spectra obtained for Re = 1100 and L/D = 90.

The vertical scale in each trace is arbitrary and corresponds to the signal amplitude versus frequency, i.e. the Fourier spectrum. The frequency content and magnitude vary greatly within the wake so these measurements were taken just outside the wake within a diameter of the rear of the cylinders where the frequency content is due to the shedding frequency for vortices of like sign. Thus, the

observed spectral peak is defined as f_s. The solid triangle on the frequency axis of each spectrum indicates the expected shedding frequency based on the Independence Principle. The observed value of f_s becomes progressively larger than expected for increasing yaw angle. At the same time the bandwidth, taken between the 70 percent amplitude points, increases more than tenfold and the amplitude of f_s compared to the background spectrum levels decreases by a factor of about three. These numbers are qualitative but are representative of the influences of yaw angle upon wake spectra [53].

The differences between the observed and expected shedding frequencies were not confined to a Reynolds number of 1100 as can be seen in Figure 14. This figure is a replotting of the largest aspect ratio data from Figure 12. Except for the Re = 160 data the spread is greatly reduced and the shedding frequency seems to follow cos θ up to 35° whereupon it exceeds cos θ but is less than Van Atta's empirical relation. One is tempted to conclude that the cosine laws are valid for angles less than 35° but this is not appropriate as will be shown later. In any case it is quite apparent that the Independence Principle cannot account for the behavior at Re = 160 and this is the first indication of the form of finite-length effects.

For Re = 160 and yaw angles between 10° and 30° there are two points for each angle. Each pair of data points corresponds to measurements in two shedding modes behind the same cylinder. The modes are typified by the flow visualization photograph of Fig. 15. In the photo the test cylinder is leaning to the left in a flow from left to right. Two hot-wire probes, a reference and a measurement probe,, are also in the photograph together with a portion of one strobe light. The lines of aerosol in the wake indicate the instantaneous positions of the vortex filaments. The two vortex shedding modes are easily distinguished by a large difference in the shedding angle. The "upper" or "tip" mode in the photograph was first observed at a yaw angle between 10° and 15°.

For increasing yaw angles the "tip" mode progressed further "down" the cylinder until $\theta = 30°$, where it appeared to cover the entire span (about 90 diameters). It seems reasonable to interpret the "upper" and "lower" vortex shedding modes as being influenced and largely uninfluenced by the free end, respectively, however this interpretation will be subject to some refinement shortly. Only a single mode was observed for $Re \geq 460$, which is consistent with the frequency measurements and is indicative of a strong Reynolds number influence on the flow.

Further insight can be gained from a comparison between the changes in the shedding frequency St/St_n and the corresponding changes in the shedding angle α. Figs. 16 and 17 present these comparisons for Re = 160 and Re = 460, respectively. After some examination of Fig. 16 it appears that frequencies less than cos θ correspond to shedding angles greater than the yaw angle while frequencies greater than or equal to cos θ are associated with shedding angles less than or equal to the yaw angle. If one accepts the interpretation that the "tip" mode is a consequence of end effects then shedding angles that are greater than the yaw angle become connected with end effects. This reasoning is consistent with the earlier considerations (Section 1.1.2) of the vorticity discharged into the wake. There it was shown that the shedding angle ought to be less than the yaw angle in the absence of end effects. If one is to remain true to this interpretation then one must also conclude that lesser end effects occur for $\theta < 35°$ because the shedding angle is often greater than the yaw angle in this range as well. It is not possible to draw any firm conclusions other than to say there is an apparent interrelationship between the shedding angle and the shedding frequency and to say there is an association of end effects with shedding angles greater than the yaw angle.

The preceding discussion concerns free-ended cylinders of fixed length with a flat free-end. The next series of experiments were performed in order to study the effects of varying length, i.e. aspect ratio L/D over a wider

range and to examine the influence of different free-end geometries. These end geometries included a hemisphere and a 45° cone, which were selected for their simplicity and symmetry. The Strouhal number ratios St/St_n for these cylinders consist of the data in Fig. 12 minus the data in Fig. 14. Much of the apparent scatter of the data in Fig. 12 can now be attributed to the progression of end effects "down" the span of the cylinder, but the entire story is more complex. At low Reynolds numbers and large yaw angles the wakes of the cylinders were not always a vortex wake of the von Karman type. Instead, a steady trailing vortex pattern often emerged as shown in the typical flow visualization photograph of Fig. 18. This flow pattern is of the type studied by some earlier investigators of the missile flight problem [37,56] and discussed previously (see Fig. 2). Of interest here is the low Reynolds number occurrence of the phenomenon and the fact that it was observed for yaw angles as small as 40°. From the entire set of flow visualization photographs it is possible to outline three regimes of wake flow which include regular alternate vortex shedding, a steady trailing vortex pattern, and a transition between the two regimes.

The outlines of the regimes as functions of Reynolds number, yaw angle, and aspect ratio are presented in Figs. 19a through 19c for the hemispherical, coned and flat ends, respectively. Each vertical bar on the graphs represents one series of photographs of a cylinder wake at one Reynolds number and various yaw angles. For example, consider the leftmost bar in Fig. 19a which corresponds to a cylinder with a hemispherical end at a Reynolds number about 200. For yaw angles from -10° to 25° the wake is of the typical von Karman vortex pattern. For angles between 25° and 40° there is a transition to the steady trailing pattern which becomes clearly established for $\theta > 45°$. At other Reynolds numbers two or three adjacent bars are used to represent two or three series at the same Reynolds number and end condition but with different

diameters to produce different aspect ratios. The three bars at Re ≈ 460 correspond to a 2:1 range in aspect ratio and demonstrate that the transition between vortex patterns is not dependent on the aspect ratio and is indeed an end effect. In the case of different aspect ratios it was the onset of each regime that is indicated in the graphs because the "longer" cylinder (in diameters) will have to be rotated to a larger yaw angle before the steady trailing pattern encompasses the entire span. In other words the transition starts at the free end, progresses along the cylinder, and is followed by the formation of a steady trailing pattern over the upper portion of the cylinder. The photographic series corresponding to the Re ≈ 160 bar in Fig. 19c serves to illustrate the changes that take place.

The photographs are shown in Fig. 20 and clearly indicate the two modes of the vortex shedding regime ($\theta < 35°$) followed by a transition regime ($35° < \theta < 50°$) that ultimately leads to a steady trailing pattern ($\theta > 50°$). An interesting insight into the transition process can also be gained from a study of the photographs. Typically, the shedding angle just prior to transition is greater than the yaw angle ("tip" mode). At a small yaw angle the vortex filaments clearly begin to loop over at the "top" of the wake after the fashion postulated by Gerrard [16] some years ago. If the yaw angle is increased further the loops eventually detach from the shedding vortex filaments and form a wavy line that streams out behind the cylinder. The looping process then occurs "lower" in the wake along the cylinder. At still larger yaw angles the looping process continues to move down, more wavy lines are formed, and the first wavy lines straighten to form a steady trailing pattern. The loop formation alternates such that the trailing vortices emanate from alternating sides of the cylinder with opposing circulation (see Fig. 2). Returning to the outlines of the various regimes in Figs. 19a-c there is an indication of a Reynolds number influence that diminishes with increasing Reynolds number. The most striking

feature of the three graphs is the basic similarity between the hemispherical and coned-end results as contrasted with the flat-end results. As will be discussed in the next section this is probably a result of the difference in spanwise flow engendered by the flat end as compared to the hemispherical and coned ends.

The final series of experiments with a free-ended cylinder was undertaken to consider another question relating to the influence of finite length. Since all the measurements were obtained by inclining a fixed length cylinder, some measurements were repeated for a cylinder length that varied as $(\cos\theta)^{-1}$. After some initial difficulty it was determined that small changes in the distance of the free-end from the wind tunnel wall could produce very different results as shown, for example, in Fig. 21. When the cylinder was in contact with the wall the Strouhal number ratio was close to or below $\cos\theta$, while a cylinder that was displaced several diameters from the wall appeared to follow Van Atta's empirical curve until $\theta = 55°$. Also, the scatter of the results was greater than had previously been the case. During these experiments the aspect ratio was large (L/D>90) by usual standards, and yet the influence of the tunnel wall seemed to extend over the entire span.

3.1.2 Cylinders With End Plates. The results of the free ended cylinder experiments indicated the form of end effects and that these effects could be significant for the entire span even for large aspect ratios, so a series of experiments was undertaken using cylinders fitted with end plates. It was quickly determined that the conditions at the upstream end of the cylinder dominated the flow, therefore subsequent tests concentrated on that end of the cylinder and left the downstream end effectively imbedded in a wall. In the belief that the spanwise flow along the cylinder was responsible for the various phenomena just discussed, the end plate angle was varied in an attempt to influence the spanwise flow. The end plate angle β was measured from the vertical (θ=0) such that β =

90° corresponds to an end plate aligned with the freestream and $\beta = 90° + \theta$ corresponds to an end plate normal to the cylinder axis. The end plate angles were estimated from the photographs, but the angles appear only as a parameter and the form of the results do not depend on the accuracy of this measurement.

The shedding frequency and shedding angle measurements for two Reynolds numbers Re = 160 and 460, and two yaw angles $\theta = 30°$ and 50°, are shown in Figs. 22 and 23. Several features are common to all of the figures. First, there is an essentially inverse relationship between the shedding angle and the shedding frequency. Second, the sensitivity to end plate angle is greatest when the end plates are approximately aligned with the free stream ($\beta \simeq 90°$-110°). Third, it is possible to obtain results identical to the use of the Independence Principle or identical to van Atta's empirical shedding frequency relation within a very small range of end plate angles. In fact it is also possible to have shedding frequencies comparable to an unyawed cylinder. Clearly, the use of flat end plates on yawed cylinders must be undertaken with some care and even in the best of circumstances could produce results that are difficult to interpret. This sensitivity of the shedding frequency to the end condition is no doubt responsible for the wall influence in the constant aspect-ratio tests of the previous section and probably accounts for much of the unexpected scatter in those measurements. A comparison between Figs. 23 and 24 indicates that the sensitivity to end plate orientation lessens with increasing Reynolds number but this trend could not be pursued without exceeding the capacity of the flow visualization aerosol generator. A series of flow visualization photographs that approximately matches the conditions of Figs. 23a and 23b is shown in Fig. 24. The individual photographs are presented in two columns in order of increasing β except for the first photograph which shows the wake of the free-ended cylinder under the same conditions.

In order to evaluate these results in the context of an infinitely long cylinder it becomes necessary to understand the mechanism by which the flow is altered by varying the end condition. This is discussed in some detail in Appendix A and the salient points are presented here. An inclined endplate will deflect the freestream flow somewhat and this can be used to define a "pseudo" flow direction and magnitude. However, this is not sufficient to account for the large changes that occur or for the strong influence of Reynolds number. Thus one is ultimately led to consider the flow induced in the base region by the difference between the base pressure P_b and the pressure on the endplate P_p. For endplate angles β less than or equal to 90° the pressure on the plate will be equal to or greater than the static pressure P_o which in turn is greater than P_b. Thus a flow 'down' the cylinder will be promoted. For endplate angles greater than 90° P_p is less than P_o and for certain combinations (see Appendix A) of the yaw angle θ and the endplate angle β the plate pressure will also be less than P_b. In the latter case the flow in the base region will tend to change direction and flow 'up' the cylinder. This will affect the mixing and vortex formation processes in a manner analagous to the wake inference experiments in the two-dimensional bluff body flows. Also, it might be expected that the vortex street would have to adjust its flow directions via changes in the shedding angle α to match the base region flows. Similar reasoning applies to the free-ended cylinders where the hemispherical and cone ended cylinders tend to promote a different spanwise base flow than the flatended cylinder.

These considerations along with the earlier vorticity discharge considerations can be combined with the observed wake behavior to draw some definite conclusions. First, a number of flow patterns can be realized for a given cylinder, yaw angle and Reynolds number; the particular flow in any case is dictated by the end condition(s). Second, an interrelationship between shedding angle and shedding frequency exists such that $St/St_n < \cos\theta$ corresponds to $\alpha > \theta$ and

$St/St_n \geq \cos\theta$ corresponds to $\alpha < \theta$. Third and most important, the configurations and conditions most appropriate to an infinitely long cylinder ought to produce shedding angles less than the yaw angle which in turn requires that the shedding frequency be greater than that given by the Independence Principle.

3.2 Vortex Wake Parameters and Base Pressure. The previous experiments provided a study of the influence of yaw angle and finite length upon the shedding frequency and wake configuration of circular cylinders. To complete the study it was desirable to measure the base pressures, and the wake parameters ℓ_F and d_F. However, it was not possible to accurately measure pressures for combinations of velocities and diameters less than a Reynolds number of Re = 500. Thus some of the spectacular changes observed in the flow at low Reynolds numbers could not be matched with base pressure measurements. Nonetheless, trends were matched that can probably account for all of the phenomena seen and discussed previously.

The wake width d_F and the formation length ℓ_F were measured behind several free-ended cylinders with a flat free-end. This geometry was selected because of its simplicity and because the extensive baseline data in the earlier sections showed that $St/St_n \geq \cos\theta$ and $\alpha < \theta$ for this configuration when $Re > 400$. The formation length ℓ_F is defined as the distance from the cylinder axis to the initial position of a fully formed vortex and can be measured by any of the following criteria:

- The minimum of the mean pressure on the wake axis [45];
- The maximum of the second harmonic of the fluctuating velocity on the wake axis [6];
- The minimum of low frequency modulation of the vortex signal [5];
- The minimum transverse spacing from the wake axis of the peaks of the maximum fluctuating velocity [1].

The second criterion was employed in the present study. The linearized output from the anemometer was bandpass filtered at a center frequency of $2f_s$ with

upper and lower cutoffs (3db down) at $\pm$ fs/10, respectively. A typical trace of the filtered RMS value of $2f_s$ is shown in Fig. 25a. The probe traversed in the freestream direction. Once the value of ℓ_F was determined, the filter was removed from the circuit and an RMS velocity profile was measured across the wake at $x = \ell_F$. The transverse profile corresponding to Fig. 25a is shown in Fig. 25b. The transverse distance between the maxima of the RMS profile is defined as the wake width d_F at formation [23,52]. This width is not precisely equal to the distance between the free shear layers that has been called d_F earlier, but the differences are small and it has become customary to use the two quantities interchangeably [23]. According to the Independence Principle the wake width ought not to be influenced by yaw angle and the formation length, measured normal to the cylinder axis, should also be independent of yaw angle. In the present range of Reynolds numbers both d_F and ℓ_F are dependent on Re and this introduces some additional complication. However, it should be possible to reconcile this with the use of Re_n if the Independence Principle is valid.

The measured values of d_F and $\ell_F \cdot \cos\theta$ are presented in Figs. 26a and 26b, respectively, as a function of Re_n. Clearly, the Cosine Laws have failed to scale the results properly. Both the wake width and the formation length become less than expected as the yaw angle is increased. The freestream Reynolds number Re tends to scale the wake width results better than Re_n but this is probably peculiar to this range of Reynolds number because Smith, Kao, & Moon have also reported a narrowing of the wake with increasing yaw angle. Based on Roshko's free-streamline theory [47] one would expect increasing base pressure to be associated with decreasing wake width. On the other hand, experience with other bluff body flows [1] has shown that the base pressure decreases as the formation length shrinks. The apparent paradox presented by Figs. 26a and 26b can be resolved by noting that this presentation of formation length has included a $\cos\theta$ owing to the Independence Principle. Dividing the data in Fig. 26b by cos

θ removes the Independence Principle so that ℓ_F, measured in the freestream direction, increases with yaw angle and the two wake measurements become consistent. This also suggests that perhaps the freestream flow direction may be the dominating influence and perhaps U_n ought to be discarded altogether. However, the use of Re_n is necessary to appropriately shift the curve shapes in Figs. 26a and b. Therefore, the normal component of velocity is the proper characteristic velocity for a yawed cylinder. It should be noted that the unyawed data in Figs. 26 a and 26b compare well to previous reports [5,40,46].

The base pressure measurements were a difficult matter. The largest measured pressure difference was less than 2 mm of water column and typically the pressures were less than 1 mm of water. Although the manometer indicated a resolution of 0.01 mm it was found that, in practice, the resolution was more nearly 0.02 - 0.03 mm. Meanwhile, the accuracy from experiment to experiment was no better than $\pm$0.03 mm. Thus the relative changes in base pressure during a particular experiment could be judged better than the absolute value of base pressure under any conditions. This is evident in the base pressure measurements shown in Figure 27 for an unyawed cylinder during two separate experiments. The two symbols represent separate experiments and demonstrate the difficulties discussed above. Nonetheless the measured base pressure coefficients for the unyawed cylinder compare remarkably well with reports of base pressure for similar Reynolds numbers [46]. They also reflect the strong Reynolds number dependence that is typical of this range of Re.

The yawed cylinder base pressure measurements were obtained from a series of yaw angles for one cylinder at two values of the freestream velocity corresponding to Re = 550 and 750. The base pressure coefficients are presented in Figure 28 in terms of the Independence Principle definition,

$$C_{P_{b_n}} = \frac{P_b - P_o}{1/2\rho U_n^2}, \quad U_n = U_o \cos\theta . \tag{18}$$

which ought to collapse the data onto the curve of Fig. 27 by using Re_n. As suggested by the wake width and formation length measurements the measured base pressure does not follow the Cosine Laws. In fact the base pressure is lower than predicted which will produce a drag greater than predicted. The excess of drag over that predicted by the Independence Principle is indicated by the ratio of $C_{p_{b_n}}$ to C_{p_b} evaluated at $Re_n = Re$. The values of this ratio which are plotted in Fig. 29 versus the yaw angle demonstrate an excess of drag that increases by 12-24 percent at $\theta = 60°$. Also plotted in the figure are similar data obtained from the published results of Smith, Kao, & Moon and Relf & Powell; both studies done at larger Reynolds numbers. Smith et al observed somewhat larger drag increases but the trends are unmistakable and the agreement with the results of Relf & Powell is good. These favorable comparisons also serve to extend the present findings to larger Reynolds numbers.

The base pressure coefficients for the unyawed cylinder were plotted against formation length with the aid of Fig. 26b. The result is shown in Fig. 30 and confirms an inverse relationship between base pressure and the formation length found in other experiments [1] and suggested by Riabouchinsky's analysis. Of interest here is a comparison of this relationship to the yawed cylinder results. This was again determined with the aid of Fig. 26b and is plotted in Fig. 31. An inverse relationship also exists but evidently a different one than the normal incidence case represented by the dashed line. The formation length plotted in the figure is the formation distance normal to the cylinder, $\ell_F \frac{\cos \theta}{D}$. A plot of ℓ_F does not improve agreement between the yawed and unyawed cylinder data because the yawed data is shifted too far to the right. The possibility remains that some intermediate direction, defined by the shedding angle, is appropriate but this was not investigated.

In effect, the Independence Principle replaces U_o by U_n in all relationships for the normal incidence case and then assumes that these same relations

will hold for the yawed cylinder. Thus the Cosine Laws predict that Roshko's universal Reynolds number is valid if the nondimensional quantities

$$S_n^* = \frac{f_s d_F}{U_{b_n}} = \frac{f_s D}{U_n} \frac{U_n}{U_{b_n}} \frac{d_F}{D} , \frac{U_{b_n}}{U_n} = k; \tag{19}$$

and

$$R_n^* = \frac{U_{b_n} d_F}{\nu} = \frac{Re_n \cdot k \cdot d_F}{D} , k = \sqrt{1-C_{p_b}}; \tag{20}$$

are employed. The present experiments have shown that the Cosine Laws fail to describe the observed f_s, the observed d_F, and the measured $C_{p_{b_n}}$. However, it was noticed that the observed variations could be off-setting within the universal Strouhal number, S_n^*. For the unyawed cylinder values of S^* were computed using the measured quantities f_s, U_o, C_{p_b}, and d_F together with the cylinder diameter D. For the yawed cylinder values of S_n^* were also computed using f_s, U_n, C_{pb_n}, d_F, and D. Some difficulty was encountered with the wake width d_F; this difficulty was caused by the dependence of d_F on both the yaw angle θ and the Reynolds number Re_n which changed together in a single experiment. Rather than impose a small variation in d_F that was not warranted by experimental accuracy it was decided to set $d_F/D = 1.1$ throughout the computations. This implies that the effects of Re_n and θ are completely balancing, which upon reference to Fig. 26 is a fair approximation that may slightly overestimate d_F at the largest yaw angles, i.e. the lowest Re_n. It must be emphasized that this approximation is valid only in this particular range of Re_n. The universal Strouhal numbers S^* and S_n^* computed according to the above method, are plotted in Fig. 32 and agree quite well with one another for both yawed and unyawed cylinders. Moreover, the results of both yawed and unyawed cylinders agree very well with the results of previous investigations of normal incidence bluff body flows that include both wake interference and resonant vibrations. To appreciate the degree of collapse of the data one might consider that in the present yawed cylinder experiments

the base pressure coefficients varied by as much as 60 percent, the wake widths by as much as 20 percent, and the Strouhal numbers St_n by as much as 50 percent. Despite these large changes virtually all of the values of S^* and S_n^* obtained in the present investigation are within 6 percent of the mean and within 10 percent of the S^* versus R^* relation found previously for a wide variety of two-dimensional bluff body flows [23].

4.0 RESULTS FOR VIBRATING YAWED CYLINDERS

The stationary cylinder experiments demonstrated that the separated flow is very sensitive to end conditions and that the conditions most representative of an infinitely long cylinder do not produce flows in accordance to the Independence Principle. King's data for vortex-excited, vibrating yawed cylinders [32] were also influenced by end conditions. For one of two sets of conditions King was able to scale both the onset and magnitude of yawed cylinder vibrations by using the Independence Principle. For the second set only the onset of vibrations could be scaled by cos θ and then only approximately; the vibration amplitudes were greatly reduced in this latter case. Therefore, one aim of the present study was to reconcile for the differences in King's two sets of results and to assess which set of results is representative of the general response of yawed cylinders that are resonantly excited by vortex shedding.

An outcome of King's experiments that is consistent with the present stationary cylinder experiments is the verification of $U_n = U_o \cos \theta$ as the proper characteristic velocity for yawed cylinders. Hence, the non-dimensional reduced velocity (see Section 1.1.4, Eq. 13) becomes

$$V_r = \frac{U_n}{f_d D} \tag{21}$$

where f_d is the driving frequency in the present forced vibration experiments. Once the yaw angle θ and the peak-to-peak amplitude of vibration a/D are selected, the reduced velocity is the independent variable for which the wake responses are to be determined.

4.1 Lock-in Regimes. The onset of vortex-induced vibrations corresponds to the "capture" of the natural vortex shedding by the cylinder motion. Identification of these "locked-in" or synchronized conditions for yawed cylinders was the first goal of the forced vibration experiments. The procedure was to oscillate a

yawed cylinder at particular values of frequency f_d and amplitude a/D and then to vary the flow speed in search of the wake capture. The capture of the vortex shedding was evidenced by a suppression of the natural shedding frequency $f_v = f_s$ in favor of $f_v = f_d$ or some multiple of f_d. This was determined by positioning a hot-wire probe to one side of the wake and recording the fluctuating velocity spectrum at each flow speed. The question of end effects was addressed by performing the test a number of times with different end conditions. For comparison purposes the stationary cylinder shedding frequencies were recorded as a function of flow speed for each configuration. It was anticipated that different end conditions would produce different stationary cylinder frequency curves which could be compared to the various forced responses. The first tests were performed at Re = 160 and $\theta = 30°$ with endplate inclination angles of $\beta \approx 85°$ and $\beta = 95°$. These endplate angles were selected in the belief that the stationary cylinder frequency was most sensitive to changes in β for $\beta \approx 90°$. There was surprisingly little difference in the measured shedding frequencies for the two endplate configurations because, as later analysis showed (see Appendix A), the greatest sensitivity to endplate inclination is actually nearer $\beta = 110°$. This was not a serious error and was compensated for by the results of the Re = 160, $\theta = 50°$ tests that followed.

The data from the $\theta = 30°$ tests are plotted in Fig. 33 in terms of the frequency ratio f_v/f_d and the reduced velocity V_r. The open symbols correspond to the stationary cylinder results ($f_v = f_s$) and, as discussed above, are essentially the same for $\beta = 85°$ and 95°. Moreover, the frequencies are just slightly greater than those expected from the Independence Principle; these are indicated by the solid lines in the figure. The solid lines are presented in two segments corresponding to Re_n from 50 to 150 and from 300 to about 500. The solid symbols in the figure represent the forced vibration responses for $f_d = 37$ Hz and a peak-to-peak amplitude a/D = 1.0. Below $V_r \approx 4.0$ the wake frequency response is

essentially that of the stationary cylinder(s). For $V_r \geq 4.0$ the wake frequency f_v jumps to the oscillation frequency f_d which is characteristic of lock-in or wake capture. Until $V_r \simeq 6.5$ the frequency remains locked onto f_d. At $V_r \simeq 6$ the second harmonic of f_d becomes pronounced and by $V_r \simeq 7.0$ it is the dominant response. Further increases in the flow speed evoke similar changes involving frequencies at $f_v = 2f_d$ and at $f_v = 3f_d$. The responses for the two endplate configurations are quite similar for $V_r < 15$. Above this value the $\beta = 85°$ cylinder reverts to the stationary cylinder response while the $\beta = 95°$ cylinder proceeds into an $f_v = 4f_d$ response. These differences occur for conditions which are not characteristic of vortex-excited resonant vibrations, as will be discussed later, but it is interesting to note that end effects are ever present. The general influence of end effects could not be assessed, owing to the incorrect selections of β, but lock-in was observed to occur at $f_v/f_d = 1$ in the range $V_r \simeq 4.0$ to $V_r \simeq 6.5$ which does include the typical range of V_r for self-excited, two-dimensional lock-in, i.e. $V_r = 5\text{-}6$ [32,33].

Before considering the remaining lock-in experiments it is interesting to examine some of the wake spectra corresponding to the $\beta = 95°$ data of Fig. 33. The sample spectra are presented in Fig. 34 and the discrete progression of the wake frequency response can be seen for increasing values of V_r. The coexistence of harmonics at one flow speed can be seen, for example, in the second trace at $V_r = 7.5$. Combinations of the forced and stationary cylinder wake responses can be seen in the fourth, sixth, and seventh traces. These spectra can be compared to the data in the previous figure with the aid of the scales drawn overhead. One striking feature of the wake response spectra that is typical of locked-on vortex shedding is the narrow-banded character of the forced responses as compared to the bandwidths for the stationary cylinder. This is analagous to the two-dimensional case. Also there is a similarity between the increase in stationary cylinder frequency bandwidth with yaw angle and the increase in bandwidth for

the stationary, unyawed cylinder due to increasing Reynolds number, i.e. turbulence.

Since the choice of endplate angles $\beta = 90° \pm 5°$ did not produce different stationary cylinder frequencies, experiments at Re = 160, $\theta = 50°$ were performed for $\beta = 85°$ and $\beta = 105°$. This turned out to be a selection in the opposite extreme because the $\beta = 85°$ cylinder exhibited a trailing vortex pattern for Re $\leq$ 200. Nevertheless the forced vibration wake frequency measurements for the two cylinders were comparable and this was taken as evidence of the relative unimportance of end conditions upon the wake frequency response. In order to simplify the remaining experiments, a third cylinder that had a free end was briefly tested under these conditions. The results for all three cylinders are plotted in Fig. 35. The open symbols, denoting the stationary cylinder frequencies for the free-ended and $\beta = 105°$ cylinders, are comparable and exceed the Independence Principle prediction (solid line) by about 20 percent. This is in complete accord with the earlier stationary cylinder data. The forced responses of all three cylinders are comparable except that the $\beta = 85°$ cylinder "holds on" to the lower multiple of f_d for larger values of V_r. This will not be important to self-excited conditions because, as will be discussed, the spanwise coherence of the flow suffers in the latter case. Once again the $f_v/f_d = 1$ wake capture takes place in the range $V_r = 4$ to 7 which includes the typical normal incidence range of $V_r = 5$ to 6.

At this point it is necessary to identify which subranges of the forced wake responses are likely to coincide with resonant vortex-excited conditions. In the two-dimensional normal incidence case, forced vibrations are known to capture the vortex shedding for frequencies above and below the stationary cylinder or "natural" shedding frequency. However, self-excited oscillations only occur for frequencies <u>below</u> the natural structural frequency because in that range the phase between the motion and the fluctuating lift force is such that work is done on

the cylinder by the fluid forces [4]. The converse is also true, in that work is done by the cylinder on the fluid for frequencies greater than the natural shedding frequency. Without identifying a natural shedding frequency for yawed cylinders it is still possible to apply this concept to the yawed cylinder responses of the present study by noting that self-excited conditions at f_v/f_d = 1, 2, 3, 4, etc. will correspond to the larger values of V_r.

In order to supplement the Re = 160 data similar experiments were conducted for Re = 460. The amplitudes of vibration for these experiments varied from a/D = 0.15 to a/D = 1.0 and only a single, free-ended, cylinder was tested. This cylinder was selected in order to simplify the experiments and the choice was justified by the relative lack of end effects at Re = 160 and the earlier observation that end effects diminished with increasing Reynolds number. The results at amplitudes a/D = 1.0 and a/D = 0.50 were quite similar to the earlier data, so that only the a/D = 0.15 results are presented in Figures 36 and 37 for yaw angles of θ = 30° and 50°, respectively. These amplitudes are insufficient to capture the shedding process for conditions other than f_v/f_d = 1. Moreover, the extent of lock-in is quite small; encompassing a narrow span of only $V_r \approx 4.5$-6.0, but this still includes V_r = 5-6 as before.

The preceding forced vibration experiments have shown that lock-in occurred for many conditions and in a number of modes. At the same time the wake responses at f_v/f_d = 1 were largely insensitive to end conditions. Moreover, the yawed cylinder values of the reduced velocity corresponding to lock-in always included the corresponding range of normal incidence values for self-excited vibrations. However, a difficulty in defining a "natural" shedding frequency for the yawed cylinder and the influence of vibration amplitude made it difficult to directly compare the yawed and unyawed lock-in regimes.

The latter difficulties were overcome by some detailed lock-in experiments at Re = 460 using a free-ended cylinder. Five yaw angles, θ = 0°, 20°, 30°, 40°

and 50°, were examined for amplitudes ranging from 0.1D to 1.0D. In addition to the frequency criterion $f_v = n\, f_d$, $n = 1,2,3 \ldots$, a second criterion was employed to account for the phase between the motion and the lift force. This was done by observing the phase between the vortex shedding signal in the wake and the motion signal. It was required that frequency capture be accompanied by a fixed phase relationship between the signals as evidenced by a steady Lissajous pattern on an oscilliscope. This is, of course, a necessary condition for sustained, large amplitude, self-excited vibrations to occur and is always the case for lock-in at normal incidence. A visual confirmation of the lock-in that met the above criteria was produced by the flow visualization system which "froze" the vibrating cylinder wake. Satisfying these two simultaneous criteria typically ruled out wake responses for $f_v/f_d > 1$, but on those occasions when $f_v/f_d = 2$ and a steady Lissajous pattern was established flow visualization of the wake revealed a very complex three-dimensional wake structure.

Since most self-excited oscillations occur for $f_v \approx f_d$, further experiments were restricted to the lowest lock-in regime. An onset and a terminal velocity for the lock-in could be determined for each yaw angle and amplitude by slowly varying the flow speed. In order to compare the present results with previous normal incidence data (see Fig. 6) it was necessary to define an appropriate "natural" shedding frequency. Use of the corresponding measured stationary cylinder frequency did not scale the data as well as the use of the expected frequency based on the Independence Principle. Therefore the results for the boundries of the locked-in vortex shedding for yawed cylinders are plotted in Fig. 38 as functions of the vibration amplitude and the parameter $(V_r \cdot St_n)^{-1}$. The Strouhal number St_n was computed from Roshko's relation(s) using the Reynolds number Re_n. The Strouhal number St_n defines a frequency f_s' which is to be expected from the Cosine Laws so that

$$(V_r \cdot St_n)^{-1} = \left(\frac{U_n}{f_d D} \quad \frac{f_s' D}{U_n}\right)^{-1} = f_d/f_s' \,. \qquad (22)$$

A direct comparison with the normal incidence case is possible as indicated by the dashed lines in Fig. 38. An interpretation of f_s' will be taken up shortly, but first the essential similarity between the yawed and unyawed results is to be noted. The lock-in range does shrink somewhat with increasing yaw angle, but this will not diminish the magnitude of the self-excited response, rather it will simply delay its onset or hasten its completion a small amount for increasing flow speed.

An explanation of f_s' or, equivalently, an accounting for the apparent validity of the Independence Principle involves a consideration of the vortex shedding angle α during the vibrations. Up to this point in the discussion the shedding angle has been treated as a kinematical parameter that specifies the vortex street inclination. It's physical importance resides in the fact that it also reflects the spanwise coherence of vortex shedding and also ultimately reflects the spanwise correlation of the fluctuating lift force. In the case of flow at normal incidence the wake capture is accompanied by parallel vortex shedding over large cylinder spans which is, in part, responsible for the large vibration amplitudes that occur. If the Independence Principle is to be valid for describing both the onset and the magnitude of vortex-excited vibrations then the vortex-shedding must be parallel to the yawed cylinder as well.

The shedding angle was determined from photographs of the wakes of the vibrating cylinders and some typical results are plotted in Figure 39 for Re = 460. Within the ranges of V_r and a/D where lock-in occurs the observed shedding angle is essentially equal to the yaw angle. Outside the lock-in range the yaw angle may vary under some other influence. The results in Fig. 39 were obtained by vibrating a free-ended cylinder but with one exception all other vibrating cylinder

shedding angles were within a few degrees of the yaw angle[1]. The exception to capture occurred in the Re = 160, = 50° experiments with an endplate angle ≈ 85°. In this instance the shedding angles increased steadily through lock-in and exceeded the yaw angle by as much as 15 percent; this can be considered a consequence of the excessive spanwise flow engendered by the endplate. The results of this section indicate that the use of the Independence Principle is appropriate for yawed cylinder vibrations and that King's conclusions are generally valid. Moreover, it appears that the small amplitude response observed by King for one set of end conditions can be attributed to a decrease in the spanwise coherence, i.e. $\alpha \neq \theta$, brought about by severe three-dimensional end conditions.

The success of the Independence Principle in characterizing vortex-excited yawed bluff body vibrations is not a result of the Principle's general validity, but rather it is a consequence of the wake capture process itself. When a yawed cylinder vibrates it can capture the shedding frequency and it can capture the shedding angle. If it captures both, as it must for large amplitude self-excited vibrations to occur, then the appropriate "natural" shedding frequency corresponds to the shedding frequency of a stationary yawed cylinder with parallel shedding. This frequency is predicted by the Independence Principle but is not the frequency observed for an infinitely-long, yawed cylinder because, as shown in the previous sections, the infinitely-long, stationary yawed cylinder is expected to have a shedding angle less than the yaw angle and this in turn produces shedding frequencies greater than those predicted by the Independence Principle.

4.2 Vortex Wake Parameters. The results presented in the preceding section demonstrated that the Cosine Laws can be used to scale the onset and the extent of locked-in vortex shedding. It also was shown that in the absence of severe three-dimensional end conditions the spanwise coherence of vortex shedding and,

---

[1] The capture of the shedding angle by the oscillations observed in this study is a generalization of the same phenomena observed in the flow visualization photographs of Dale & Holler [10].

consequently, the unsteady lift force were unaffected by yaw angle because the vortex shedding angle was captured by the oscillations. In order to completely describe vortex-excited, yawed cylinder vibrations it is necessary to know how the fluid forces vary during lock-in. It was not possible to measure the fluctuating fluid forces in the present experiments owing to the small magnitudes of the forces in air. Moreover, the need for large vibration amplitudes placed restrictions on the allowable vibration frequencies which in turn required low flow speeds. These circumstances made it impossible to obtain base pressures during the lock-in experiments. Thus no attempts were made to measure directly either steady or unsteady fluid forces during vibrations.

Based on a known correspondence between the fluid forces and the characteristic wake length scales, ℓ_F and d_F, it is possible to infer changes in the former by measuring variations in one or both of the latter. The correspondence between changes in wake dimensions and fluid forces is the basis of Riabouchinsky's and Roshko's analyses and was observed in the present study for stationary, yawed cylinder flows. Also, the formation region length is known [22] to vary in relation to the amplitude and frequency of vibration during locked-in vortex shedding at normal incidence. Therefore it is reasonable to suppose that if the formation region length ℓ_F behind vibrating, yawed cylinders was observed to vary in the same way as behind vibrating, unyawed cylinders then a correspondence in the fluid force amplification can be concluded.

Measurements of the formation region length were obtained for yaw angles of $\theta = 40°$ and $\theta = 50°$ over a small range of Reynolds numbers near $Re = 460$. The data are plotted in Figs. 40a and 40b as functions of the reduced velocity V_r and the vibration displacement, respectively. At a fixed amplitude of oscillation, as in Fig. 40a, the formation length ℓ_F increases with reduced velocity V_r. This can be compared to the known results at normal incidence [22] by recalling that $V_r^{-1} \propto f/f_s'$ from the previous section, so that ℓ_F is indeed

inversely proportional to f/f_s' for cylinder vibrations at both yawed and normal incidence. The vortex formation region lengths measured in the wakes of yawed, vibrating cylinders can be compared to the stationary cylinder measurements at the same Reynolds number Re_n. These latter results appear in an earlier section of this study. At $V_r = 5.0$ the formation lengths are $\ell_F = 1.26D$ and $\ell_F = 2.6D$ for the vibrating and stationary cylinders, respectively. At $V_r = 6.0$ the two formation lengths become 2.16D and 2.9D, respectively. This reduction in the length of the formation region is direct evidence of an amplification in fluid forces during the locking-on [12,25]. At fixed values of the reduced velocity the length of the formation region decreases with vibration amplitude in the same manner as has been found for a cylinder at normal incidence [22]. The formation region length for the vibrating cylinder in Fig. 40b can be compared to the stationary cylinder results by noting that the stationary cylinder data are listed on the figure. Once again the decrease in ℓ_F with increasing amplitude of oscillation is a measure of the amplification in the fluid forces during the locking-in or wake capture.

Although these results imply a direct correspondence between the amplification of the fluid forces during lock-in for both yawed and unyawed cylinders, the absolute magnitudes of the fluid forces are not determined here. The logical deduction is that, given the same amplification of fluid forces for both yawed and unyawed vibrations, the actual force magnitudes for the two cases can be related through their stationary cylinder counterparts. After all, these are the force values that are being amplified by the vibrations. The difficulty with this conclusion is that it is not possible to decide whether the appropriate stationary yawed cylinder forces are the measured values or those predicted by the Cosine Laws. The existence of this choice is analagous to the earlier problem in selecting a "natural" shedding frequency f_s' for the vibrations of yawed cylinders and stems from the capture of the shedding angle during the oscillations. The

selection which is consistent with the earlier interpretation is to use the stationary cylinder forces predicted by the Cosine Laws. In this case all facets of the vortex-excited vibrations of yawed cylinders can be scaled from the vibrations at normal incidence via the Cosine Laws. It must be noted that this conclusion is not directly proved by force measurements, rather it is based upon consistent physical interpretation of measured flow characteristics. Additional support for this conclusion can be found in King's results where measurements of the vortex-excited vibration responses of yawed circular cylinders were properly scaled by the use of Cosine Laws.

5.0 SUMMARY AND CONCLUSIONS

The results of the present investigation into the vortex wakes of yawed circular cylinders have been compared with the results of adopting the Independence Principle. This principle states that the proper characteristic velocity for yawed bodies is the component of the freestream velocity perpendicular to the cylinder and that if this velocity is incorporated into any and all relations found for the normal incidence flow, then these same relations will also describe the flow over a yawed cylinder. In practice the influence of end conditions upon the Independence Principle has been unknown, so that a study of their effects was undertaken as part of the present investigation.

The first conclusion of the present study is that the use of the Independence is not valid for separated, yawed body flows except in two special cases. The first instance pertains to forced or self-excited transverse oscillations of yawed, circular cylinders. This finding implies a simple extension of existing vortex-induced vibration models [4] to include the influence of yaw angle. The second instance involves the influence of end conditions whereby a particular cylinder-endplate configuration can produce a flow pattern consistent with the Independence Principle. However, this particular configuration - endplates aligned with the freestream flow - is not consistent with the flow over an infinitely long cylinder. Interestingly enough, this configuration or a similar one has often been adopted during previous investigations of the yawed body problem and may account for the varying reports of the validity of the Independence Principle. These results are based on a number of experiments and analyses summarized below. Another important finding of the present study is that the universal Strouhal number concept originally advanced by Roshko for bluff body flows at normal incidence can be modified to include yawed cylinders.

Measurements of the vortex shedding frequency, the shedding angle, the base pressure, the vortex formation region length and the wake width were obtained for

stationary, yawed cylinders ($\theta = 0° - 60°$) in the Reynolds number range $Re = 150$-1100. The experiments were performed for various end conditions, including free-ended cylinders and cylinders fitted with adjustable endplates. The results were very sensitive to end conditions, especially at the lower Reynolds numbers of the present study.

An interdependence between the shedding frequency and the shedding angle was found and was used to determine, from simple discharged vorticity considerations, the type(s) of end conditions appropriate to the simulation of an infinitely long cylinder. A later consideration of the interaction between the end flow and the base region flow (Appendix A) yielded similar conclusions. In the case of a cylinder with endplates, the appropriate configuration involves inclined endplates; the amount of inclination depends on the yaw angle but is not precisely specified. Nevertheless for these configurations the shedding frequency is greater than expected from the Independence Principle while the shedding angle, the vortex formation length, the base pressure and the wake width are all less than expected. Within the framework of a universal Strouhal number S^* [23,49,52] these variations are offsetting, and the present results for yawed cylinders agree quite well with previous reports of S^* for a wide variety of bluff bodies at normal incidence. Since the Independence Principle automatically satisfies this universality concept it was concluded that a number of flows could be realized for finite length yawed cylinders; the flow in any particular case is dictated by the end conditions. Thus, the validity of the Principle could not have been determined by any previous investigation.

Measurements of the wake response frequency, the shedding angle and the vortex formation region length[1] were obtained for vibrating yawed cylinders

---

[1] Base pressure measurements were not possible for the vibrating cylinders owing to the experimental requirements of low frequency oscillations which in turn required air speeds too low for measurable pressures.

in the range of Reynolds numbers between Re = 160 and 460. Wake capture was accompanied by a frequency lock-in between the vortex wake and the cylinder motion and was also accompanied by vortex shedding parallel to the cylinder axis unless the end flows were severely three-dimensional. Due to the parallel shedding the proper characteristic frequency is equal to the shedding frequency predicted by the Cosine Laws. Therefore, the locked-in vortex wakes of vibrating yawed cylinders in the majority of cases can be described by means of the Independence Principle even though the Principle fails for the stationary cylinder. Measurements of the bounds of the lock-in regime for yawed cylinders compare well to the normal incidence case.

6.0 RECOMMENDATIONS

Recommendations for further study fall into two categories: those which will add directly to an understanding of the fluid dynamic processes, and those which will supplement the measurements of the present study.

In the first category a basic study of the differences between yawed and unyawed boundary layer separation and base region flow is desirable. The influence of end conditions also should be considered and could lead to a better definition of "severe three-dimensional end flows". This is a complicated task which might be simplified through the use of bluff bodies with fixed separation points such as flat plates or wedges. In these cases the free-streamline velocity at separation U_b can be measured directly and can be used to determine if the influence of yaw angle is wholly upon the separation process, wholly upon the vortex formation processes, or is some combination of these. The manner of end influence could be determined in the same sense. Flow visualization is recommended as an integral part of such an investigation. Perhaps a multi-colored aerosol or dye could be used to identify flow paths and directions or even to indicate the mixing processes that occur.

A recommendation that falls into the second category is a verification of the universal Strouhal number concept for vibrating yawed cylinders. The validity of this concept is implied by the present experiments, but it is not confirmed owing to the absence of base pressure measurements for the vibrating cylinder. Verification need not involve base pressure measurements if, as Griffin [23] has done in the normal incidence case, a correspondence between base pressure and vortex strength can be determined or assumed. The vortex strengths can be computed from the fit of a suitable vortex street model to the measured velocity profiles in the wake [25]. Another recommendation is to examine the vortex street wakes behind yawed cylinders to see how the usual two-dimensional vortex street analyses carry over to the inclined vortex streets observed in this study.

7.0 ACKNOWLEDGMENT

This research was submitted to the Catholic University of America in partial fulfillment of the degree, Doctor of Philosophy. The author wishes to thank the members of the dissertation committee, Professors Mario J. Casarella and Timothy W. Kao of Catholic University and Dr. Owen M. Griffin of NRL, for their contributions.

REFERENCES

1. Bearman, P.W., "Investigation of the Flow Behind a Two-Dimensional Model With a Blunt Trailing Edge and Fitted with Splitter Plates," Journal of Fluid Mechanics, Vol. 21, Part 2, 1965, pp. 241-255.

2. Berger, E., "Unterdruckung der laminaren Wirbelstromung and des Turbulenzeinsatzes der Karmanschen Wirbelstrasse im Nachlauf eines schwingenden Zylinders bei kleinen Reynoldszahlen," Jahrbuch der WGLR, pp. 164-172, 1964.

3. Berger, E., & Wille, R., "Periodic Flow Phenomena, "Annual Review of Fluid Mechanics, Vol. 4, 1972, pp. 313-340.

4. Blevins, R.D., Flow-induced Vibration, Van Nostrand Reinhold, New York, 1977.

5. Bloor, M.S. "The Transition to Turbulence in the Wake of a Circular Cylinder," Journal of Fluid Mechanics, Vol. 19, Part 2, 1964, pp. 290-304.

6. Bloor, M.S., & Gerrard, J.H., "Measurements on Turbulent Vortices in a Cylinder Wake," Proceedings of the Royal Society, London, England, Series A, Vol. 294, 1966, pp. 319-342.

7. Bursnall, W.J. & Lofting, L.W., "Experimental Investigation of the Pressure Distribution About a Yawed Circular Cylinder in the Critical Reynolds Number Range," NACA TN #2463, 1951.

8. Chiu, W.S., "The Boundary Layer Formation and Vortex Shedding on Yawed Cylinders," Wash. State University, College of Engineering Bulletin 299, 1966.

9. Chiu, W.S. & Lienhard, J.H., "On Real Fluid Flow Over Yawed Circular Cylinders, Trans. ASME, Series D, J. Basic Eng. Vol. 89, (1967), pp. 851-857.

10. Dale, J., & Holler, R.A., "Vortex Wakes from Flexible Circular Cylinders at Low Reynolds Numbers," USNADC Report AE-7011, 1970.

11. Dale, J., Menzel, H. & McCandless, J., "Dynamic Characteristics of Underwater Cables: Flow Induced Transverse Vibrations," U.S. Naval Air Development Center Report NADC-AE-6620, 1966.

12. Davies, M.E., "A Comparison of the Wake Structure of a Stationary and Oscillating Bluff Body, Using a Conditional Averaging Technique," J. Fluid Mech., Vol. 75, 1976, pp. 209-231.

13. Echols, W.H., & Young, J.A., "Studies of Portable Air-Operated Aerosol Generators," Naval Research Laboratory (NRL) Report 5929 (1963).

14. Etzold, J., "Strukturanalyse des Stromungsfeldes in Windshatten quer angestromter Zylunderstumpfe," Ph.D. dissertation at the Technical University of Berlin, 1974.

15. Etzold, F. & Fiedler, H., "The Near-Wake Structures of a Cantilevered Cylinder in a Crossflow," Z. Flugwiss, Vol. 24, 1976, pp. 77-82.

16. Fage, A., & Johansen, F.C., "On the Flow of Air Behind an Inclined Flat Plate of Infinite Span," Proc. Roy. Soc. (London), Ser. A, Vol. 116, No. 773, 1927, pp. 170-197.

17. Ferguson, N. & Parkinson, G.V., "Surface and Wake Flow Phenomena of the Vortex-Excited Oscillation of a Circular Cylinder," Journal of Engineering for Industry, Trans. ASME, Series B. Vol. 89, No. 4, Nov. 1967, pp. 831-838.

18. Gerrard, J.H., "The Three-Dimensional Structure of the Wake of a Circular Cylinder," Journal of Fluid Mechanics, Vol. 25, Part 1, 1966, pp. 143-164

19. Gerrard, J.H., "The Mechanics of the Formation of Region of Vortices Behind Bluff Bodies," Journal of Fluid Mechanics, Vol. 25, Part 2, 1966, pp. 401-413.

20. Glenny, D.E., "A Review of Flow Around Circular Cylinders, Stranded Cylinders and Struts Inclined to the Flow Direction," Australian Department of Supply, Mechanical Engineering, Note 284, 1966.

21. Graham, J.M.R., "The Effect of End-Plates on the Two-Dimensionality of a Vortex Wake," Aero. Quarterly, pp. 237-247, August, 1969.

22. Griffin, O.M., "The Unsteady Wake of an Oscillating Cylinder at Low Reynolds Number," Journal of Applied Mechanics, Trans, ASME, Vol. 38, Dec. 1971, pp. 729-738.

23. Griffin, O.M., "A Universal Strouhal Number for the 'Locking-on' of Vortex Shedding to the Vibrations of Bluff Cylinders," Journal of Fluid Mechanics, Vol. 85, Part 3, 1978, pp. 591-607.

24. Griffin, O.M., & Ramberg, S.E., "The Vortex-Street Wakes of Vibrating Cylinders," Journal of Fluid Mechanics, Vol. 66, Part 3, 1974, pp. 553-576.

25. Griffin, O.M., & Ramberg, S.E., "On Vortex Strength and Drag in Bluff-Body Wakes," Journal of Fluid Mechanics, Vol. 69, Part 4, 1975, pp. 721-728.

26. Griffin, O.M. & Ramberg, S.E., "Vortex Shedding from a Cylinder Vibrating in Line with an Incident Uniform Flow," Journal of Fluid Mechanics, Vol. 75, Part 2, 1976, pp. 257-271.

27. Griffin, O.M., Ramberg, S.E., Votaw, C.W., & Kelleher, M.D., "The Generation of Liquid Aerosols for the Visualization of Oscillatory Flows," Proc. Int. Cong. for Instr. in Aero. and Space Facil., Trans IEEE, pp. 133, 1973.

28. Griffin, O.M. & Votaw, C.W., "The Vortex Street in the Wake of a Vibrating Cylinder," Journal of Fluid Mechanics, Vol. 55, 1972, pp. 31-48.

29. Hanson, A.R., "Vortex Shedding from Yawed Cylinders," J. AIAA, Vol. 4, 1966, pp. 738-740.

30. Honji, H. & Ishi-I, K., "Wake Shedding from a Distorted Cylinder," J. Physical Soc. Japan, Vol. No. 3, 1976, pp. 1089-1090.

31. Honji, H. & Taneda, S., "Vortex Wakes of Oscillating Circular Cylinders," Reports of Research Institute for Applied Mechanics, Kyushu Univ., Vol. 16, 1968, pp. 211-222.

32. King, R., "Vortex Excited Oscillations of Yawed Circular Cylinders," J. Fluids Engineering, Trans. ASME, Vol. 99, No. 3, 1977,, pp. 495-502.

33. King, R., Prosser, M.J., & Johns, D.J., "On Vortex Excitation of Model Piles in Water," Journal of Sound and Vibration, Vol. 29, 1973, pp. 169-188.

34. Kochin, N.E., Kibel', I.A. & Roze, N.V., "Theoretical Hydromechanics," New York: Interscience Publishers (Wiley and Sons), 1964.

35. Koopmann, G.H., "The Vortex Wakes of Vibrating Cylinders at Low Reynolds Numbers," Journal of Fluid Mechanics, Vol. 28, 1967, pp. 501-512.

36. Koopmann, G.H., "Wind-Induced Vibrations of Skewed Circular Cylinders," Civil and Mech. Eng. Dept. Report 70-11, Catholic University of America, Washington, D.C., 1970.

37. Lamont, P.J. & Hunt, B.L., "Pressure and Force Distributions on a Sharp-Nosed Circular Cylinder at Large Angles of Inclination to a Uniform Subsonic Stream," Journal of Fluid Mechanics, Vol. 76, Part 3, pp. 519-559, 1976.

38. McCroskey, W.J., "Some Current Research in Unsteady Fluid Dynamics," Freeman Scholar Lecture, ASME 1976 Winter Annual Meeting, (published in ASME J. Fluids Eng., Vol. 99, No. 1, 1977, pp. 8-39).

39. Novak, M. & Tanaka, H., "Pressure Correlations on a Vibrating Cylinder," presented at the Conf. on Wind Effects on Buildings and Structures, London (1975).

40. Ramberg, S.E., & Griffin, O.M., "Vortex Formation in the Wake of a Vibrating, Flexible Cable," Journal of Fluids Engineering, Trans. ASME, Vol. 96, Series I, No. 4, 1974, pp. 317-322.

41. Ramberg, S.E. & Griffin, O.M., "Velocity Correlation and Vortex Spacing in the Wake of a Vibrating Cable," Journal of Fluids Engineering, Trans. ASME, Vol. 98, Series I, No. 1, 1976, pp. 10-18.

42. Relf, E.H. & Powell, C.H., "Tests on Smooth and Stranded Wires Inclined to the Wind Direction and a Comparison of the Results on Stranded Wires in Air and Water," British A.R.C., 1917.

43. Riabouchinsky, D., "On Steady Fluid Motions with Free Surfaces," Proc. London Math. Soc., Vol. 19, 1921, pp. 206-215.

44. Richter, A., & Naudascher, E., "Fluctuating Forces on a Rigid Circular Cylinder in a Confined Flow," Journal of Fluid Mechanics, Vol. 78, Part 3, 1976, pp. 561-576.

45. Roshko, A., "On the Development of Turbulent Wakes from Vortex Streets," NACA Report 1191, Washington, D.C., 1954.

46. Roshko, A., "A New Hodograph for Free-Streamline Theory," NACA TN3168, July, 1954.

47. Roshko,, A., "On the Wake and Drag of Bluff Bodies," Journal Aeronautical Sciences, Vol. 22, No. 2, 1955, pp. 124-132.

48. Roshko, A., a discussion of Ref. [9], Journal of Basic Engineering, Trans. ASME, Vol. 91, No. 1, Series D, 1969, pp. 132.

49. Sainsbury, R.N. & King, R., "The Flow-Induced Oscillations of Marine Structures," Proc. Instn. Civil Engrs., Vol. 49, 1971, pp. 269-302.

50. Sarpkaya, T., "Separated Flow about Lifting Bodies and Impulsive Flow about Cylinders," AIAA J., Vol. 4, 1966, pp. 414-420.

51. Schlichting, H., Boundary Layer Theory, 6th ed. McGraw-Hill, New York, 1968.

52. Simmons, J.E.L., "Similarities Between Two-Dimensional and Axisymmetric Vortex Wakes," The Aero. Quart. Vol. XXVIII, Pt. 1, 1977, pp. 15-20.

53. Smith, R.A., Moon, W.T. & Kao, T.W., "Experiments on Flow about a Yawed Circular Cylinder," Trans. ASME, J. Basic Eng., Vol. 94, 1972, pp. 771-776.

54. Stansby, P.K., "The Effects of End Plates on the Base Pressure Coefficient of a Circular Cylinder," Aeronautical Journal, Vol. 78, January 1974, pp. 36-37.

55. Surry, J., "Experimental Investigation of the Characteristics of Flow about Curved Circular Cylinders," University of Toronto Institute for Aerospace Studies Technical Note 89, 1965.

56. Thomson, K.D. & Morrison, D.F., "The Spacing Position and Strength of Vortices in the Wake of Slender Cylindrical Bodies at Large Incidence," JFM, Vol. 50, Part 4, pp. 751-783, 1971.

57. Toebes, G.H., "The Unsteady Flow and Wake Near an Oscillating Cylinder," Journal of Basic Engineering, Trans. ASME, Series D, Vol. 91, No. 3, Sept. 1969, pp. 493-502.

58. Van Atta, C.W., "Experiments on Vortex Shedding from Yawed Circular Cylinders," J. AIAA, Vol. 6, pp. 931-933, 1968.

59. Votaw, C.W., & Griffin,, O.M., "Vortex Shedding from Smooth Cylinders and Stranded Cables," J. Basic Engineering, Trans. ASME, Series D, Vol. 93, pp. 457-460, 1971.

60. Williams, J.C., III, "Incompressible Boundary-Layer Separation," Annual Review of Fluid Mechanics, Vol. 9, 1977, pp. 113-144.

61. Wootton, L.R., Warner, M.H., Sainsbury, R.N., & Cooper, D.H., "Oscillation of Piles in Marine Structures," London: Construction Industry Research and Information Association, Report CIRIA 41, (1972).

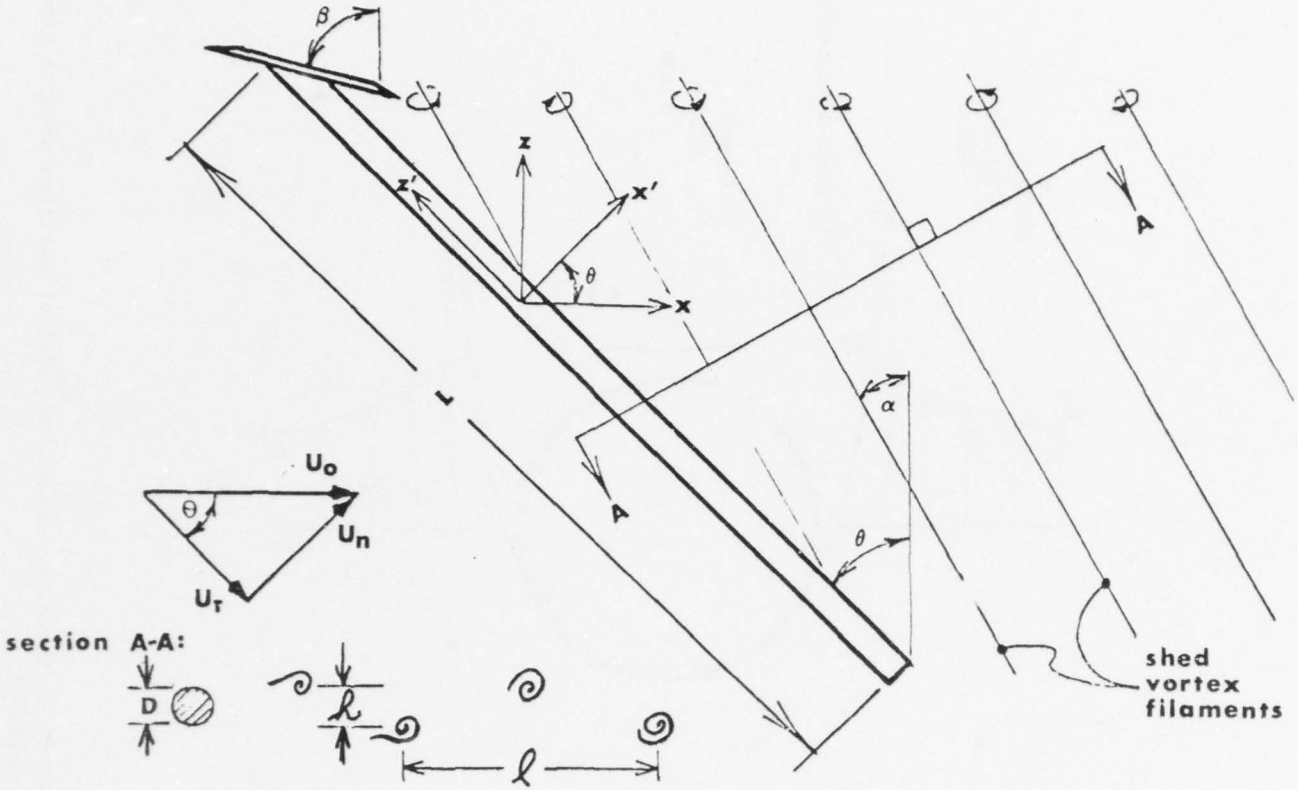

Figure 1 - A schematic of the flow over a finite length yawed cylinder, indicating the nomenclature employed in this study.

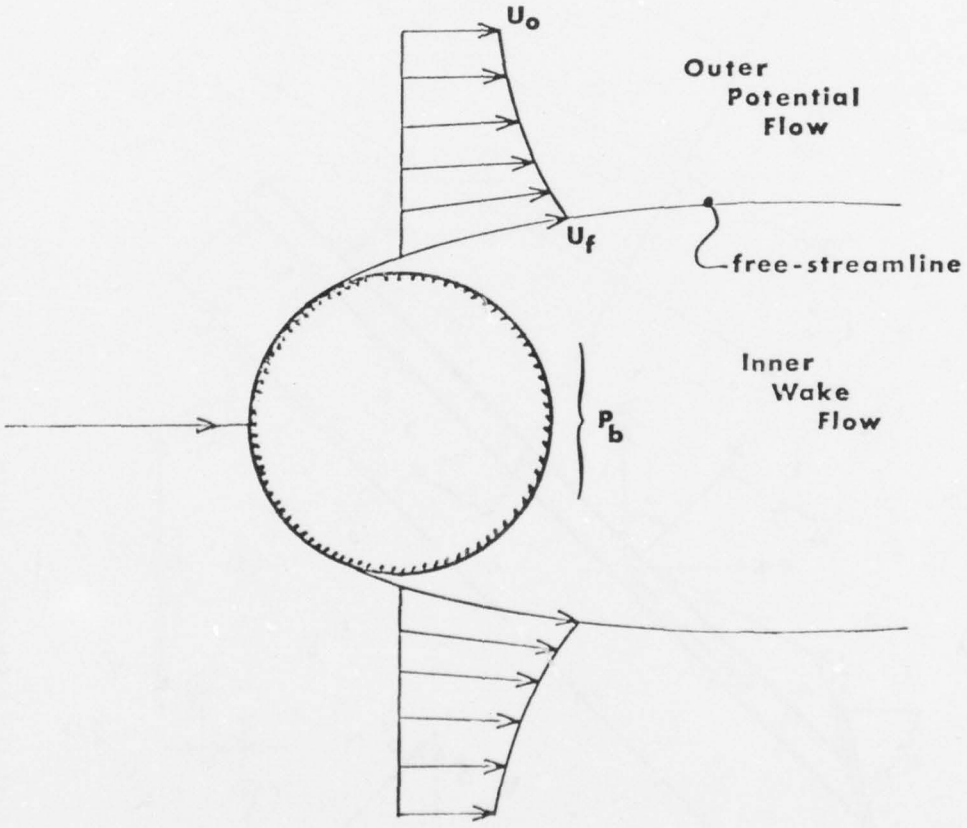

Figure 2 - A sketch of the free-streamline model of the flow about a circular cylinder.

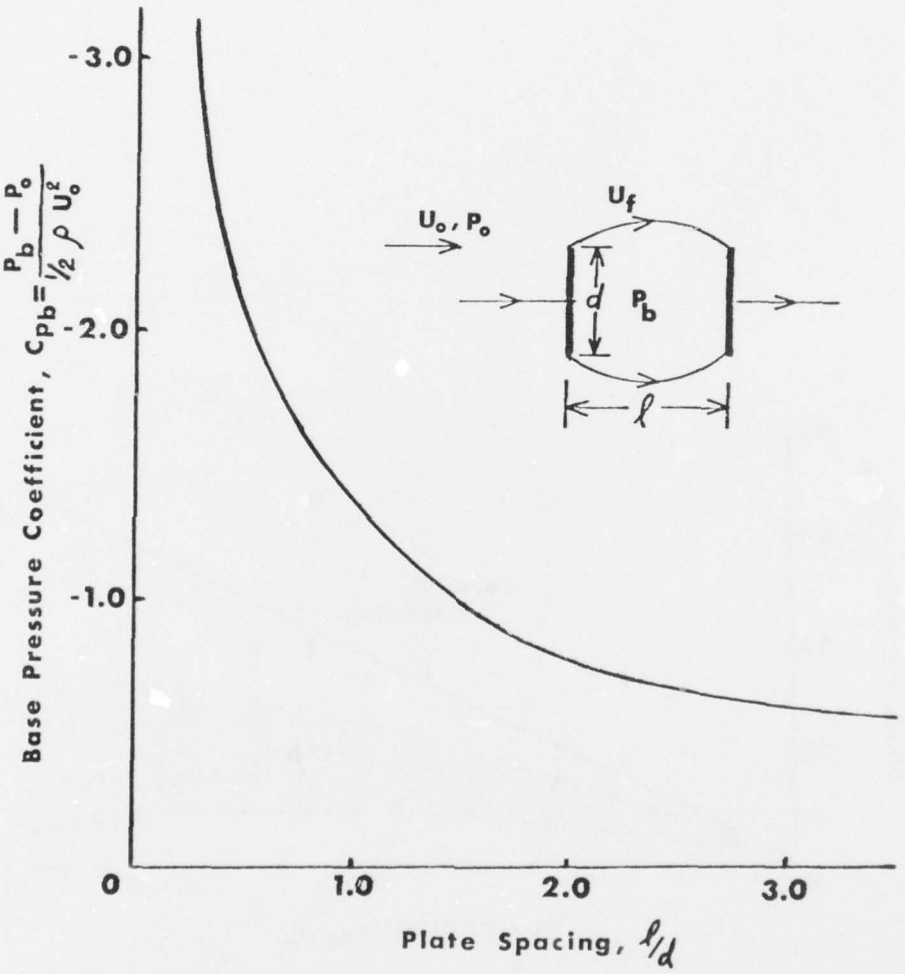

Figure 3 - A plot of Riabouchinsky's free-streamline theory [43] results for the base pressure of a flat plate as a function of the image plate position.

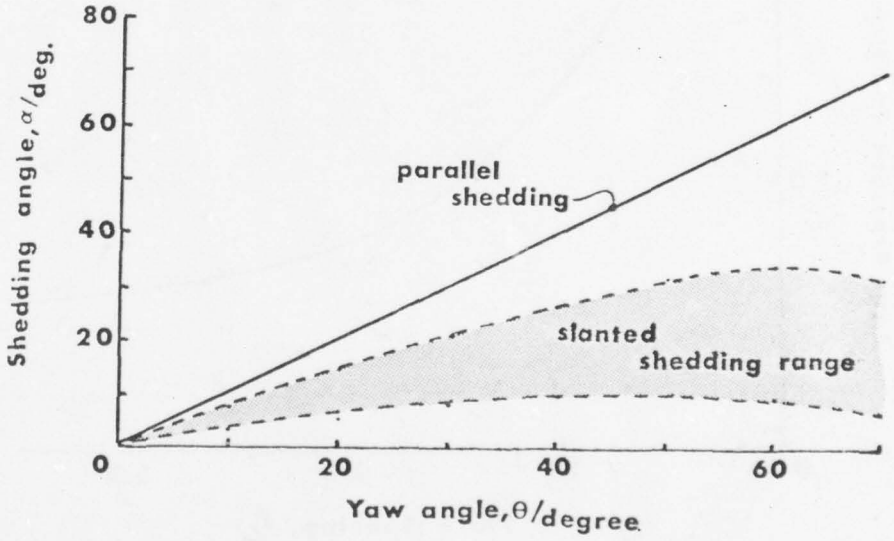

Figure 4 - Estimates of the expected shedding angle behind a yawed cylinder according to simple vorticity considerations.

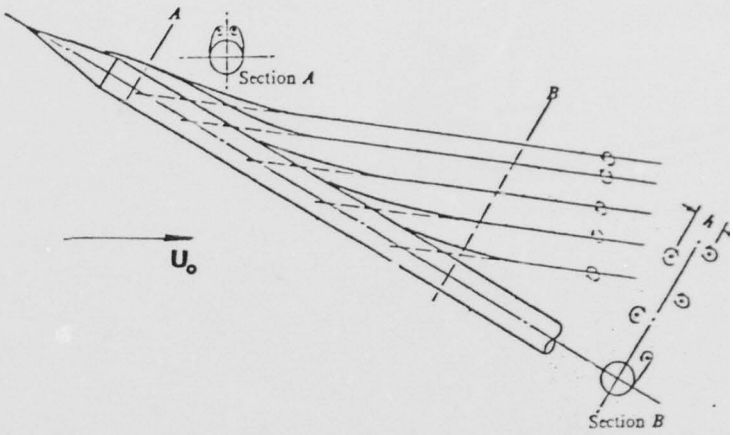

Figure 5 - A sketch of the steady trailing vortex pattern behind a finit length cylinder at large incidence; from Ref. [37].

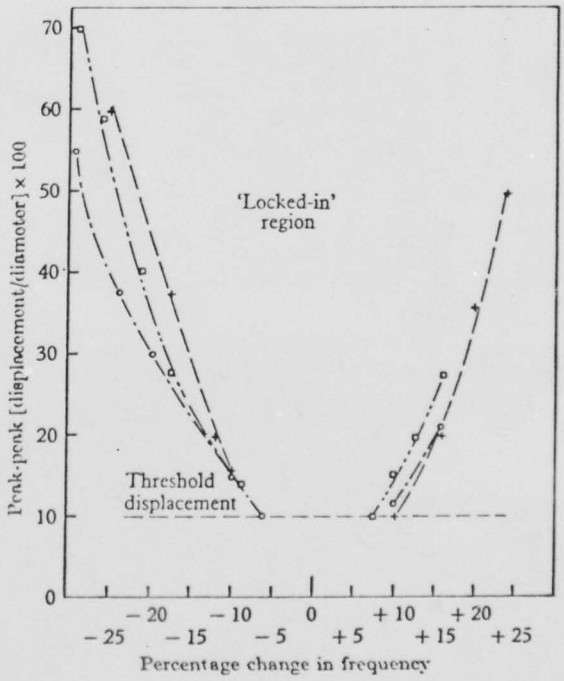

Figure 6 - The lock-in region for a circular cylinder at normal incidenc from Ref. [35].

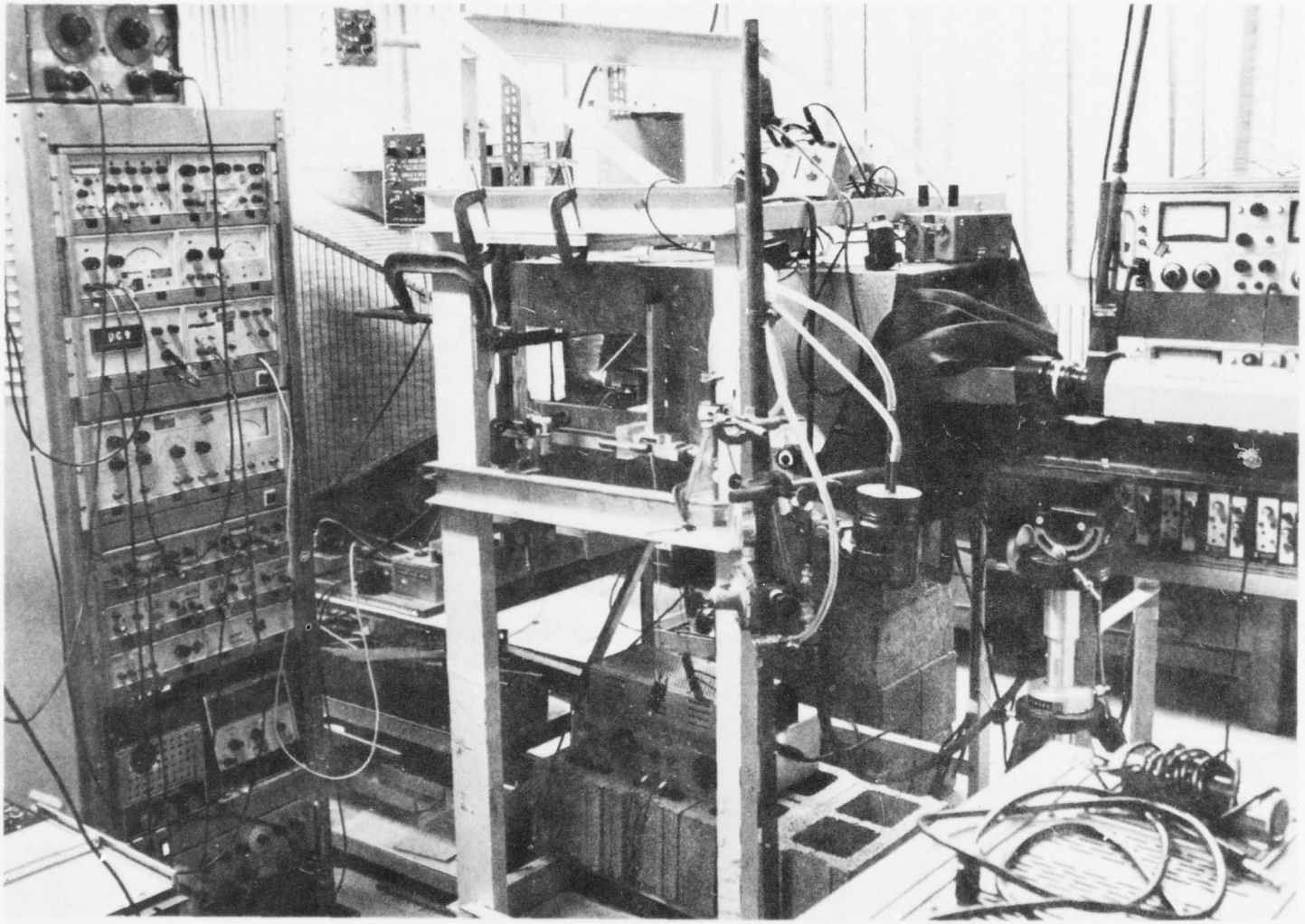

Figure 7 — A photograph of the wind tunnel and supporting equipment.

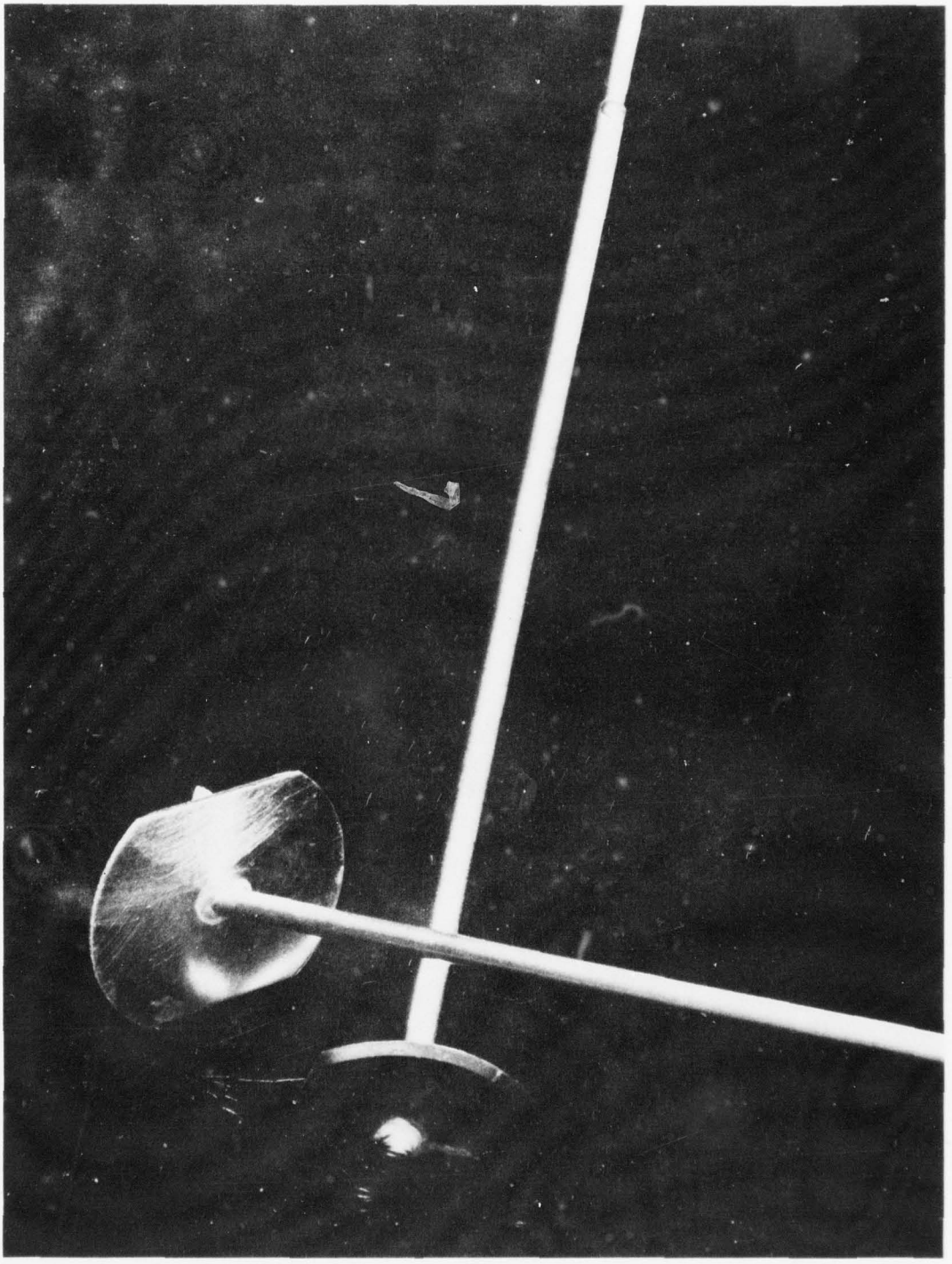

Figure 8 — A photograph of several test cylinders fitted with endplates.

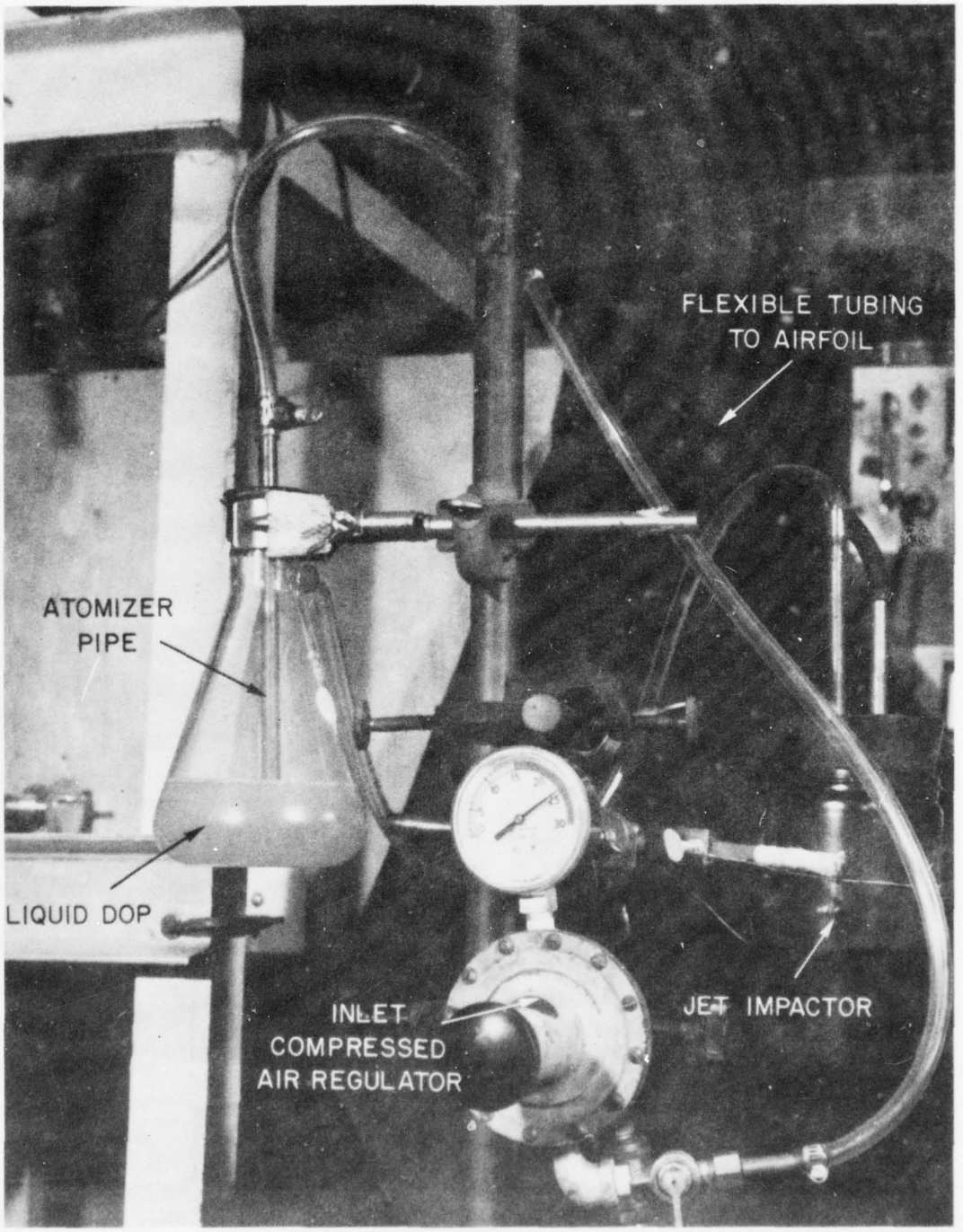

Figure 9 — A photograph of the flow visualization aerosol generator.

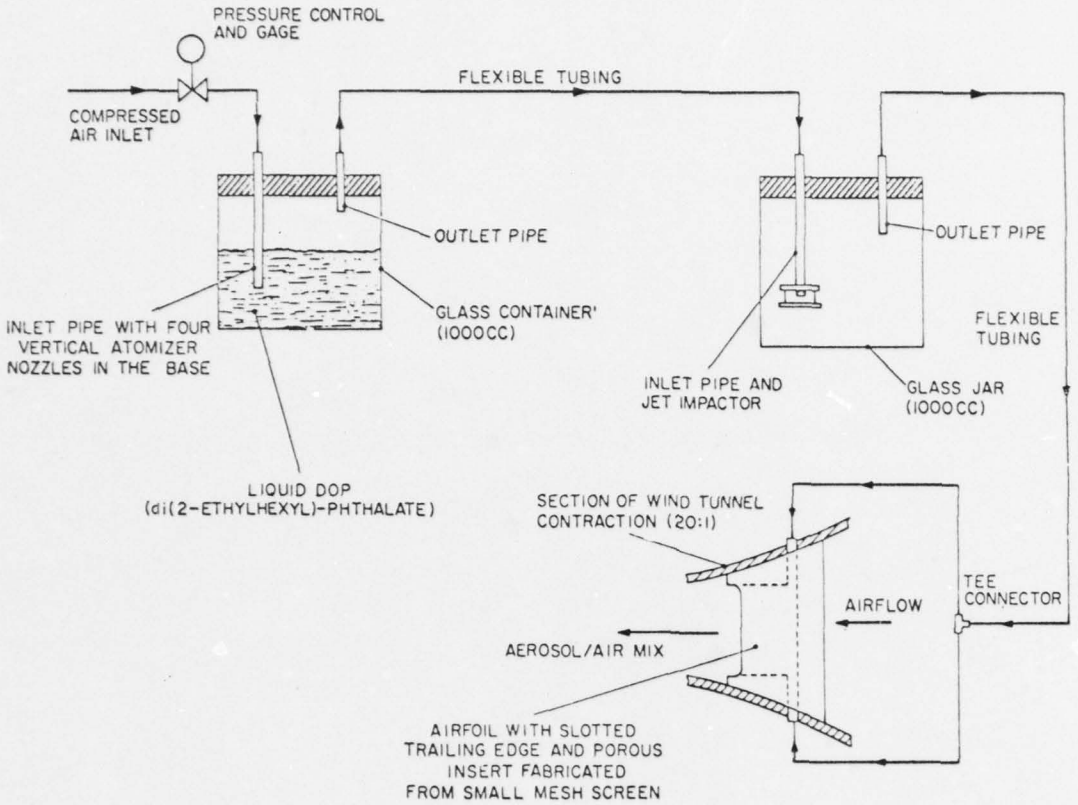

Figure 10 - A schematic of the flow visualization system.

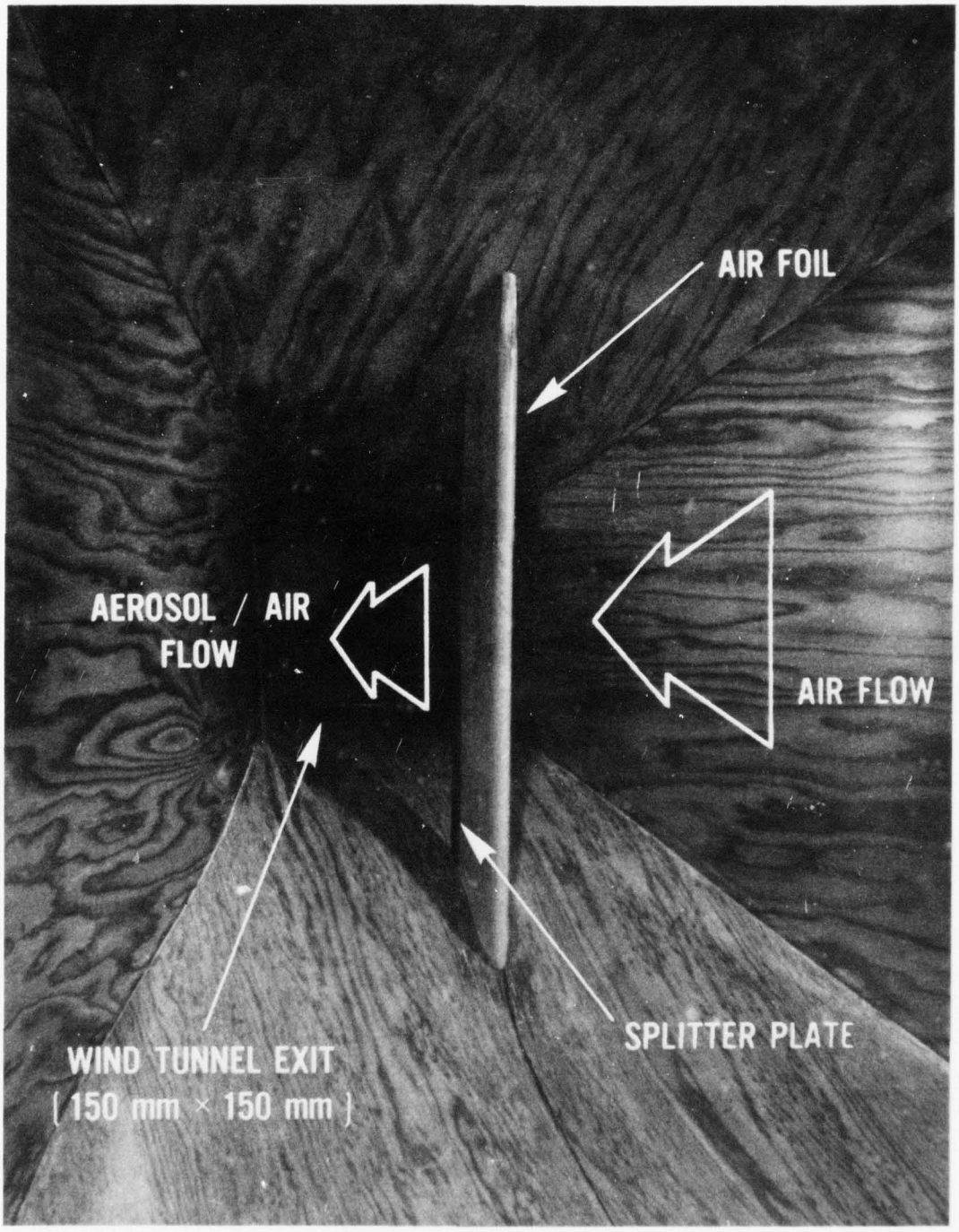

Figure 11 — A photograph of the aerosol injection airfoil mounted in the contraction section of the wind tunnel.

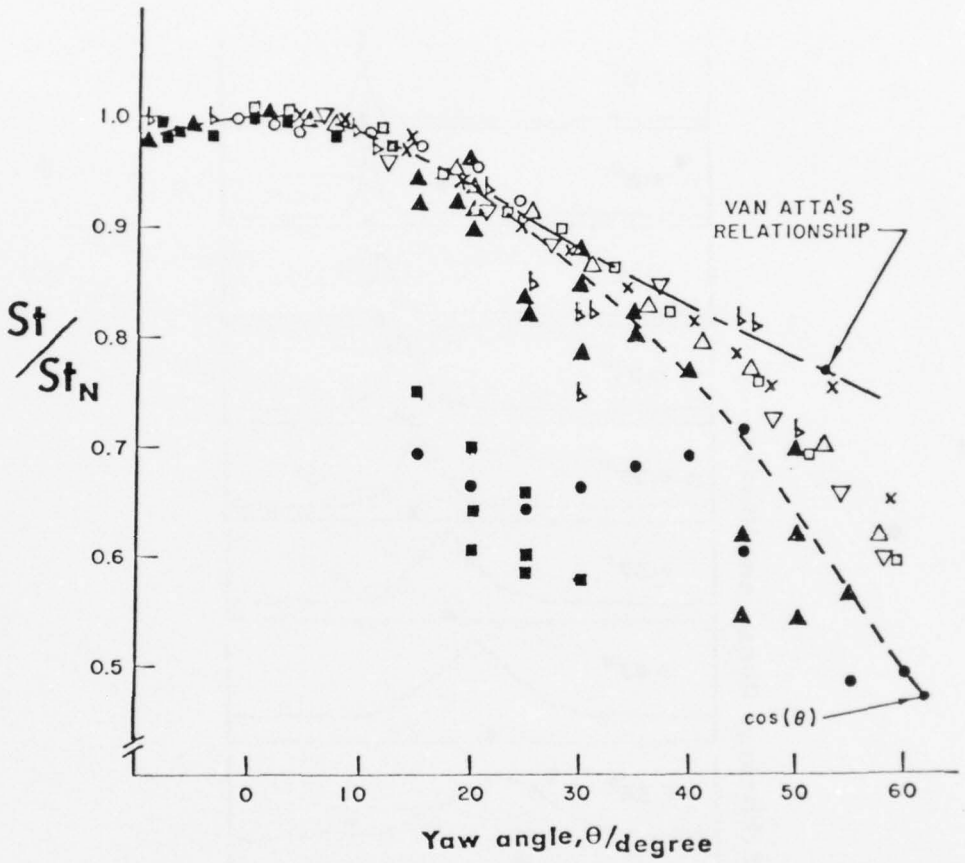

Figure 12 - A plot of the normalized Strouhal numbers as a function ofyaw angle for a variety of free-ended, inclined cylinders, $St_n = 0.212(1-A/Re_n)$.

Legend for data:

- ■ - Re = 210, L/D = 20-40
- ▷ - Re = 320, L/D = 20-40
- ▲ - Re = 460, L/D = 20-40
- o,● - Re = 160, L/D = 90
- × - Re = 460, L/D = 90
- □ - Re = 700, L/D = 90
- △ - Re = 900, L/D = 90
- ▽ - Re = 1100, L/D = 90

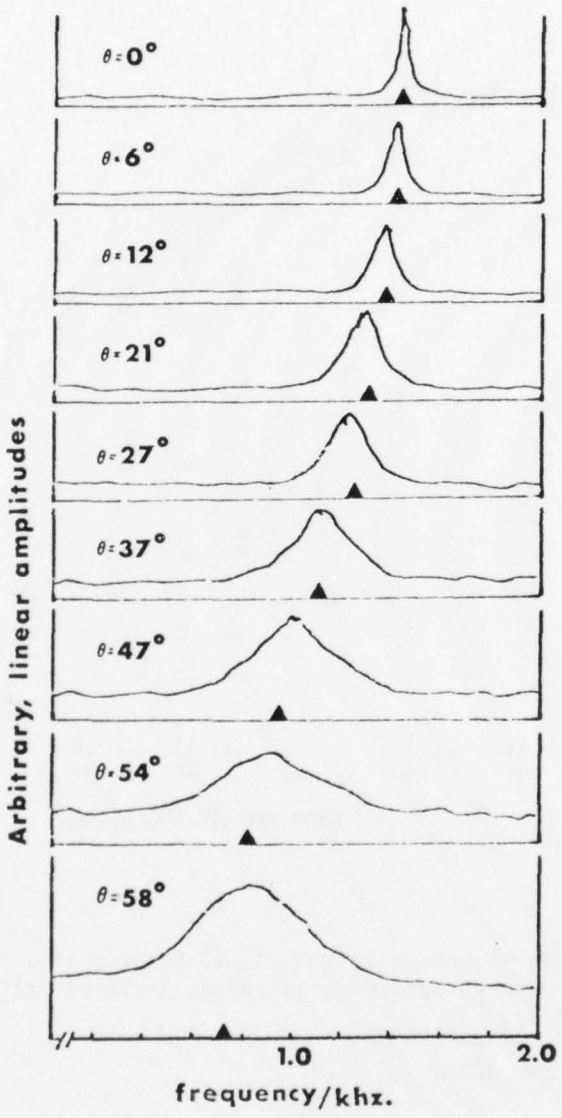

Figure.13 - Sample spectra of the fluctuating velocity corresponding to the Re = 1100 data plotted in Figure 12. The solid triangles indicate the Cosine Law prediction of the shedding frequency.

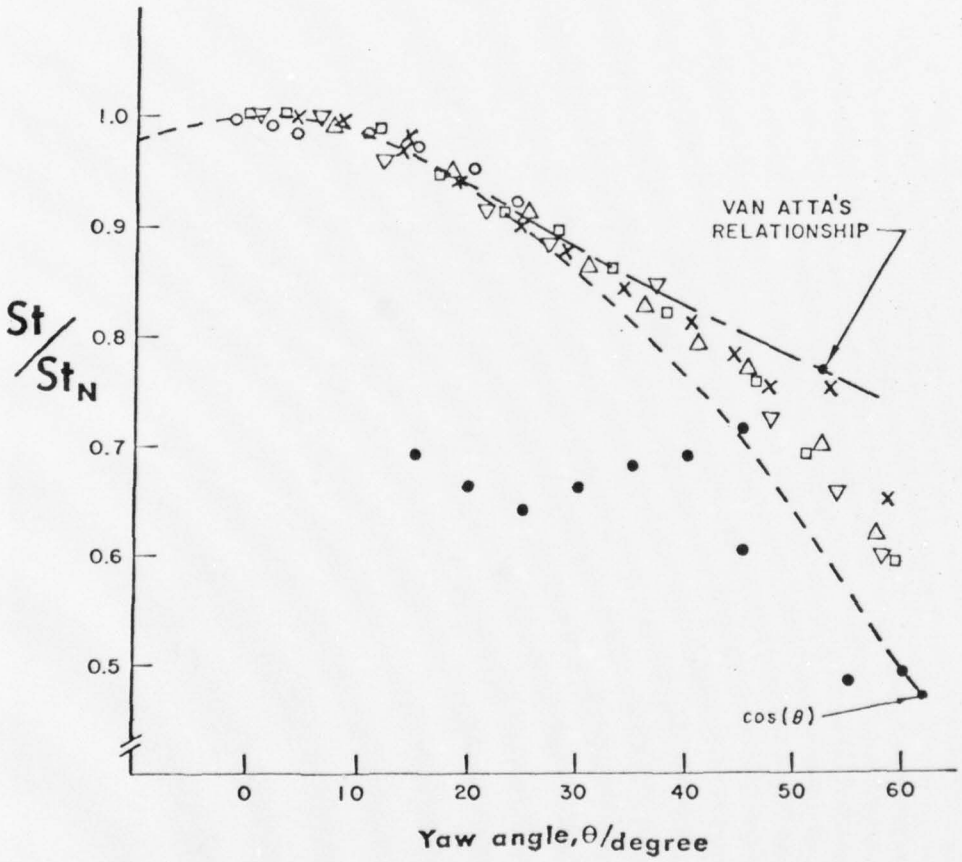

Figure 14 - A replotting of the largest aspect-ratio data from Figure 12.

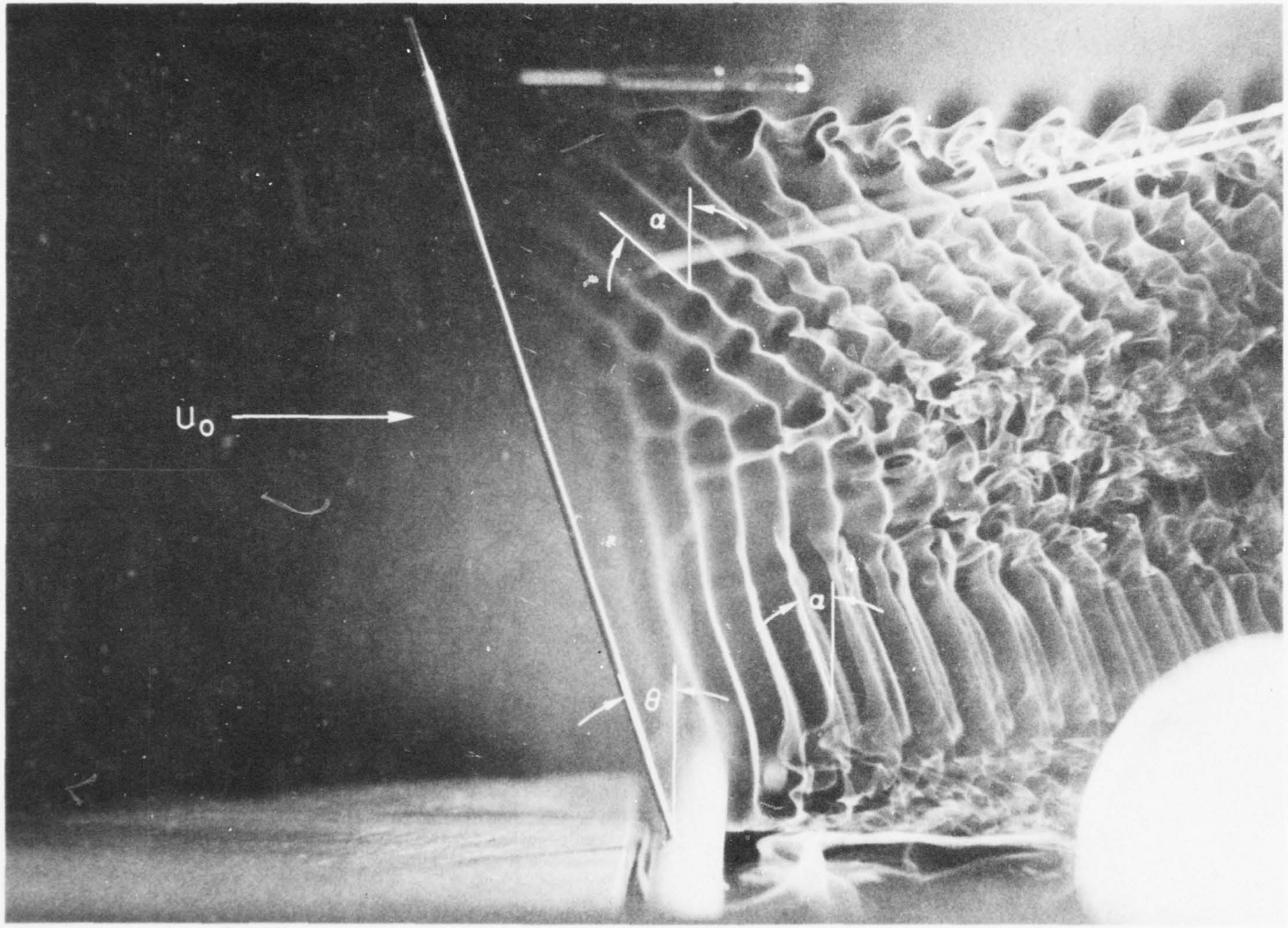

Figure 15 — A flow visualization photograph of the two modes of vortex shedding from an inclined cylinder at Re = 160.

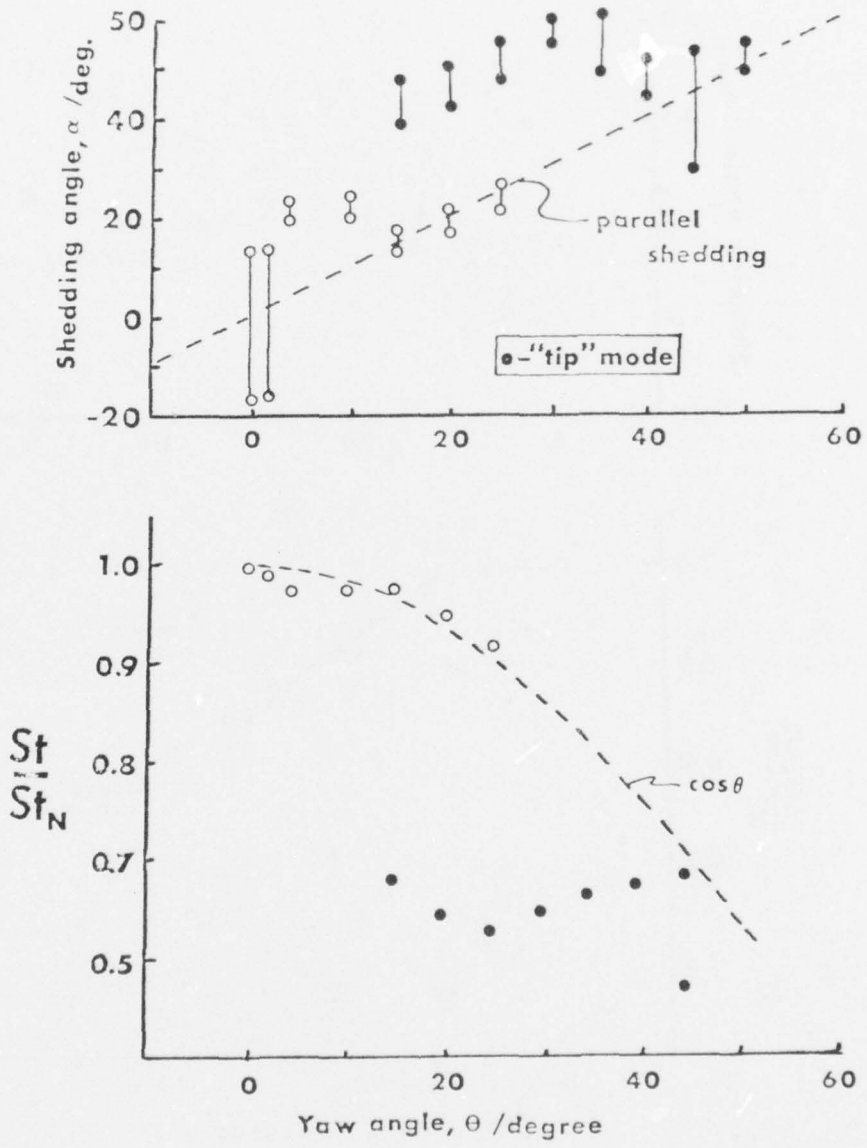

Figure 16 - A comparison of the shedding angles and shedding frequencies measured for Re = 160.
a) Shedding angle as a function of yaw angle.
b) Shedding frequency as a function of yaw angle.

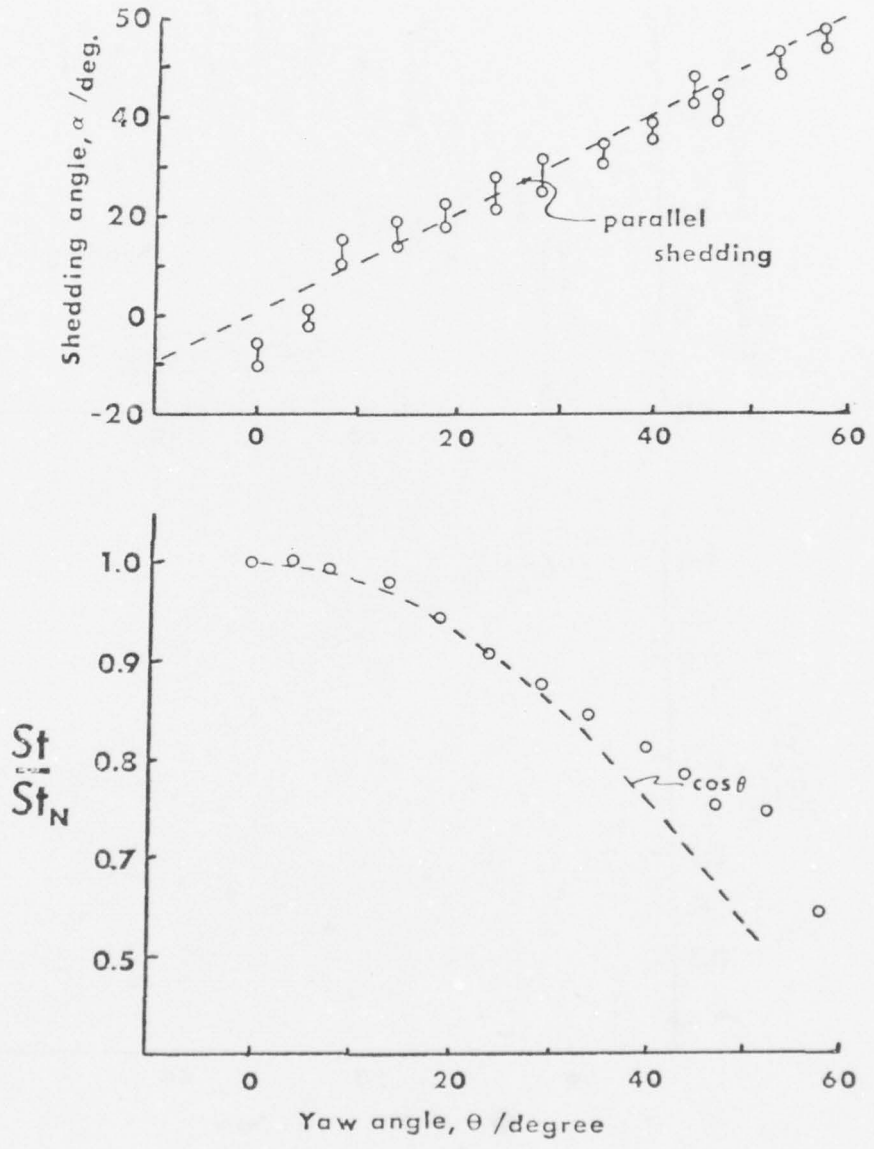

Figure 17 - A comparison of the shedding angles and shedding frequencies measured for Re = 460.
a) Shedding angle as a function of yaw angle.
b) Shedding frequency as a function of yaw angle.

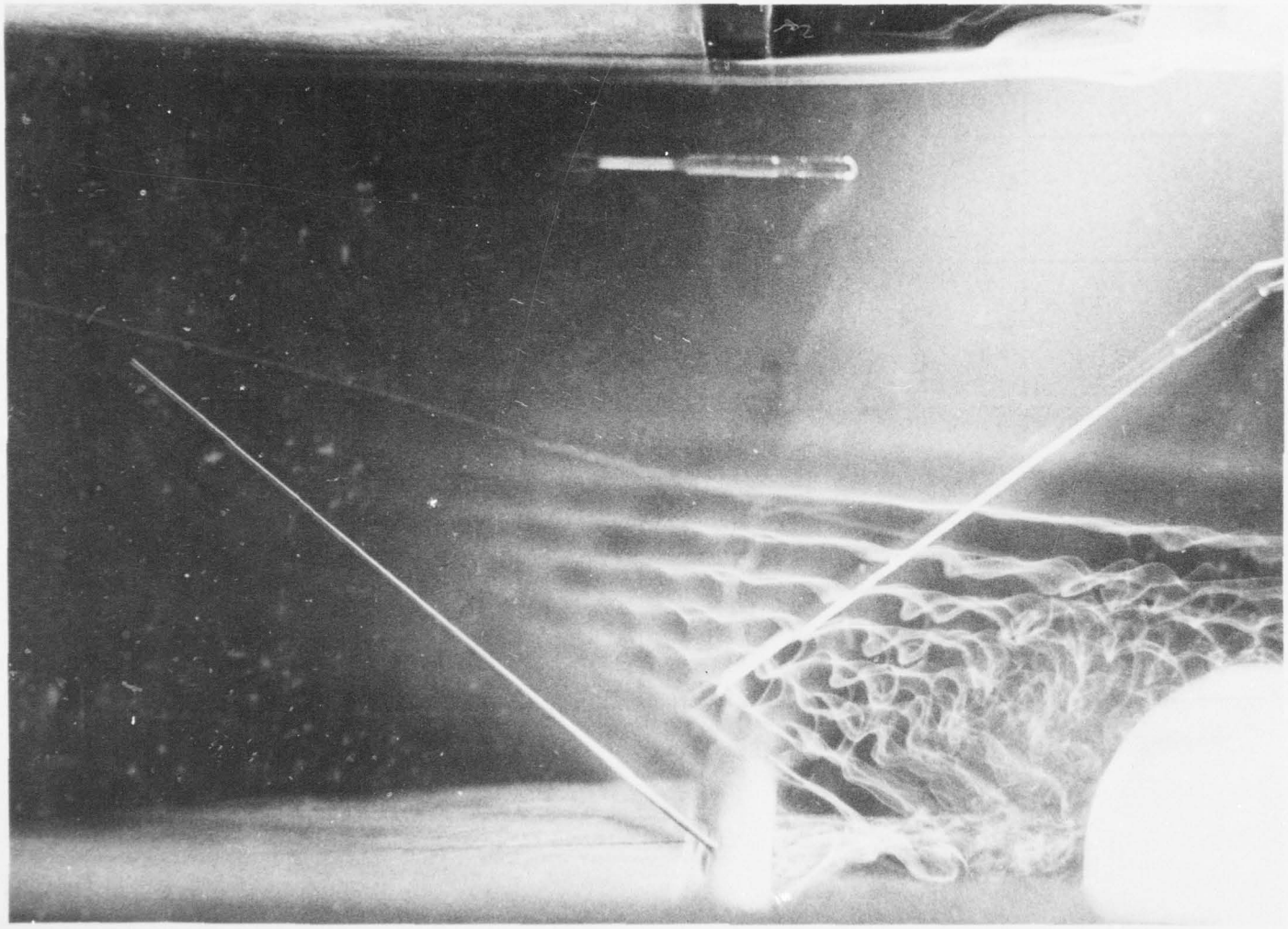

Figure 18 — A flow visualization photograph of the incipient trailing vortex pattern behind finite length yawed cylinders, for large yaw angles, at a Reynolds number, Re = 160.

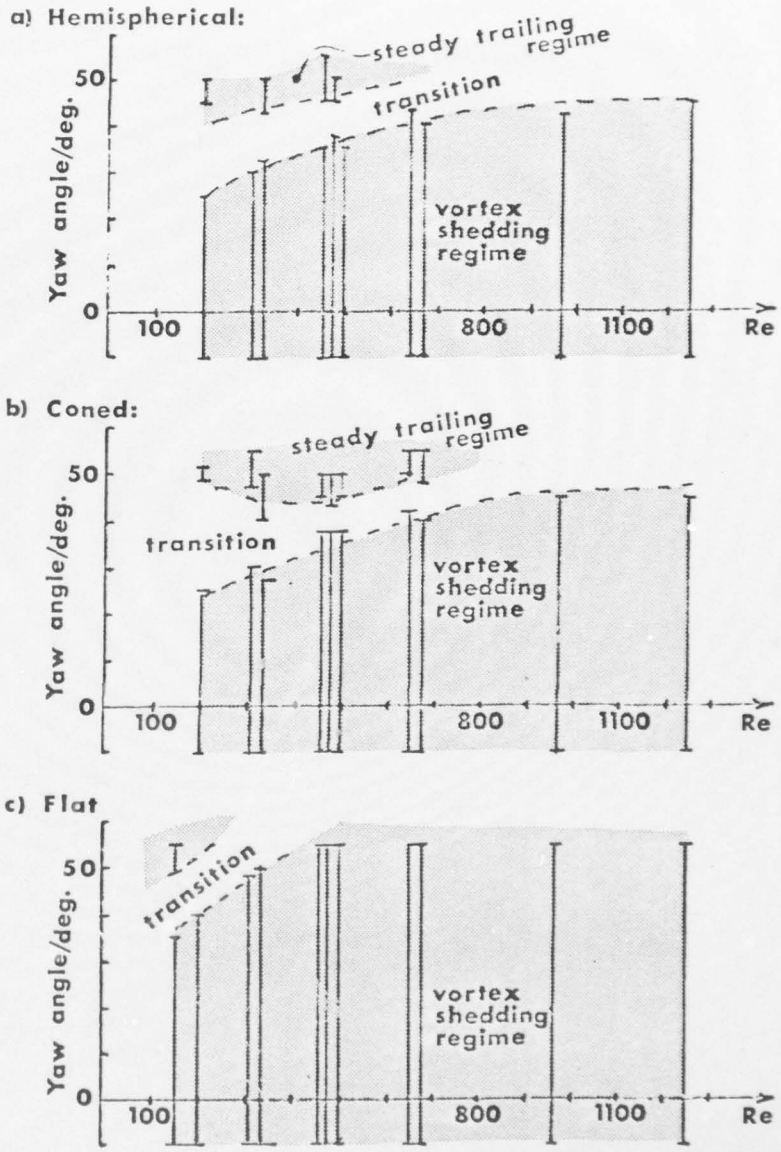

Figure 19 - Outlines of the three regimes of wake flow behind finite len
yawed cylinders.

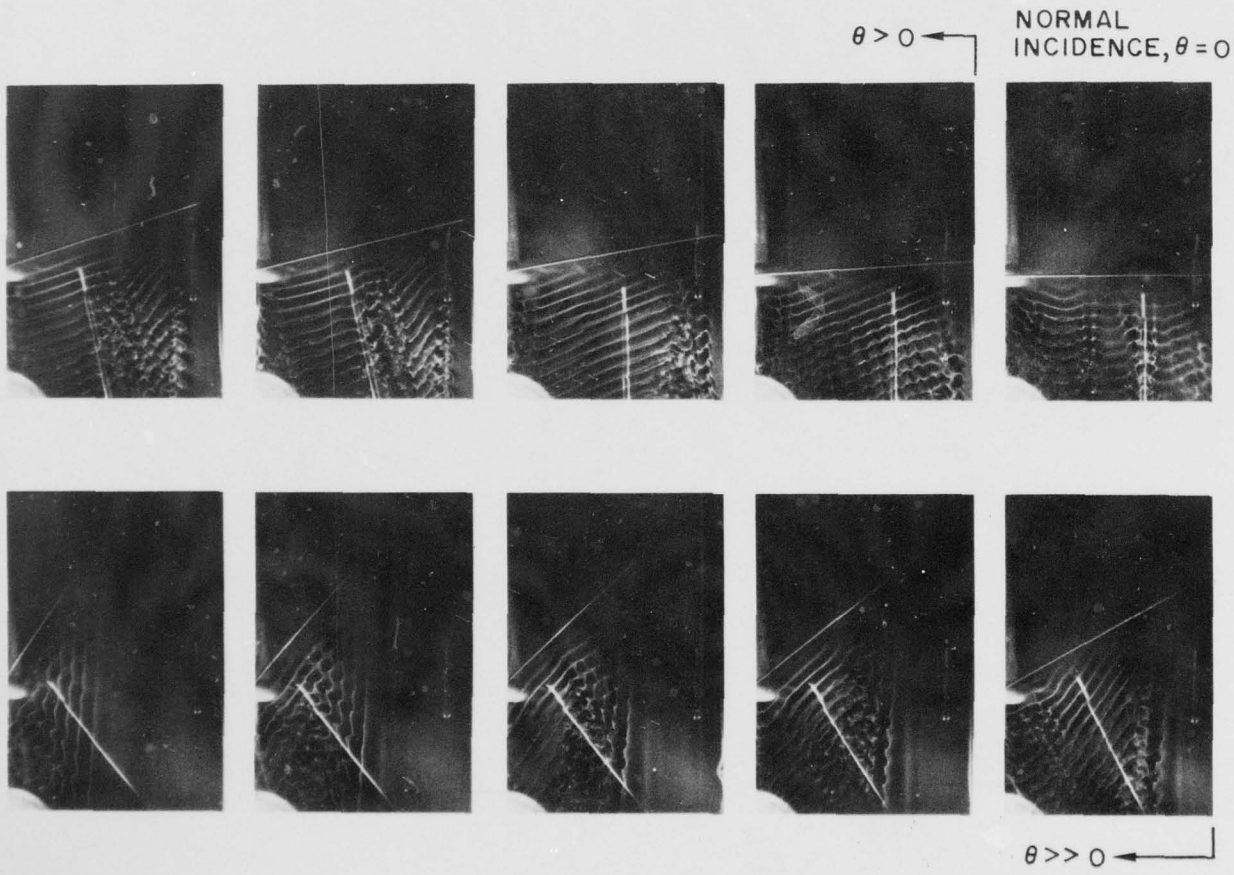
θ > 0
NORMAL
INCIDENCE, θ = 0°
θ >> 0

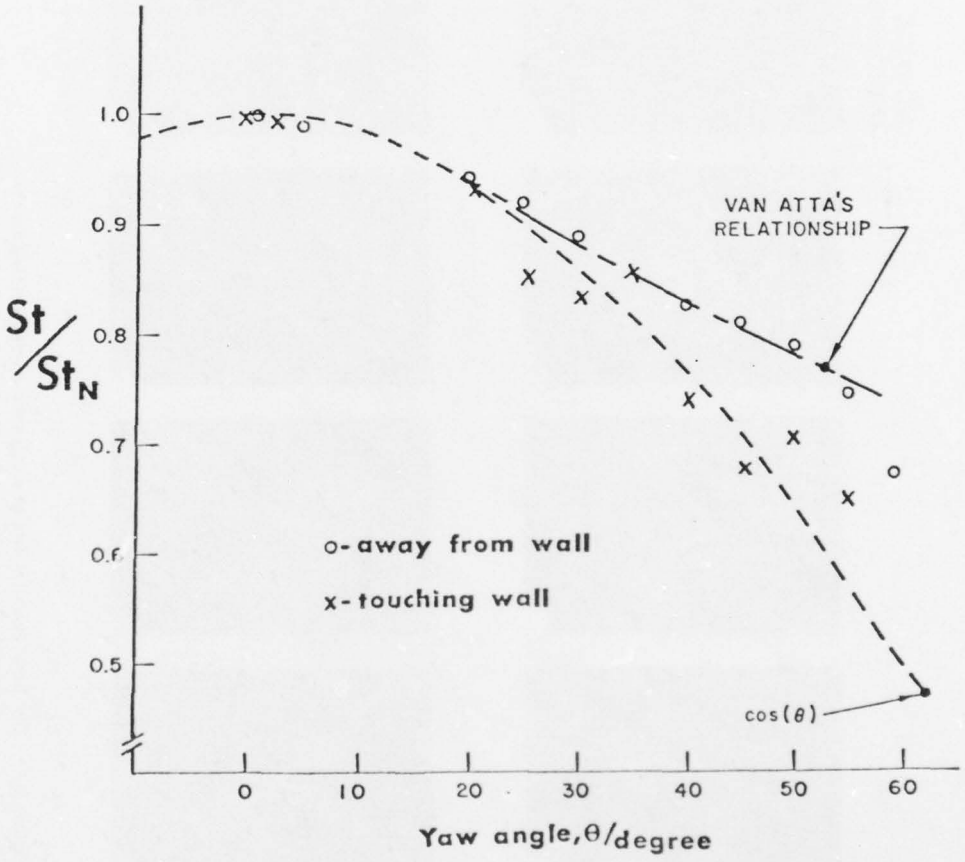

Figure 21 - A comparison of the shedding frequencies for two cylinders of nearly constant aspect ratio but slightly different free-end displacements from the wind tunnel wall, Re = 460.

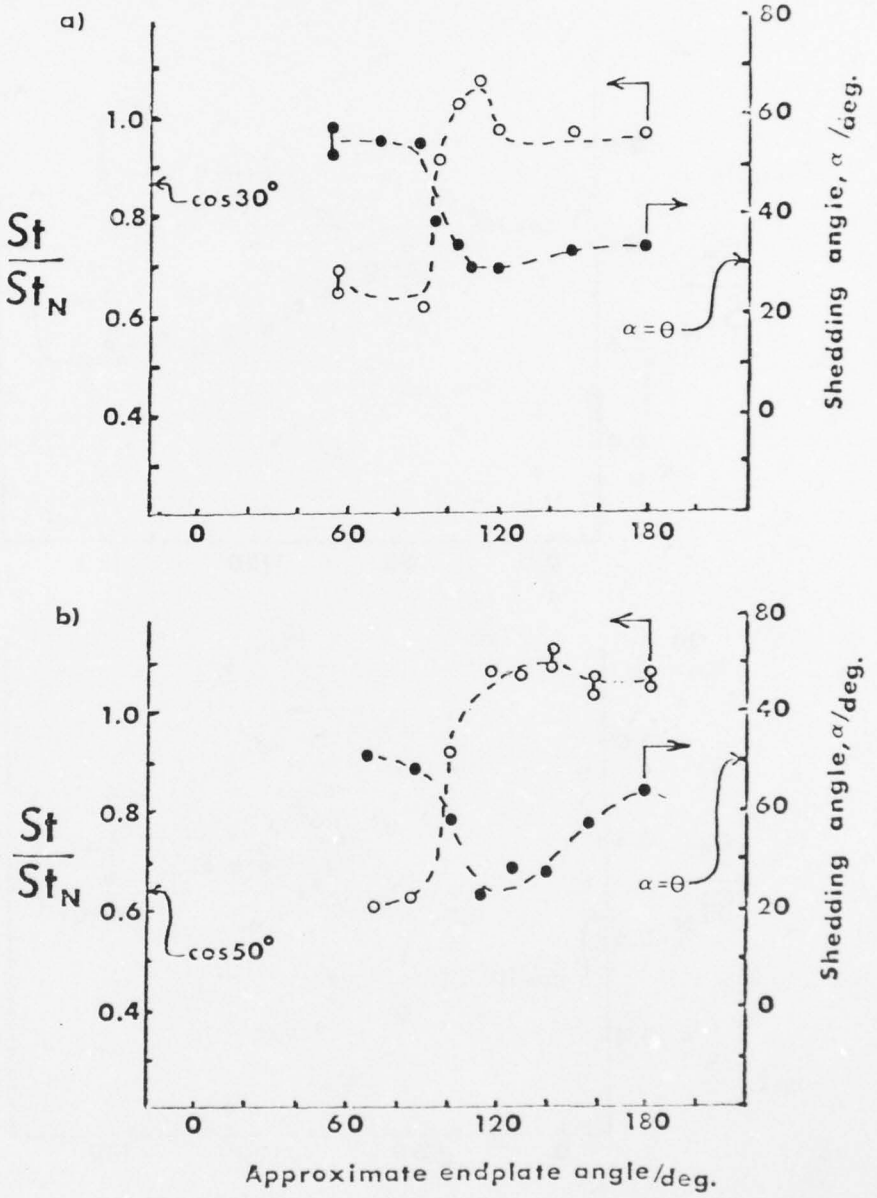

Figure 22 - The influence of endplate inclination angle upon the vortex shedding frequency and shedding angle for Re = 160.

a) Yaw angle, $\theta = 30°$.
b) Yaw angle, $\theta = 50°$.

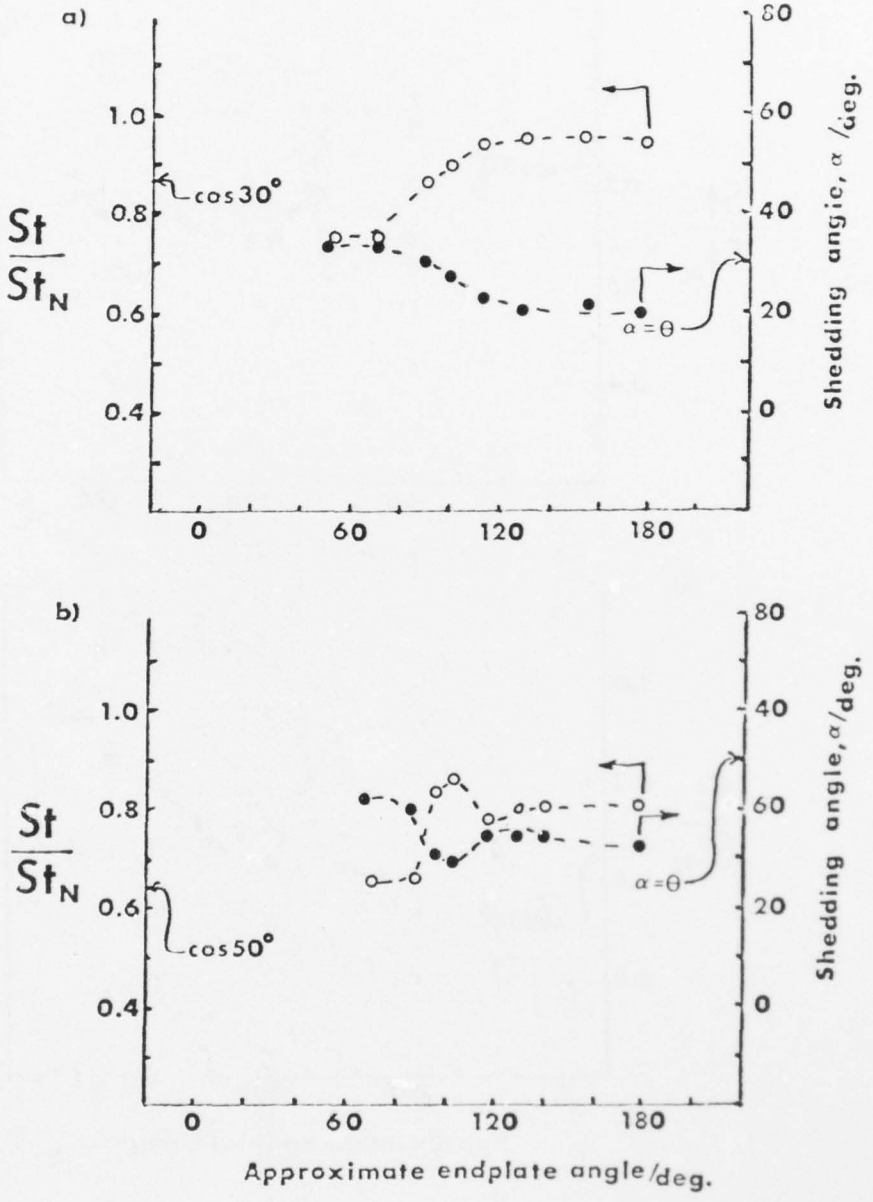

Figure 23 - The influence of endplate inclination angle upon the vortex shedding frequency and shedding angle for Re = 460.

a) Yaw angle, $\theta = 30°$.
b) Yaw angle, $\theta = 50°$.

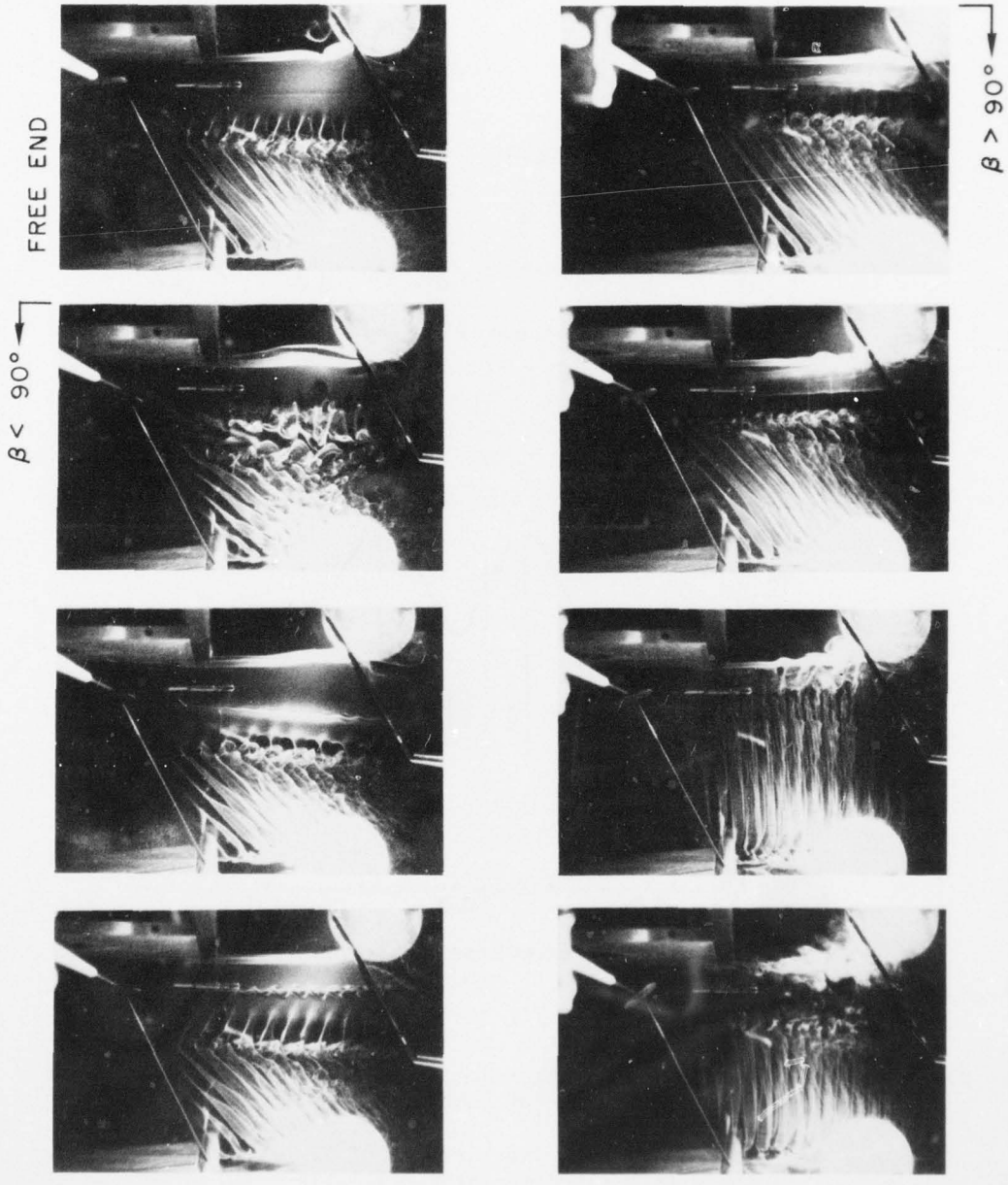

Figure 24 — A series of flow visualization photographs showing the influence of endplate angle upon the wake flow for Re = 160, and a yaw angle θ = 40°.

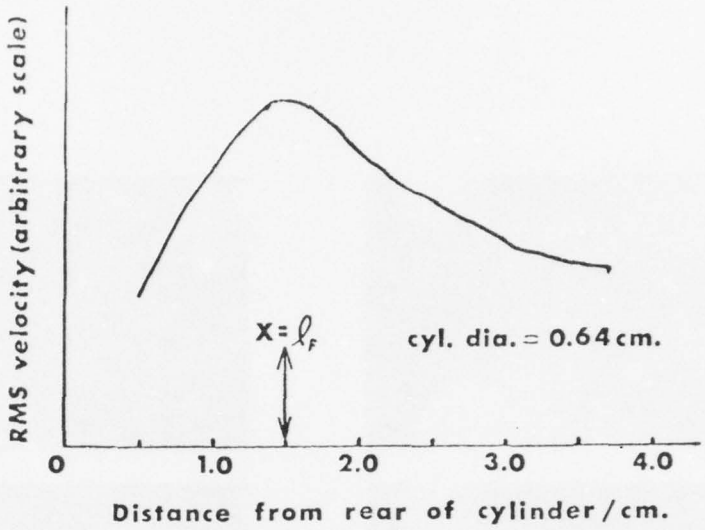

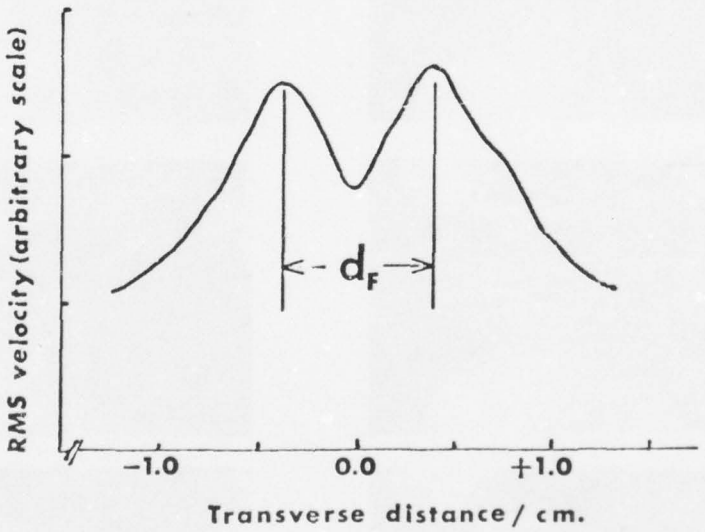

Figure 25 - Profiles of the fluctuating velocity in the wake of a stationary yawed cylinder for a Reynolds number Re_n = 425, yaw angle $\theta = 30°$.

a) The RMS velocity distribution of $2f_s$ along the wake axis with a characteristic peak at $\bar{x} = \ell_F$.

b) The RMS velocity distribution across the wake measured at $x = \ell_F$. The wake width d_F is determined from this trace.

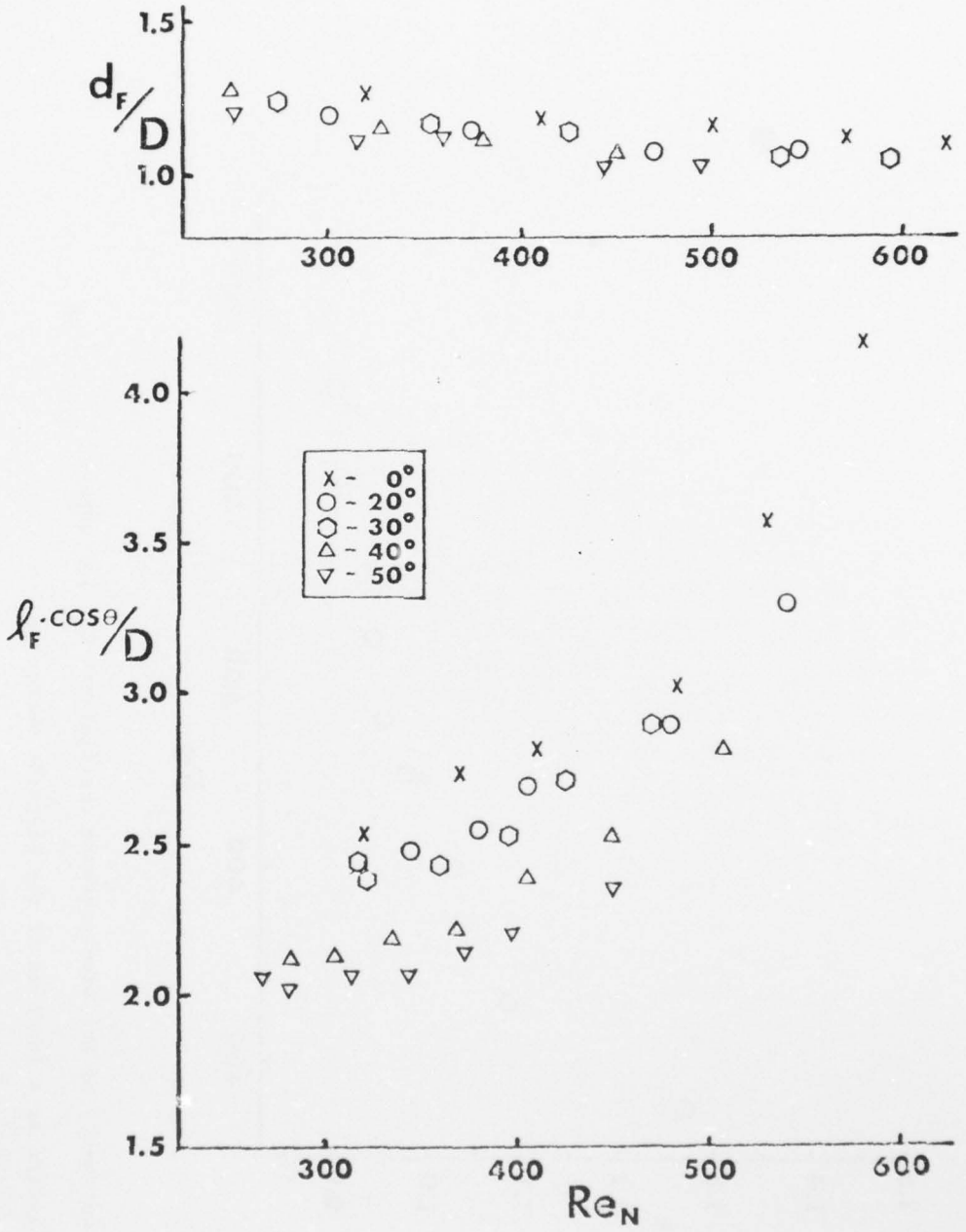

Figure 26 - The characteristic wake dimensions for yawed, stationary cylinders.

a) The wake widths.
b) The vortex formation lengths.

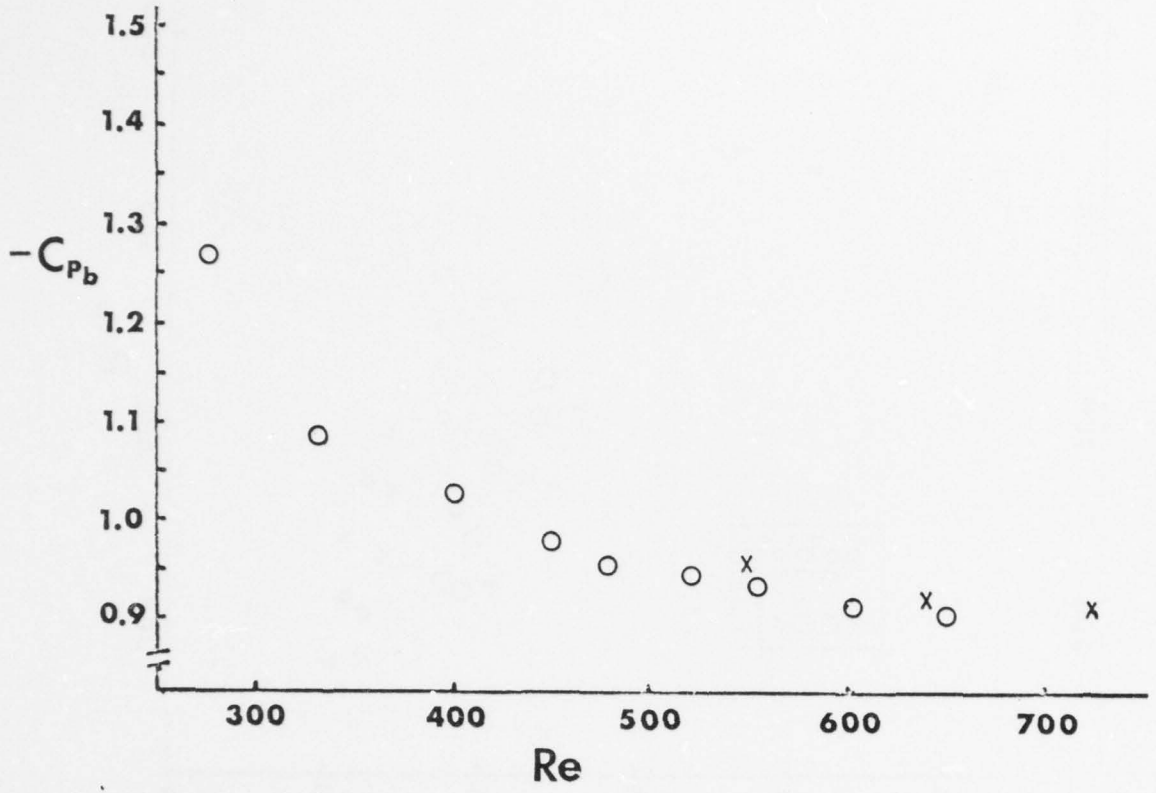

Figure 27 - Measurements of the base pressure coefficients C_{P_b} for unyawed cylinders as a function of the Reynolds number Re_n.

O - First test
X - Second test

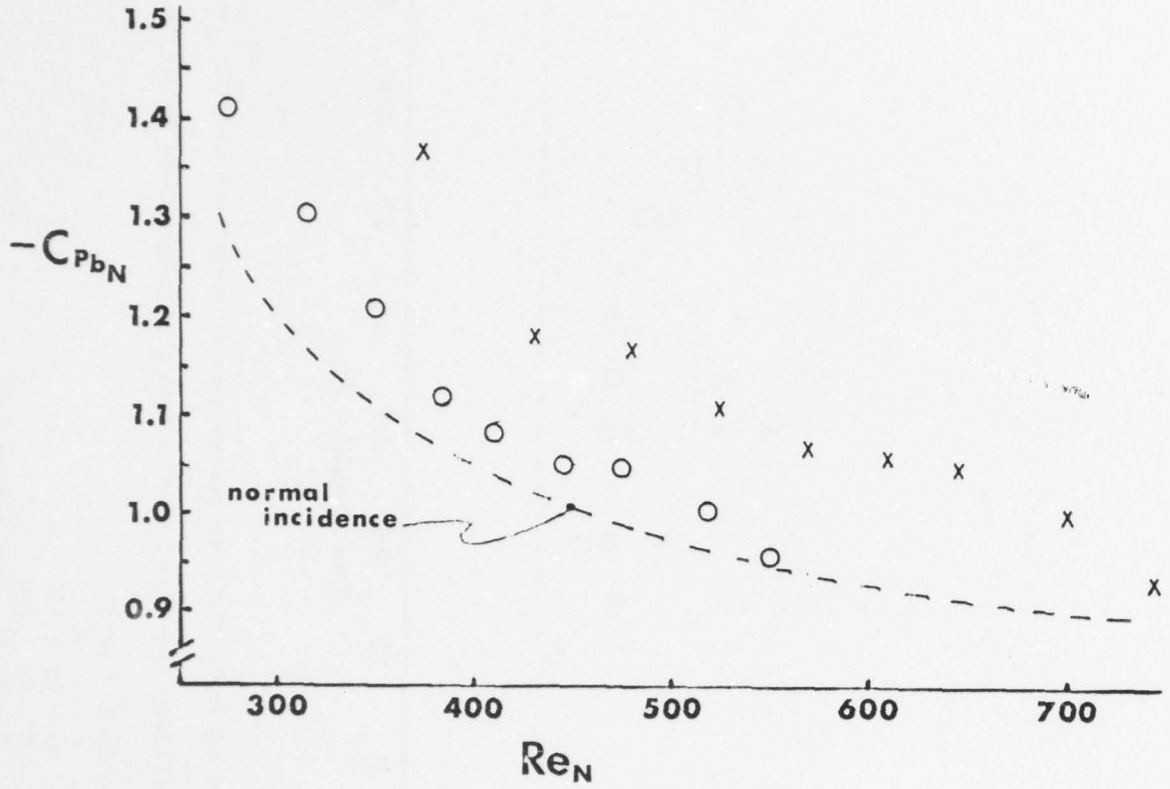

Figure 28 - Measurements of the base pressure coefficients $C_{P_{b_n}}$ for yawed cylinders as a function of the Reynolds number Re_n.

O - Re = 550
X - Re = 750

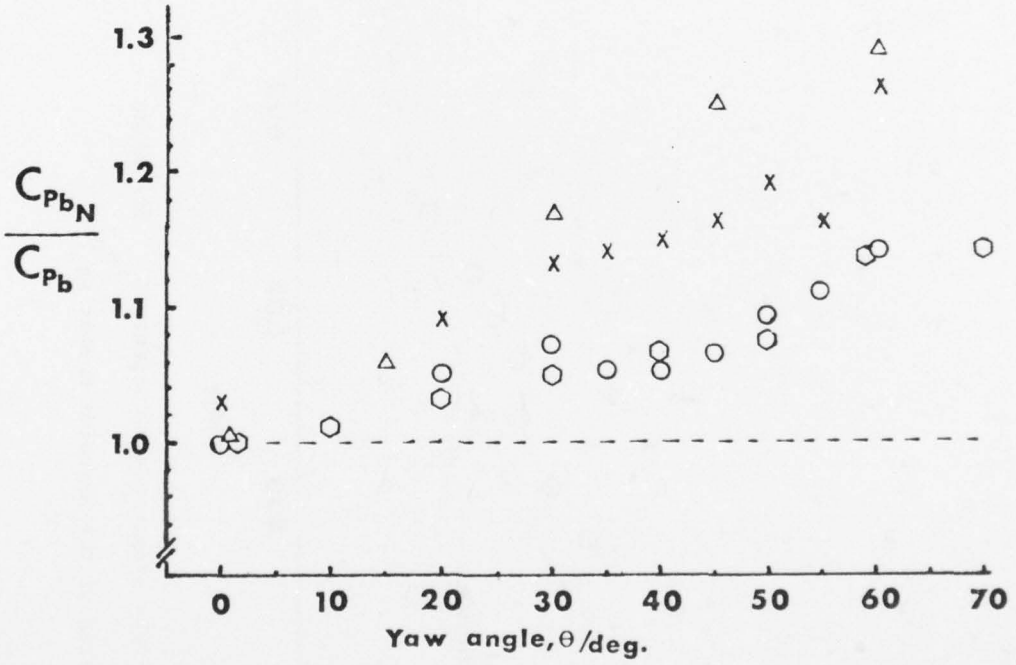

Figure 29 - The ratio of the base pressure coefficients measured for yawed cylinders to those expected from the Independence Principle.

Legend for data:

O - Re = 550
X - Re = 750
△ - Smith, Kao, & Moon [53]
⬡ - Relf & Powell [42]

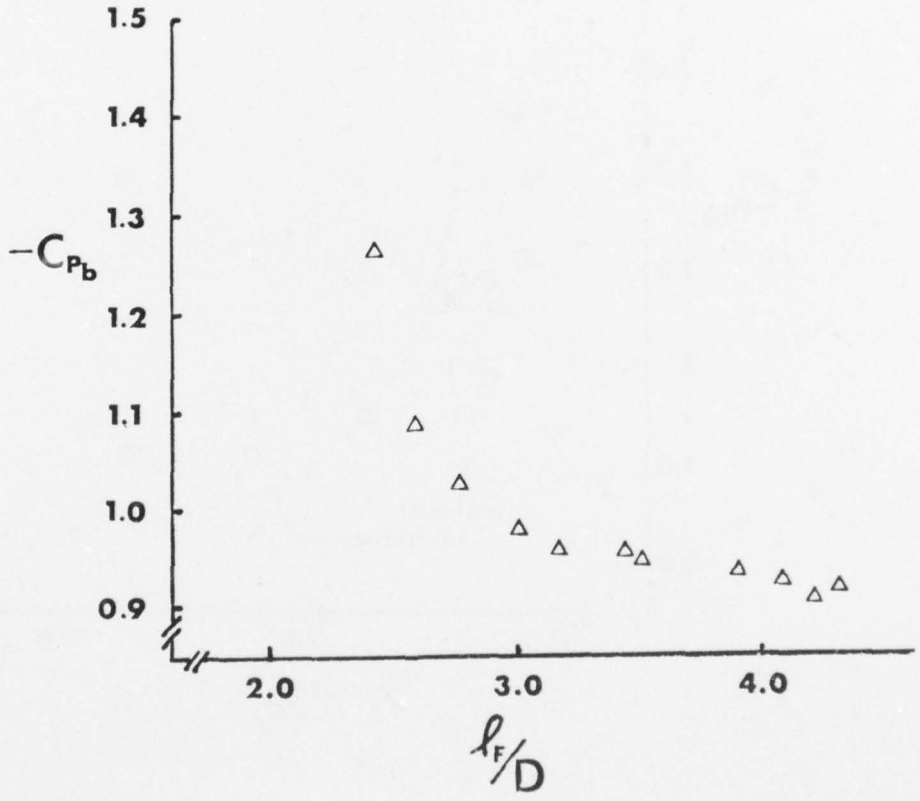

Figure 30 - The base pressure coefficient C_{P_b} plotted against the formation length ℓ_F for cylinders normal to the incident flow.

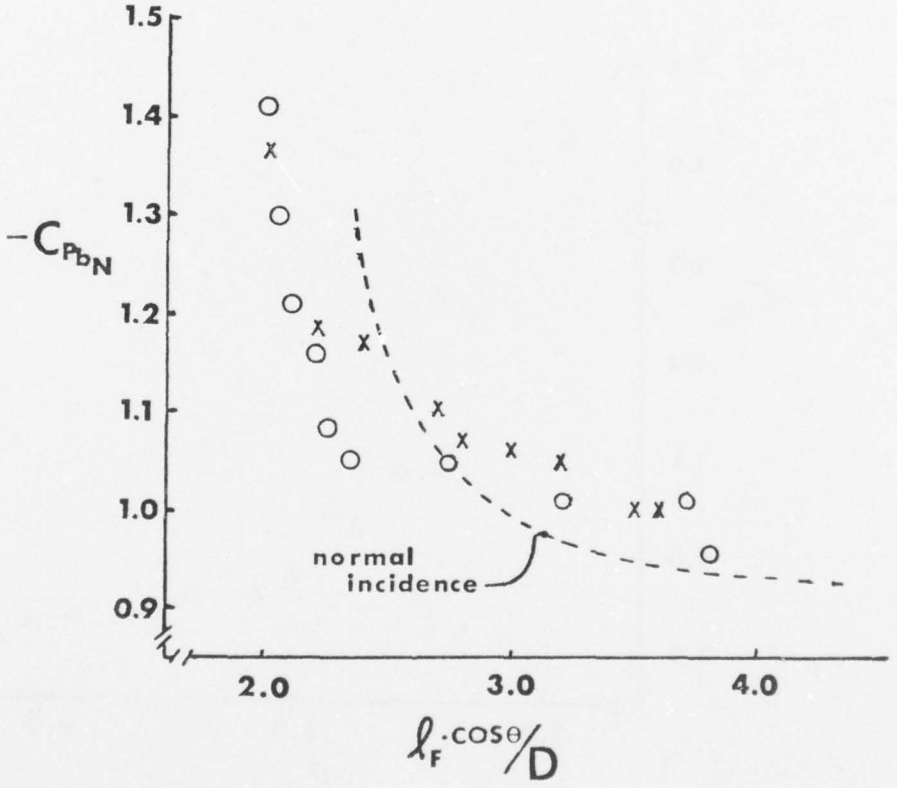

Figure 31 - The base pressure coefficients $C_{P_{b_n}}$ as a function of the formation length for yawed cylinders.

O - Re = 550
X - Re = 750

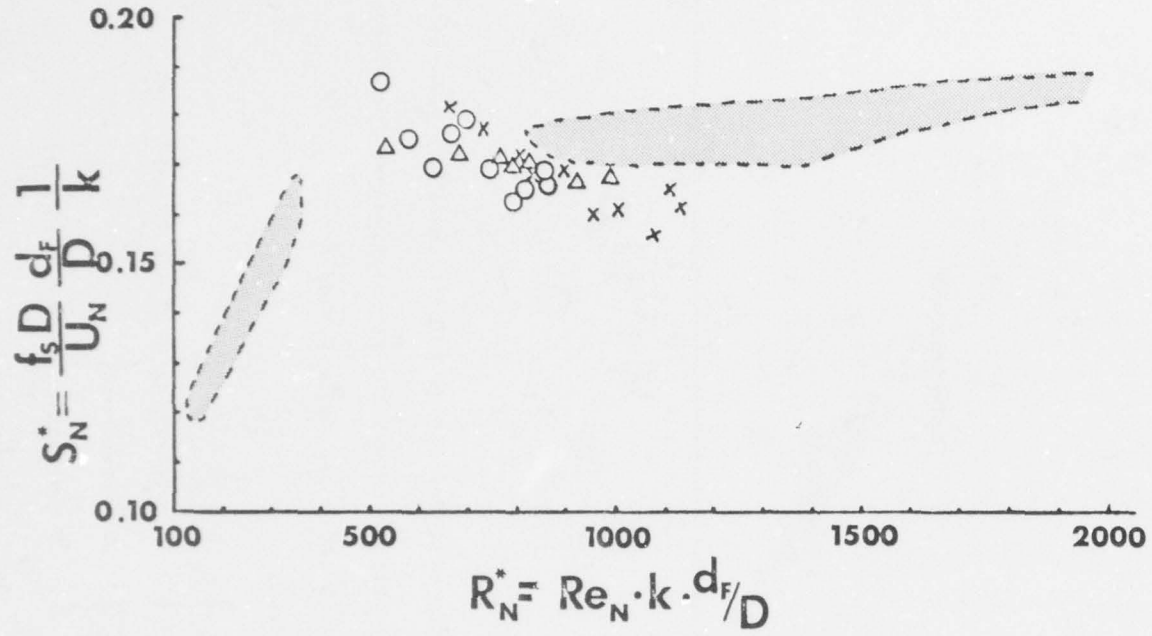

Figure 32 - The 'universal' Strouhal number S^* as a function of the Reynolds number R_n^* for yawed and unyawed bluff body flows.

Legend for data:

- △ - Unyawed, present experiments.
- O - Yawed, Re = 550, present experiments.
- X - Yawed, Re = 750, present experiments.
- ⋯ - Previous data for nominally two-dimensional bluff body flows (stationary and vibrating cylinder).

AD-A062 417 NAVAL RESEARCH LAB WASHINGTON D C F/G 20/4
THE INFLUENCE OF YAW ANGLE UPON THE VORTEX WAKES OF STATIONARY --ETC(U)
AUG 78 S E RAMBERG
UNCLASSIFIED NRL-MR-3822 SBIE-AD-E000 238 NL

2 OF 2
AD
A062417

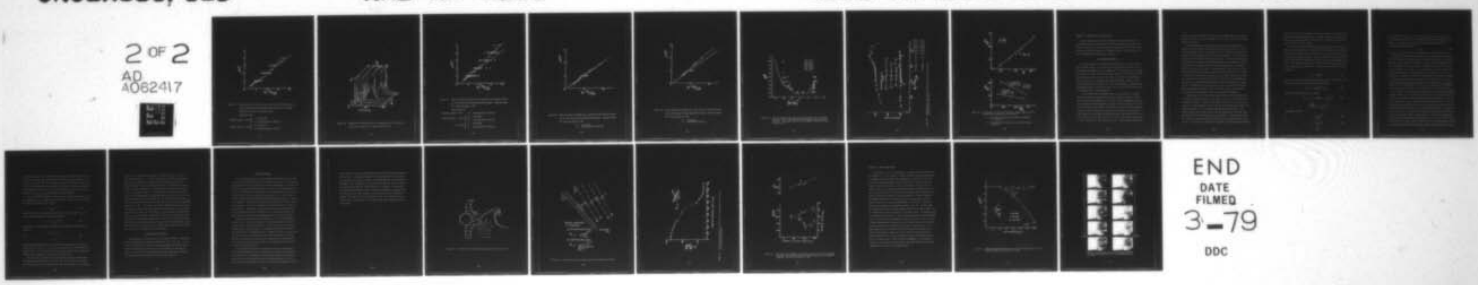

END
DATE
FILMED
3-79
DDC

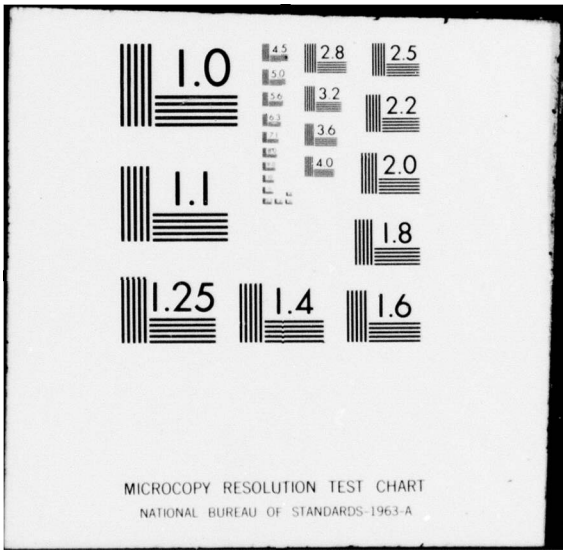
1.0
1.1
1.25
1.4
1.6
1.8
2.0
2.2
2.5
2.8
3.2
3.6
4.0
4.5
5.0
5.6
MICROCOPY RESOLUTION TEST CHART
NATIONAL BUREAU OF STANDARDS-1963-A

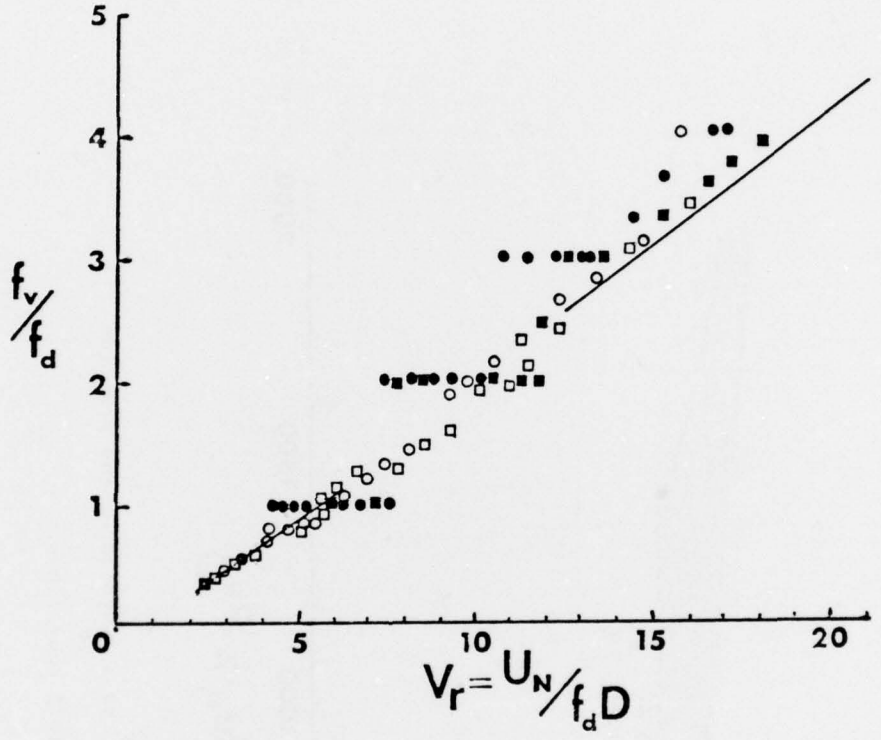

Figure 33 - Wake frequency measurements as a function of the reduced velocity V_r for stationary and vibrating yawed cylinders for a Reynolds number Re = 160 and a yaw angle $\theta = 30°$.

Legend for data:

Endplate angle, $\beta = 95°$ { o = Stationary; ● = Vibrating (a/D = 1.0D p-p)

Endplate angle, $\beta = 85°$ { □ = Stationary; ■ = Vibrating (a/D = 1.0D p-p)

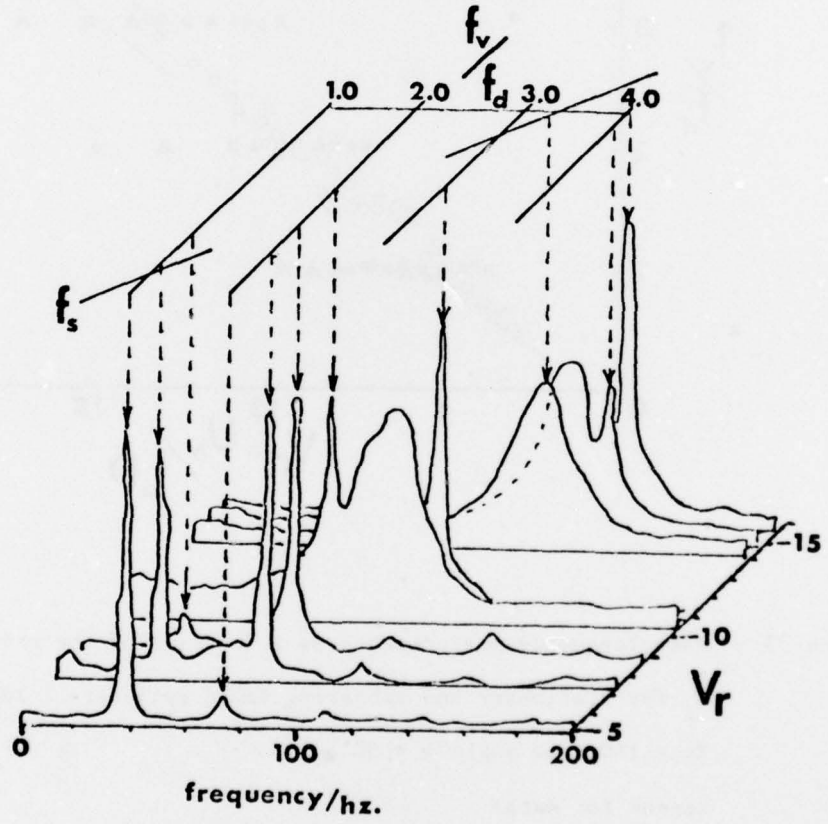

Figure 34 - Typical wake velocity spectra corresponding to the vibrating cylinder data in Figure 33. Endplate angle $\beta = 95°$.

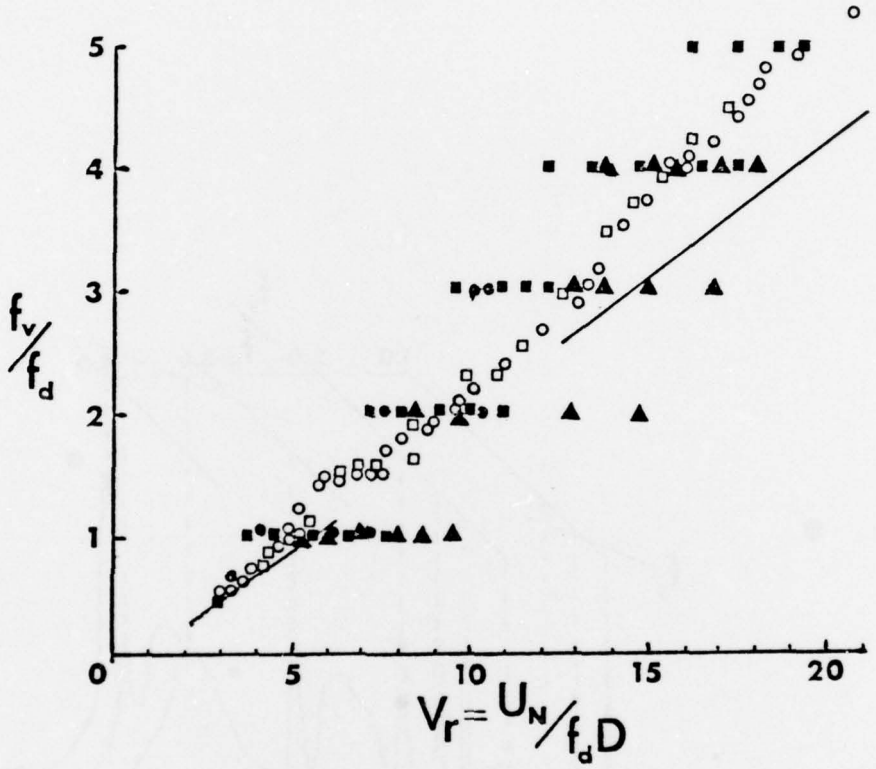

Figure 35 - Wake frequency measurements as a function of the reduced velocity V_r for stationary and vibrating yawed cylinders. Reynolds number Re = 160, yaw angle $\theta = 50°$.

Legend for data:

Endplate angle, $\beta = 85°$ ▲ - Vibrating (a/D =1.0D p-p)

Endplate angle, $\beta = 105°$ { □ - Stationary; ■ - Vibrating (a/D =1.0D p-p)

free-end { o - Stationary; • - Vibrating (a/D =1.0D p-p)

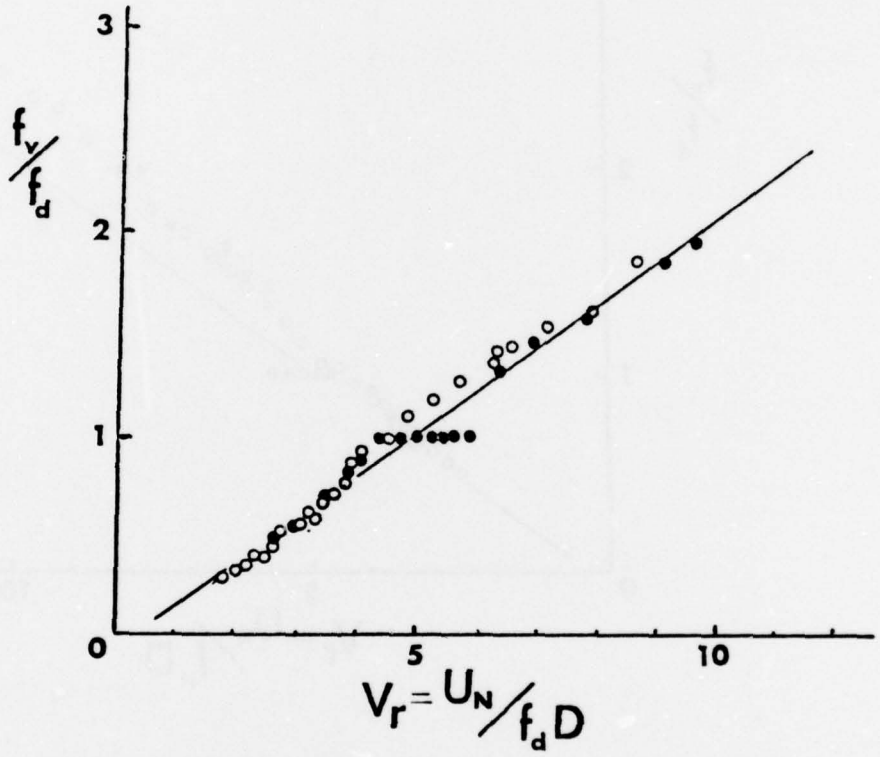

Figure 36 - Wake frequency measurements as a function of the reduced velocity V_r for stationary and vibrating yawed cylinders. Reynolds number Re = 460, yaw angle $\theta = 30°$.

o - Stationary
• - Vibrating (a/D =0.15D p-p)

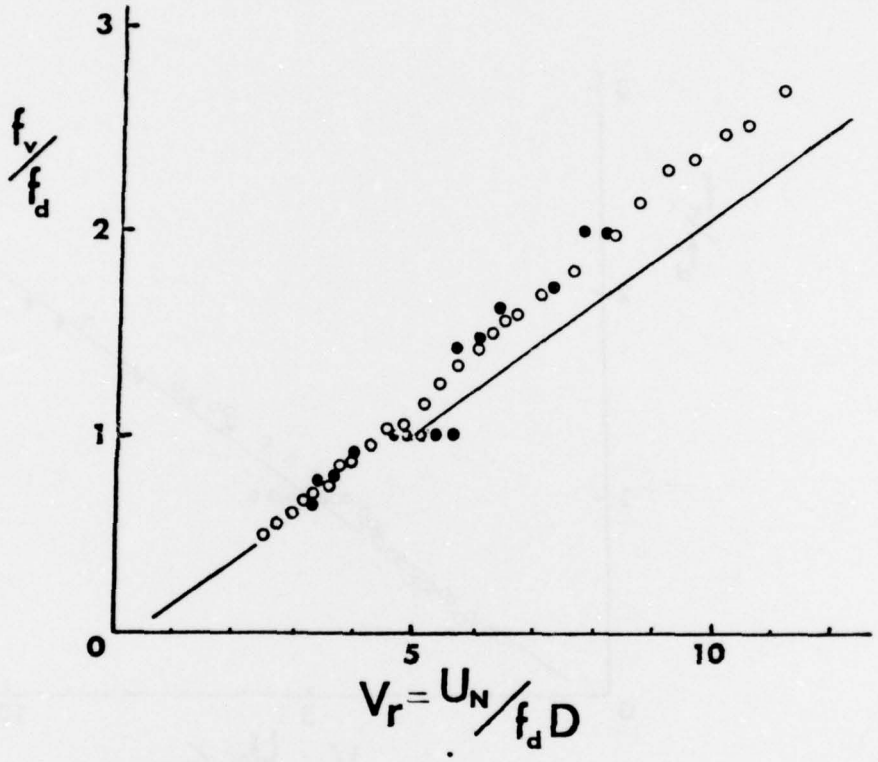

Figure 37 - Wake frequency measurements as a function of the reduced velocity V_r for stationary and vibrating yawed cylinders. Reynolds number Re = 460, yaw angle $\theta = 50°$.

o - stationary
• - vibrating (0.15D p-p)

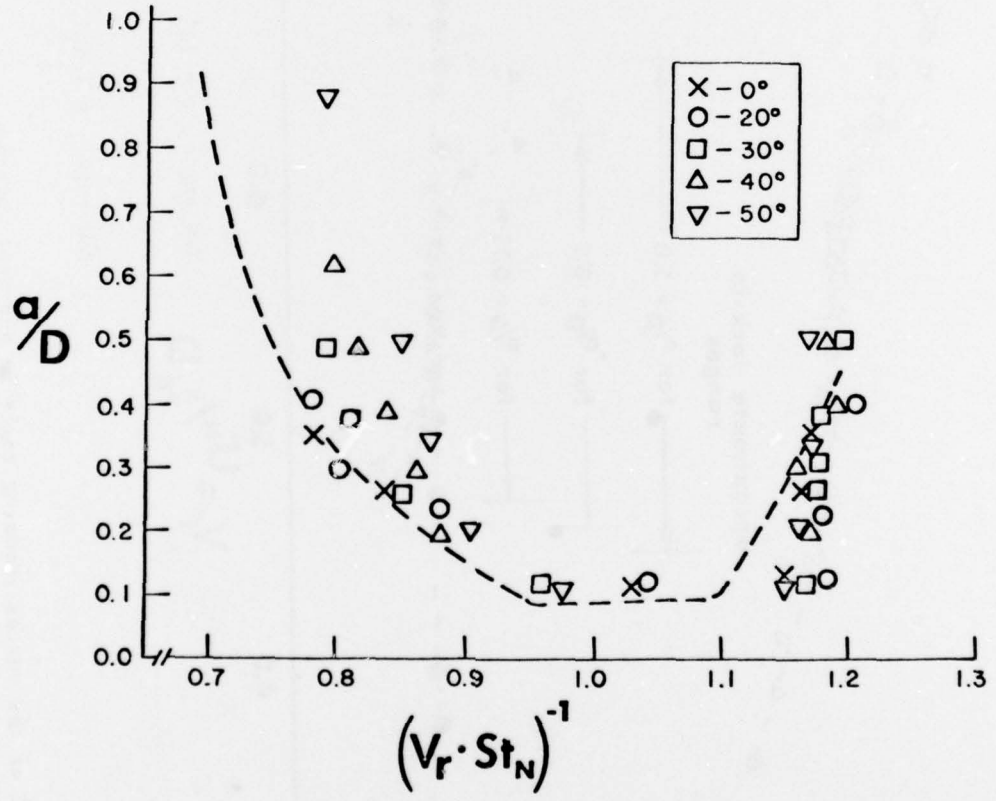

Figure 38 - Lock-in boundaries for vibrating yawed cylinders for a Reynolds number Re = 460. Wake capture occurs inside the area bounded by the data. The dashed lines are for the normal incidence cylinder from Ref. [3].

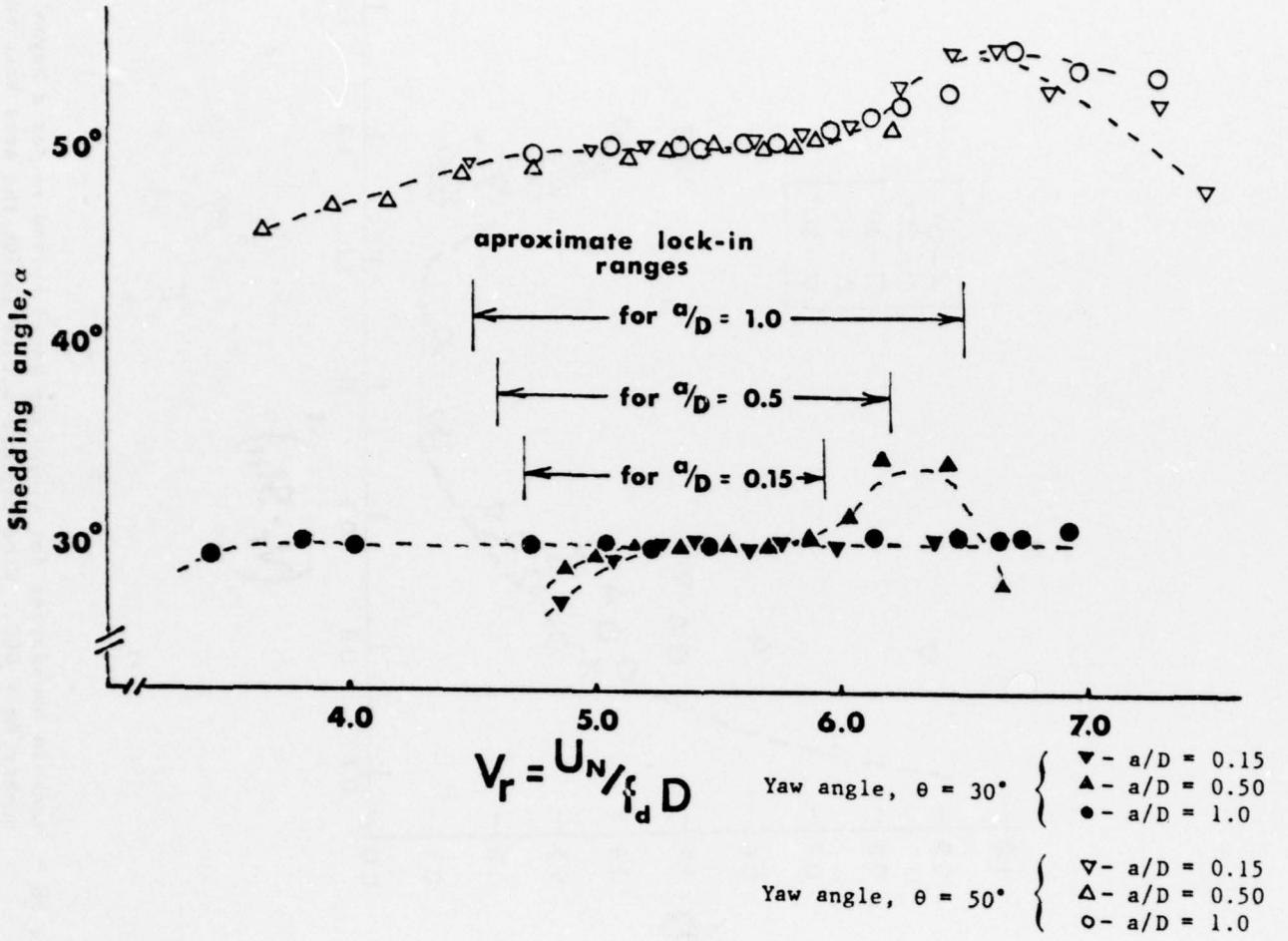

Figure 39 - Measurements of the vortex shedding angle in and near lock-in. Reynolds number Re = 460.

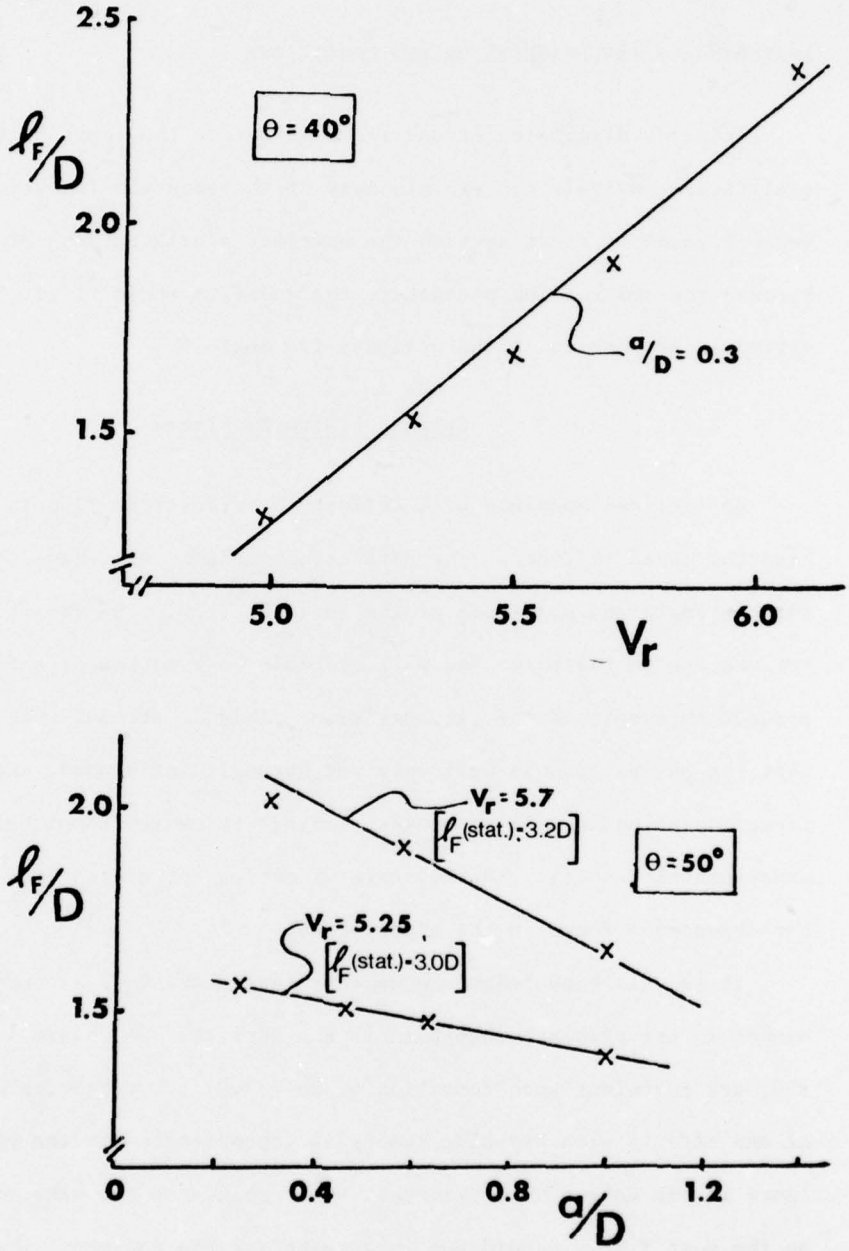

Figure 40 - Measurements of the vortex formation region length ℓ_F for vibrating yawed cylinders as a function of

a) the reduced velocity V_r (at constant amplitude of vibration,

b) the amplitude of vibration (at constant reduced velocity).

APPENDIX A - INFLUENCE(s) OF END CONDITIONS

An exact discussion of end flows is beyond the scope of this study but a qualitative analysis can explain many of the observed features. The most convenient place to start is with the endplate configurations of the present study because the controlling parameter, the endplate angle β, is obvious and can be varied independently of the cylinder yaw angle θ.

Cylinders With Endplates

An inclined endplate will deflect the freestream flow in front of and behind the yawed cylinder. The deflection in front will have the effect of varying the angle and magnitude of the incident flow. The variations will be greatest nearest to the plate and will decrease to a matter of a few degrees or a few percent over most of the cylinder span. This is at odds with the observation that the entire span is uniformly and strongly influenced. Moreover, the deflection influence will be weakest for $\beta \approx 90°$ which completely contradicts the experimental results. Lastly, this effect cannot account for the Reynolds number dependence found in the experiments.

It is well-known that the wake processes are very dependent on Reynolds number in the present range because the vortices, which are laminar below Re $\approx$ 150, are turbulent upon formation by Re $\approx$ 300. Thus the diminishing influence of end effects with Reynolds number is concomitant with the transition to turbulence in the wake of the cylinder. This points to the wake formation processes as the most likely candidates to account for the influence of end conditions. A simple deflection of the wake flow may explain some of the observations but, as in the deflection of the flow in front, it is not a strong enough influence near $\beta \approx 90°$ to effect most of the changes that occur. A more promising explanation

involves the interaction between the flow over the endplate and the base region flow of the cylinder. This will be taken up after a brief discussion of the base region flow structure.

In two-dimensional bluff body flows the base region is bounded by the oscillating free shear layers that alternately roll-up to form vortices. During the vortex formation process outer potential fluid is swept into the forming vortex street as shown schematically in the sketch of Figure A1. At any instant all velocities are contained in the plane of the figure. In contrast, the yawed cylinder base flow is inherently three-dimensional owing to the additional spanwise vorticity and the changing direction of the freestream flow as it accelerates around the cylinder and its wake. The complex nature of this flow can be seen in the flow visualization photographs taken by King [32] and Chiu [8]. An attempt to illustrate the major features of this flow in a sketch is presented in Figure A2. One feature of the sketch is the "fan" or "spiral" of the flow magnitudes and directions at separation which can influence the wake formation in a number of ways. For example, the outer potential flow that is swept into the forming wake will have axial components. Also, the vorticity within the shear layer has a directional distribution as well as a distribution of magnitude.

Another aspect of the sketch is an axial flow within the base region which is intuitively expected and is, in fact, equal to $U_t = U_o \sin \theta$ according to the Independence Principle. Whether the base flow is equal to U_t or to some other value is of lesser importance than the fact that it must exist and it ought to be "down" the cylinder. If the flow about an infinitely long cylinder is to be matched using a finite length cylinder then the spanwise flow in the base region must be provided by the termination(s) of the cylinder. Near the end this must be a result of a pressure gradient driving the fluid into and then down the base region. In the case of a cylinder with an endplate, the driving pressure gradient

will be the result of the difference between the pressure on the plate P_p and the pressure within the base region P_b. Actually, this type of flow was one aspect of the problem studied by Etzold [14] for cantilevered circular cylinders ($L/D \leq 10$) at normal incidence.

In order to pursue this discussion further some simplifications are necessary. First, the pressure on the endplate will be assumed to be uniform, unaffected by the presence of the cylinder, and equal to the pressure on an infinitely long inclined flat plate. Second, the base pressure of the cylinder will be taken as the undisturbed value on the face of the plate toward the cylinder. This rudimentary approach is not only justified by necessity but also by the results that can be obtained. The pressure on the face of the plate is given by

$$P_p = P_o + 1/2\rho U_o^2 C \ , \tag{A1}$$

where C is the pressure coefficient of the plate and is a function of ß. The base pressure of the cylinder is similarly determined,

$$P_b = P_o + 1/2\rho U_o^2 \cos^2\theta \ C_{P_{b_n}} \ . \tag{A2}$$

The driving pressure difference is simply,

$$\Delta P \equiv P_p - P_b = 1/2\rho U_o^2 \ (C - C_{P_{b_n}} \cos^2\theta) \tag{A3}$$

or

$$\frac{\Delta P}{1/2\rho U_o^2} = C - C_{P_{b_n}} \cos^2\theta .$$

Accordingly, we have

$$C > C_{P_{b_n}} \cos^2\theta \tag{A4}$$

and

$$C < C_{P_{b_n}} \cos^2\theta \tag{A5}$$

as conditions for flow into or out of the base region, respectively. This is an interesting result because it has application to the normal incidence case as well. In that case $C_{pb_n} = C_{pb}$ and in order to prevent axial flow on a two-dimension model we require

$$C \simeq C_{pb} \tag{A6}$$

or, since C_{pb} is negative, the endplate ought to be tipped into the flow.

Support for this notion can be found in the careful experiments of Graham [21] who studied the two-dimensionality of the wake flow behind a D-section bluff body fitted with endplates. His spanwise velocity correlations improved markedly for endplates with an inclination of slightly greater than 4° with respect to the freestream, i.e. $\beta \simeq 94°$. It is interesting to note that Gerrard's experimental configuration [18] tipped the endplates the other way ($\beta < 90°$) which was probably responsible for many of the three-dimensional phenomena he observed, including steady, slantwise vortex shedding for an unyawed cylinder. Similar results can be obtained for yawed cylinders if the variations of C and $C_{p_{b_n}}$ are known for β and θ, respectively. The latter can be found from the experimental results of the present study but it is sufficient in this analysis to take $C_{p_{b_n}} = -1$. The variation of C with β can be estimated from the experimental measurements of Fage & Johansen [16]. Their data are plotted in Fig. A3 along with a dashed line which is a somewhat speculative representation of the behavior for all values of the angle β. In this connection it must be noted that for $\beta > -30^o$ the pressure varies significantly over the face of the plate but within the spirit of this analysis the distribution of P_p is of secondary importance. The essential result is that $C(\beta) \simeq -\cos^2\theta$ gives the endplate inclination angles for which the flow in the base region ought to change direction. For the two yaw angles $\theta = 30°$ and 50° the corresponding endplate angles are $\beta \simeq 110°$ and $\beta \simeq 105°$. Within the accuracy of β in Figs. 22 and 23 these values of β correspond fairly well with the locations where the observed shedding frequency changes from below to above

the value predicted by the Independence Principle and the shedding angle goes from $\alpha > \theta$ to $\alpha < \theta$. Moreover, the sensitivity of this mechanism to small changes in β is greatest for $\beta \simeq 90° - 120°$, which compares very well with the data in Figs. 22 and 23. As a final observation this mechanism will not only be sensitive to Reynolds number because the base flow is influenced by turbulence but also because the coefficients C and $C_{p_{b_n}}$ are themselves Reynolds number dependent.

We can also use this approach to help select the endplate orientation(s) that best correspond to an infinitely long, yawed cylinder. On one hand, the flow must be "down" the cylinder so that we require

$$C > C_{p_{b_n}} \cos^2 \theta. \tag{A7}$$

On the other hand, the pressure on the plate ought to be less than P_o to prevent excessive flow down the cylinder and therefore

$$0 > C > C_{p_{b_n}} \cos^2 \theta \tag{A8}$$

According to all of the endplate experiments this inequality corresponds to the conditions

$$St/St_n > \cos \theta$$

and (A9)

$$\alpha < \theta .$$

This reasoning complements the vorticity discharge considerations that were employed earlier to select $\alpha < \theta$ as the condition appropriate to an infinitely long yawed cylinder. Use of either reasoning with the data of the present experiments invalidates the Independence Principle for separated flows.

This analysis has assumed that the base pressure P_b remains constant while the endplate inclination angle β is varied. This is not likely to be the case, since the universal Strouhal number concept requires that changes in the shedding

frequency f_s be accompanied by changes in the wake width and/or changes in base pressure parameter k. A single experiment was undertaken to investigate this point by simultaneously measuring the vortex shedding frequency, the shedding angle and the base pressure as functions of the endplate inclination angle β. The data, obtained for a Reynolds number Re = 550 and the yaw angle $\theta = 30°$, is presented in Fig. A4. The results for the Strouhal number ratio St/St_n and the shedding angle α compare well with the earlier data in Fig. 23a which was obtained under similar conditions. The base pressure coefficient $C_{p_{b_n}}$ also varies and reflects the frequency variation, even including an unexplained "bump" near $\beta = 100°$. This figure conclusively demonstrates the strong interaction that occurs between the end conditions and the wake flow of finite-length, yawed cylinders. This result also serves as further warning that spanwise uniformity is not an indication of the absence of end effects; Stansby [54] demonstrated this for the normal incidence case. Lastly, this data lends additional support for the notion that within the universal Strouhal number concept a multitude of flows can be realized for finite-length yawed cylinders; the particular flow in any case is determined by the end conditions.

Cylinders with a Free-End

An explanation of the end effects for a free-ended cylinder is complicated by the three-dimensional separation processes that occur at the end. It is intuitively satisfying to say that the coned and hemispherical ends will tend to promote a greater spanwise flow than the flat end because of the shapes involved. In a sense the coned and hemispherical ends become more streamlined for increasing yaw angle whereas the flat end becomes "bluffer."

Other Configurations

It is worth mentioning a few other configurations that have been utilized in previous investigations and to briefly discuss their effects. Van Atta used two configurations; one that passed the cylinders through slots in the wind tunnel walls and one that employed endplates. In view of the very large aspect ratios (L/D ≈ 500-1000) of his experiments it would appear that end effects were minimal and that is why he did observe that $St/St_n \geq \cos \theta$. Relf & Powell's smooth cylinder had two rounded free-ends and was mounted by means of a spindle at the midpoint. End effects were discounted by reducing the effective length by 4 diameters at each end or equivalently a 10 percent reduction in span for all yaw angles. According to the results of the present investigation and to those of Thompson & Morrison or Lamont & Hunt, it is entirely possible that Rolf & Powell's cylinder was not shedding vortices at the larger yaw angles.

Smith, Kao & Moon placed their cylinders in an air jet with endplates outside the jet. In this case there will be an equal tendency for "room" air to enter the base region from both ends. If this occurred, then a two angle shedding pattern could have formed. Alternately, the base flow could have been determined by an asymmetry of the jet. Whatever the cause, parallel shedding did not occur as indicated by the flow direction profiles in the wake. Moreover, the measured flow directions are consistent with a shedding angle less than the yaw angle and this accounts for the reported excess form drag over the Cosine Law prediction.

The experiments of Dale & Holler and those of King are interesting in that all were performed in water such that the free surface was one boundary of the wake flow. Air entrapment in the base region can pose a problem for sufficiently low base pressures (see King's original BHRA report) but otherwise the free surface provides a means to sustain pressure differences as well

as satisfying the vorticity theorem condition that vortex lines cannot terminate within a fluid. A spanwise base region flow must be permitted but its control can perhaps be more precisely adjusted at the downstream end. The greatest disadvantage to this configuration is that the water surface can act as a "reflecting" plane and introduce the strong influence(s) of symmetry. In other words the experimental arrangement is merely a physical representation of half of the flow that occurs for a bent cylinder. This was one difficulty encountered in attempts to generalize the results of Dale & Holler or for that matter the results of King. The importance of the symmetry influence is demonstrated in the next appendix.

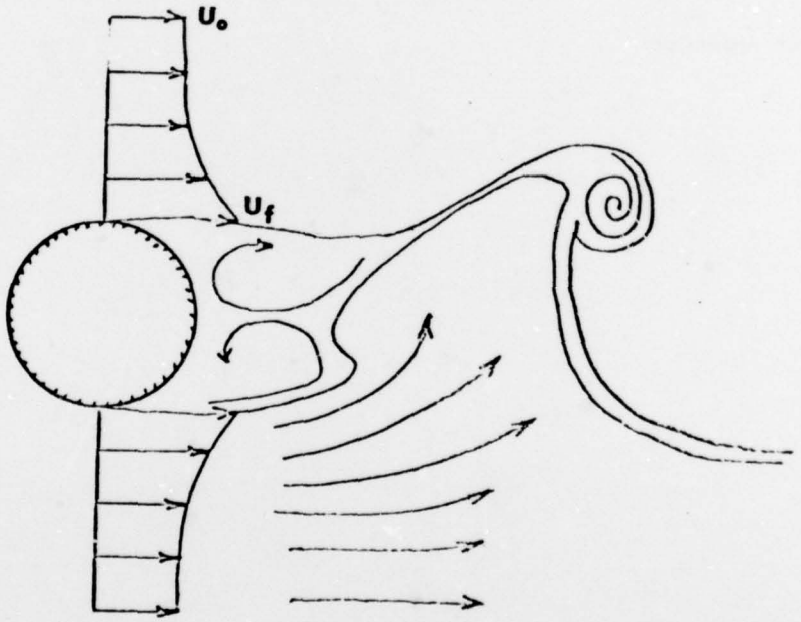

Figure A1 - A sketch of the two-dimensional vortex formation processes.

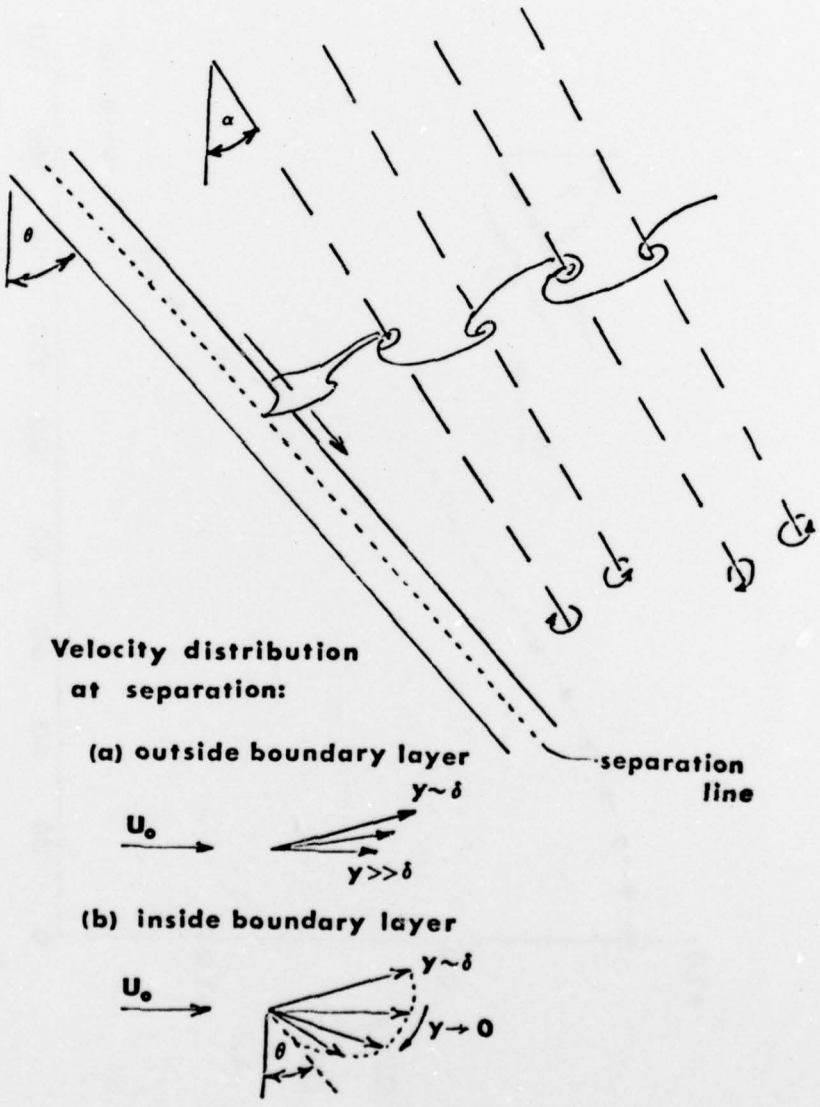

Figure A2 - A sketch of the three-dimensional vortex formation processes.

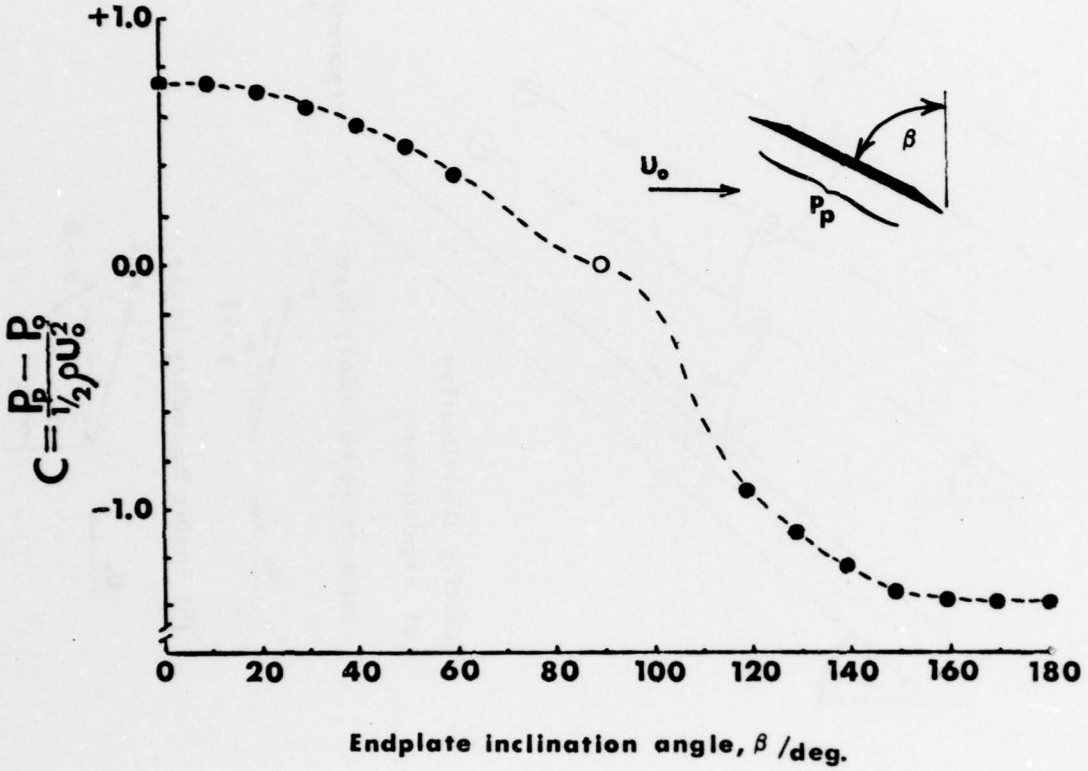

Figure A3 - The pressure coefficient C on the face of an endplate as a function of the inclination angle β.

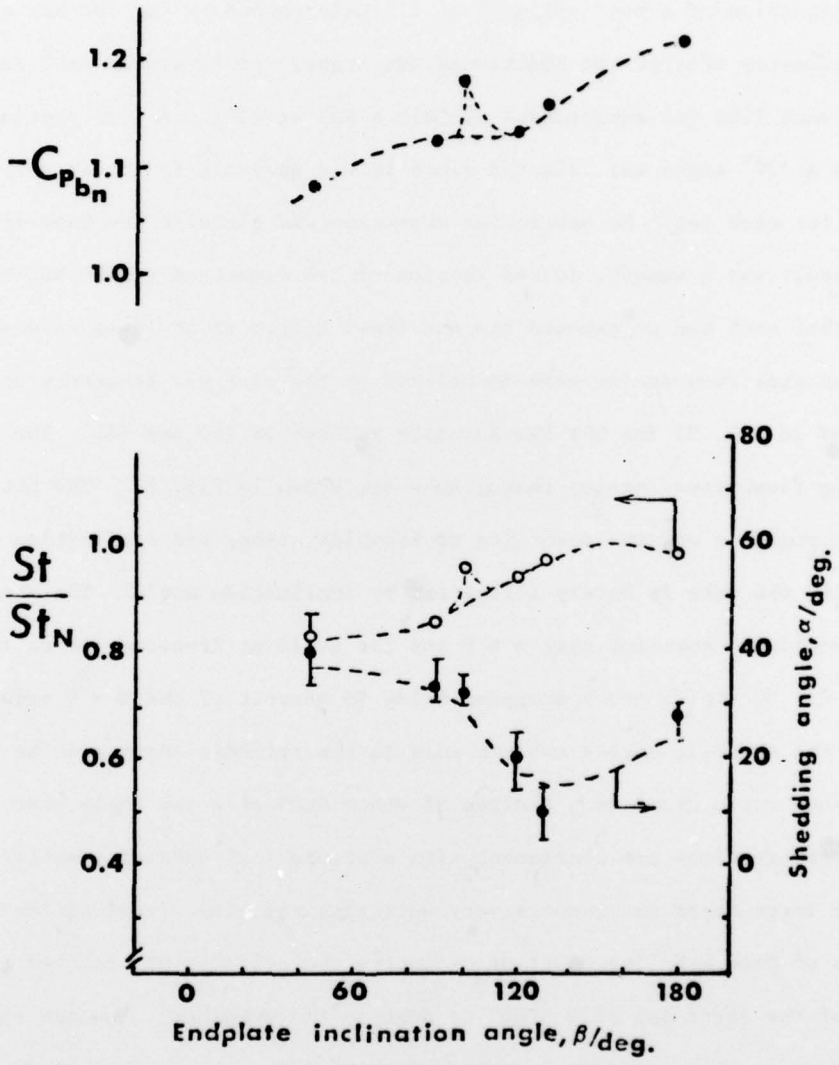

Figure A4 - The influence of endplate inclination angle upon the vortex shedding frequency, the shedding angle, and the base pressure for a Reynolds number Re = 550 and a yaw angle $\theta = 30^{\circ}$.

APPENDIX B - BENT CYLINDER FLOWS

A discussion of various configurations of some practical importance led to the suggestion of a bent cylinder as a likely candidate for further experiments. This geometry offered two additional advantages; no "upstream end" and a symmetry much like the experiments of Dale & Holler [10]. A bent section that formed a 120° angle was selected since it was possible to obtain a zero yaw angle for each leg. No particular attention was given to the bend itself and the result was a smooth, curved section of 3-4 diameters radius between the two legs that each had an exposed (to the flow) length of at least 44 diameters. The shedding frequencies were normalized by the zero yaw frequency and are plotted in Fig. B1 for the two Reynolds numbers of 160 and 460. The corresponding flow visualization photographs are shown in Fig. B2. The photographs are arranged in columns according to Reynolds number and inclination angle. For Re = 160 the wake is barely influenced by inclination angle. The shedding angle is essentially constant near $\alpha = 0$ and the shedding frequency shows some symmetry about $\theta = 30°$ while never dropping below 96 percent of the $\theta = 0$ value. For Re = 460 the shedding angles conform more to the cylinder shape and the shedding frequency ratio drops to a minimum of about 0.89 at a yaw angle near $\theta = 32°$. These observations are consistent with a strong influence of symmetry over rather large spans and compare very well with the flow visualization photographs of Dale & Holler. Out of curiosity the cylinder was rotated about the axis of the lower leg at $\theta = 30°$ to destroy the symmetry. The new shedding frequency in this instance is represented by the square symbol in Fig. B1 and compares well to the earlier free-ended results.

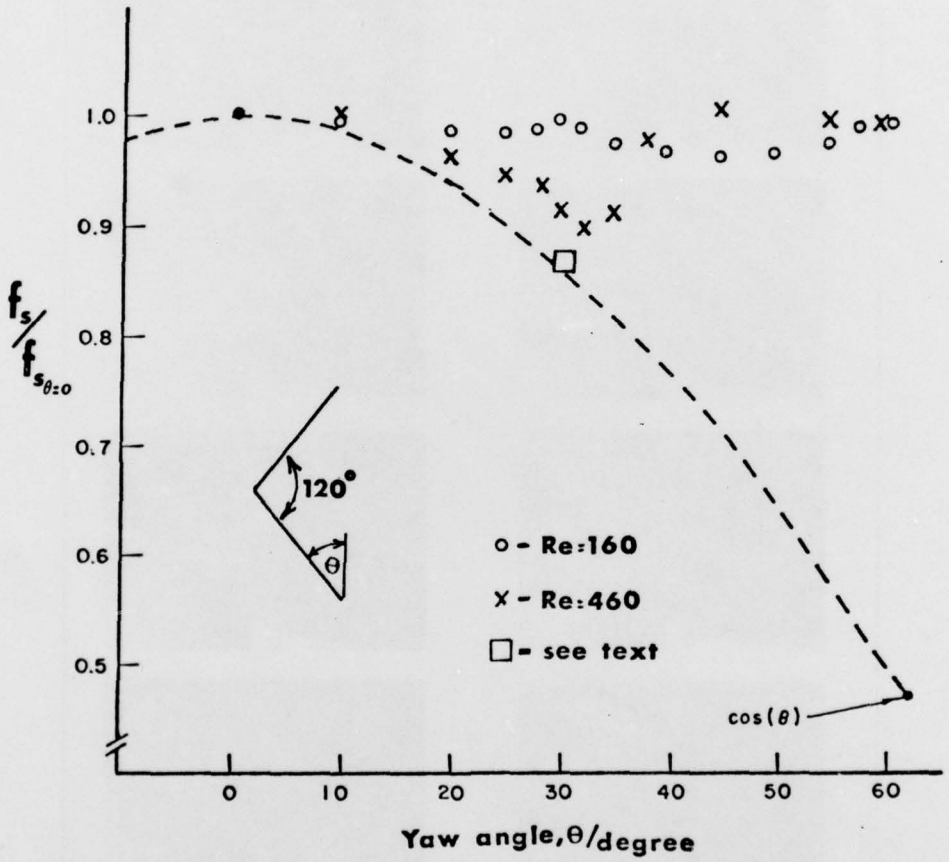

Figure B1 - Shedding frequency measurements for a bent circular cylinder at two Reynolds numbers, Re = 160 and Re = 460.

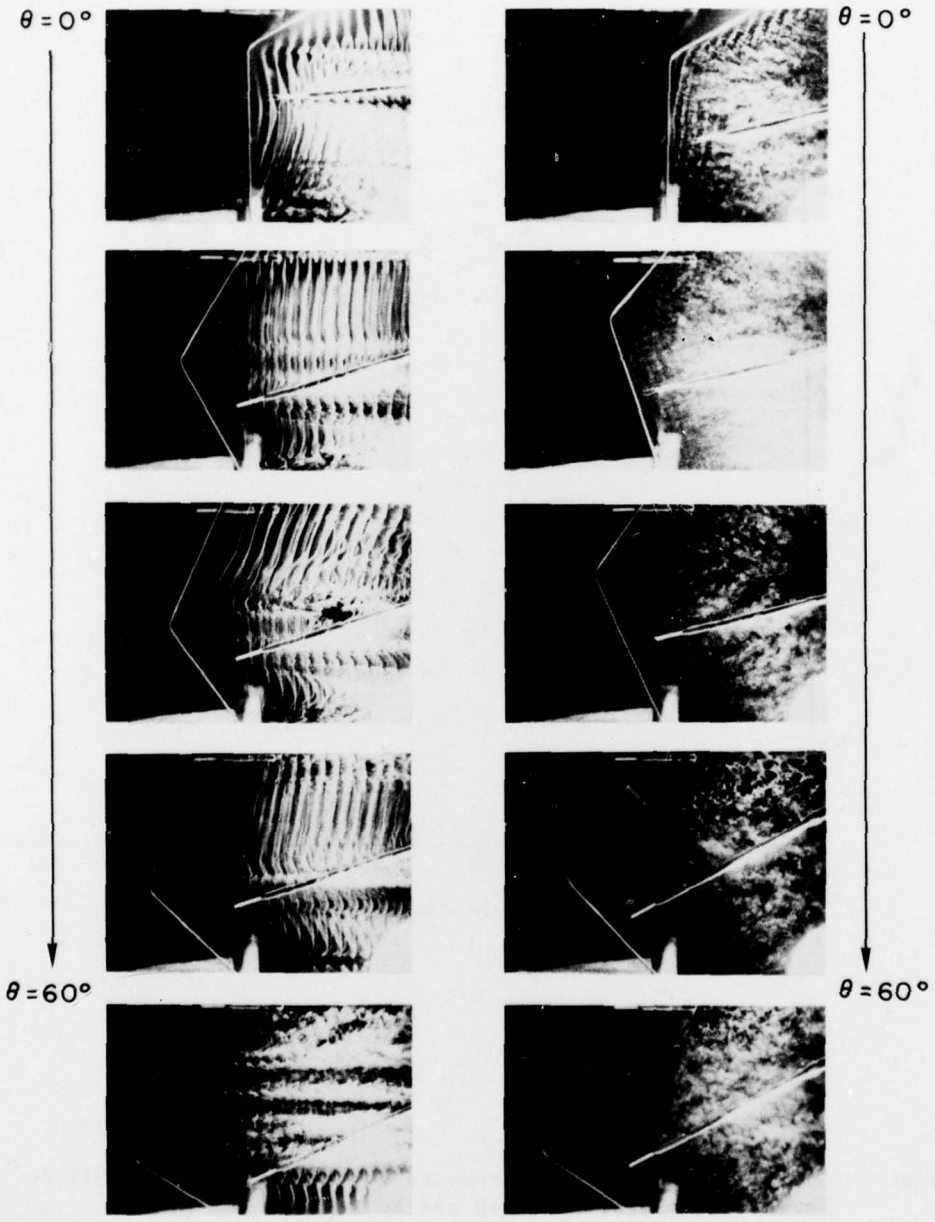

Figure B2 — A flow visualization series for the bent cylinder experiments. The lefthand column corresponds to Re = 160 and the righthand column to Re = 460.